A STUDY OF SELECTED WATER-SOLUBLE HYDRAZYL FREE RADICALS

A Thesis

Submitted to the Faculty of Graduate Studies and Research

in Partial Fulfillment of the Requirements

for the Degree of

Master of Science

in the

Department of Pharmacology

University of Saskatchewan

Saskatoon

by

Monika D. Lafond

Saskatoon, Saskatchewan

Canada

Fall 2002

DEDICATION

To my brother Michael J.R. Lafond (November 12, 1960 – June 20, 1989),

whose quiet encouragement gave me the incentive to begin my long

"educational" Odyssey,

To my grandmother Helene Däuwel (November 14, 1913 – August 21, 1999),

whose unwavering support gave that Odyssey shape and endurance,

And to my parents, Marga and Bert, whose love and understanding made the

culmination of that Odyssey possible.

ACKNOWLEDGEMENTS

I would like to thank the many people who have helped me through the numerous years of study and research:

Drs. John A. Weil (who had the idea for this project) and J. Steven Richardson, my supervisors, for their direction, constructive criticism, and commitment to high standards in both research and writing;

Mr. David F. Howarth, for his enthusiastic and invaluable help with the electron paramagnetic resonance studies and write-up, who spent considerable time "degassing" liquid solutions of the paramagnetic species, and simulating their experimental spectra to determine the EPR parameters presented in this paper;

The Scottish Rite Charitable Foundation of Canada, for their generous support in funding this basic research, and their ongoing sponsorship of research that focuses on understanding and curing neurodegenerative diseases;

Dr. J. Wilson Quail, for his dedication to crystallography, and his help in obtaining and understanding the molecular structures presented herein, who generously performed all the x-ray diffraction work and its demanding computer-based analysis;

Dr. Keith C. Brown, for his expertise and help with the nuclear magnetic resonance studies, who obtained the 500 MHz low temperature NMR spectra of the diamagnetic compounds;

Dr. J. R. Dimmock, for his willingness to serve on my Advisory Committee, and for his idea to send our molecules for external testing and his help in so doing;

Drs. J. Tuchek and R. A. Hickie, for their willingness to serve on my Advisory Committee and for their understanding that a pharmacology thesis can be based on organic chemistry;

Dr. Parvaneh Rahimi-Moggadam, for her untiring tutelage in the culturing of cells, and general pharmacology-lab procedures;

Ms. Yamini Upadrashta, for her help with the dynamic nuclear magnetic resonance studies, who performed simulations of the experimental NMR spectra to determine the rate parameters;

Mr. Rick Elvin, for his patience and willingness to design and construct special glassware used in the experimental work;

Mr. Ken Thoms, for his work in obtaining the elemental analysis of the salts prepared for this study;

The Department of Chemistry for giving me, a Pharmacology graduate student, laboratory space in which to do the necessary (and endless) organic chemistry;

The Department of Pharmacology (staff, students, and faculty), for making me feel like "one-of-the-family" even when the majority of my time was spent at the Department of Chemistry;

Dr. Alec Jokic, for his help in the preparation of the "super-duper" oxidizing agent (MnO_2) used in this study;

Dr. Zbigniew Zimpel, for the design and development of the computer-based analytical procedure used to automate the spectral-fitting process so necessary for the simulation of EPR spectra and attainment of EPR spectral parameters;

Ms. Viorica (Ibi) Bonadici, for her enthusiastic translation of several Hungarian-language papers;

Dr. Barbara R. Nelson, for her willingness to take me on as an undergraduate student and teach me proper laboratory procedures and experimental organic synthesis techniques;

Dr. Malvinder Singh, who taught me, as an undergrad, how important it is to never underestimate the apparent and hidden dangers that lurk in an organic laboratory;

And last but not least, my Burmese boys Mickey, Simon, and Boo, who kept me well-grounded in the "real world' by constantly reminding me about what is most important in life, their happiness.

ABSTRACT

Numerous diseases that afflict living organisms have been linked to cellular/biomolecular damage caused by reactive nitrogenic and oxygenic species (RNS/ROS). Many RNS/ROS are free radicals. In response, a stable water-soluble free radical able to react with other free radicals could, in theory, act as a free-radical scavenger *in vivo* and detect, decrease or eliminate harmful free-radical activity.

Salts of water-soluble analogs of the well-known free radical 2,2-diphenyl-1-(2,4,6-trinitrophenyl)hydrazyl were synthesized as were their progenitor molecules, the corresponding hydrazines. The analogs were produced by replacement of either an *ortho* or *para* nitro group ($NO_2\bullet$) with a sulfo group (SO_3^-), in the trinitrophenyl ring. The compounds have been characterized by ultraviolet-visible light spectroscopy, elemental analysis, nuclear magnetic resonance spectroscopy (the hydrazines), x-ray diffraction studies (the hydrazines), and by electron paramagnetic resonance spectroscopy (the hydrazyls). As well, the compounds were evaluated for neurotoxicity in mice and rats, for anticonvulsant activity (an assessment of the compounds' ability to penetrate the central nervous system), and for antineoplastic activity.

Potassium salts of both the *ortho* and *para* sulfo-substituted hydrazines and hydrazyls were synthesized. Surprisingly, a *para*-substituted diphenyl hydrazinium salt was obtained where the protonated (H^+) form had been the goal. All the synthesized sulfohydrazines were successfully purified, and yielded

crystals suitable for examination by x-ray diffraction. The crystal structures of the three sulfo-hydrazine salts are included herein.

The salts are all water-soluble; the sulfohydrazyls seem to be somewhat more "water-loving" than the sulfohydrazines. They all are stable in their solid form in air at room temperature. Properly stored in a desiccator and away from light, the solids do not decompose over time.

Solutions of the sulfohydrazyl salts dissolved in various solvents, including water, are stable at room temperature for at least two days, as followed by EPR. With few exceptions, the solutions are intensely coloured and range from a red-purple (plum) to a black-purple (violet). In solution, the sulfohydrazyls do not seem to be particularly sensitive to the presence of dioxygen (•O—O•).

Interesting pH-dependent reactions of the sulfohydrazyl salts have been seen. Addition of dilute $HClO_4$ or HNO_3 to aqueous solutions of either the *ortho*- or *para*- sulfohydrazyl anion eliminated the EPR absorption. Upon neutralization of the acidic solution by dilute aqueous NaOH, the characteristic EPR absorption of the respective sulfohydrazyl reappeared. On the other hand, addition of dilute NaOH to the sulfohydrazyls in H_2O brought about a similar quenching of the EPR signal but subsequent neutralization of the alkaline solution with acid did not result in the reappearance of the EPR absorption. However, oxidation of the neutralized solution (by MnO_2 and dioxane) did result in an EPR spectrum similar to that observed for the "precursor" sulfohydrazyl in a dioxane/water binary-solvent system.

Attempts were made to correlate the solvatochromic Kamlet-Taft β parameter to the effect of water and a series of organic solvents on ^{1}H NMR parameters of the sulfohydrazine salts and on EPR parameters of the sulfohydrazyl salts. In general, both EPR (i.e., A [^{14}N]) and NMR (i.e., chemical shift of the hydrazinic proton) parameters studied were relatively insensitive to the H-bonding characteristics of the solvent.

TABLE OF CONTENTS

GLOSSARY OF ACRONYMS AND SYMBOLS

ATCC: American Type Culture Collection

BSA: bovine serum albumin

cAMP: cyclic adenosine-3',5'-monophosphate

CD_2Cl_2: perdeuterated dichloromethane (methylene chloride)

DH_2-H: 2,2-diphenyl-1-(2,4,6-trinitro)phenyl hydrazine; 2,2-diphenyl-1-picryl hydrazine

DH_2•: 2,2-diphenyl-1-(2,4,6-trinitro)phenyl hydrazyl; 2,2-diphenyl-1-picryl hydrazyl

DMEM: Dulbecco's modified Eagle's medium

DMF: dimethylformamide

DMPH-H: 2,2-dimethyl-1-picrylhydrazine

DMPO: 5,5-dimethyl-1-pyroline-N-oxide

DMSO: dimethylsulfoxide

DPH: 1,1-diphenylhydrazine

DPH-DP4SH: 1,1-diphenylhydrazinium 2,2-diphenyl-1-(2,6-dinitro-4-sulfo)phenyl hydrazine

DPH-DP4SH•: 1,1-diphenylhydrazinium 2,2-diphenyl-1-(2,6-dinitro-4-sulfo)phenyl hydrazyl

ECM: extracellular matrix molecule

ELISA: enzyme linked immunosorbant assay

EtOH: ethanol

EPR: electron paramagnetic resonance

FBS: fetal bovine serum

HPLC: high performance liquid chromatography

HS: horse serum

K-DP4SH: potassium 2,2-diphenyl-1-(2,6-dinitro-4-sulfo)phenyl hydrazine

KPH-DP4SH•: potassium 2,2-diphenyl-1-(2,6-dinitro-4-sulfo)phenyl hydrazyl

K-DP6SH: potassium 2,2-diphenyl-1-(2,4-dinitro-6-sulfo)phenyl hydrazine

K-DP6SH•: potassium 2,2-diphenyl-1-(2,4-dinitro-6-sulfo)phenyl hydrazyl

MeOH: methanol

MTT: 3-(4,5-dimethylthiazol-2-yl)-2,5-diphenyl tetrazolium bromide

NMR: nuclear magnetic resonance

PBN: N-*tert*-butyl-α-phenylnitrone

RPMI-1640: Roswell Park Memorial Institute-1640 medium

TBAB: tetra-*n*-butyl-ammonium bromide

THF: tetrahydrofuran

TMS: tetramethylsilane

TSA: thiosalicylic acid

Uv-vis: ultraviolet-visible

δ: in NMR, chemical shift

α: Kamlet-Taft solvatochromic parameter; a measure of the dipolarity/ dipolarizability of a solvent

β: Kamlet-Taft solvatochromic parameter; a measure of a solvent's ability to donate a pair of electrons to a solute-solvent hydrogen bond

π^*: Kamlet-Taft solvatochromic parameter; a measure of a solvent's ability to donate a proton to a solute-solvent hydrogen bond

$A[^{14}N]$: hyperfine coupling constant due to the interaction between the lone electron and the hydrazinic nitrogen nuclei

LIST OF TABLES

LIST OF FIGURES

1. INTRODUCTION

1.1 Free Radicals and Disease

Many of the illnesses that plague biological organisms have been linked to an increase in free-radical activity. These diseases and insults include (but are not restricted to) atherosclerosis, hypertension, diabetes, ischaemia-reperfusion, chronic inflammatory diseases (i.e., rheumatoid arthritis), lung damage, cystic fibrosis, cancer, brain injury, and neurodegenerative diseases such as Alzheimer's Disease, Parkinson's Disease and Amyotrophic Lateral Sclerosis. An increased level of free-radical activity is also associated with aging. Whether this escalated free-radical burden is causative, or an effect of the disease/aging process, is unclear.

Researchers [ZRMW95] at the University of Saskatchewan have shown that the formation of free radicals in autopsy samples of Alzheimer cortex is greater than that generated in age-matched autopsy samples of normal control cortex. In the presence of ferrous sulfate, an agent that promotes free-radical generation, Alzheimer frontal cortex samples generated almost 50% more free radicals than did the control samples. Even under basal conditions (in the absence of a promoter), 22% more free radicals were generated by the Alzheimer samples than by the controls. More recently, researchers [PLTRF98, LRF99] from the University of Pennsylvania Medical Centre found that, when compared with the frontal and temporal lobes of normal brains, free-radical activity was almost double in the autopsied brains of Alzheimer patients.

A free radical is any chemical species (atom, molecule, or group of molecules) that possesses one or more unpaired electrons. Since chemical species with paired electrons tend to be stable, free radicals are generally unstable and more reactive than non-radicals. As a tendency, free radicals generated by living organisms are extremely unstable and have very short half-lives. Because they are highly reactive, they are capable of damaging cells, tissues, and organs. In biologic systems, free radicals often function as electron acceptors and, as such, are referred to as oxidants. However, at times they are also able to function as electron donors.

The production of reactive oxygenic species is a characteristic of normal aerobic existence. These include but are not restricted to free radicals (i.e., $HO\bullet$, $O_2\bullet^-$, as well as H_2O_2). Herein, an unpaired electron is denoted by "•". Oxidants carry out key roles in a wide range of normal biologic processes. They are important in clearing infections and are crucial in the maintenance of life. They are kept in check by a balance of extra- and intra-cellular antioxidants, including both enzymatic (e.g., superoxide dismutase, catalase) and non-enzymatic (e.g., vitamins C and E) systems. Oxidants tend to react with and change normal biological constituents in the event of a decrease in antioxidant defense and/or an increase in oxidant burden. Halliwell and Gutteridge [HG99, pp. 106-7] define an antioxidant as "any substance that, when present at low concentrations compared with those of an oxidizable substrate, significantly delays or prevents oxidation of that substrate." The phrase "oxidizable

substrate" encompasses, but is not restricted to, every kind of molecule found in living cells, including proteins, lipids, carbohydrates, and DNA.

1.2 Aromatic Hydrazines and Hydrazyls

1.2.1 Hydrogen-Atom Abstraction

Aromatic hydrazines and hydrazyls both have a hydrazinic backbone that consists of two singly-bonded nitrogen atoms, N_1 and N_2. In most cases, a hydrogen atom and a 2,4,6-trinitrophenyl group are attached to N_1. N_2 has at least one (usually two) phenyl group attached, substituted or not, but no directly attached hydrogen atom. As Figure 1 shows, aromatic hydrazines differ from aromatic hydrazyls by but one hydrogen atom. Thus, an appropriate oxidant abstracts atomic hydrogen through cleavage of the N-H bond of the hydrazine. As such, hydrazines are the precursor molecules (starting materials) of hydrazyls. The lone electron of the hydrazyl is partially stabilized by delocalization over both nitrogen atoms as well as through the π-system of the

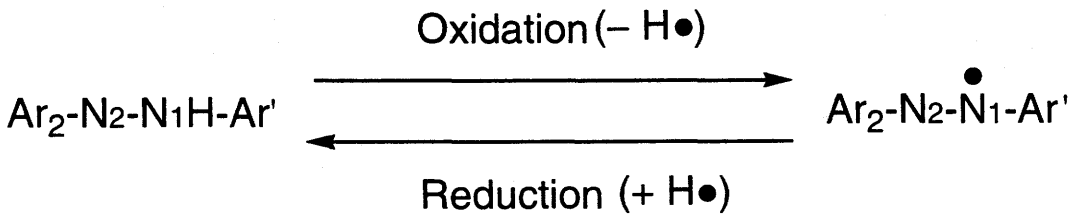

Figure 1: A hydrazine is oxidized to a hydrazyl, which in turn can be reduced back to a hydrazine

aromatic groups and their substituents (see Section 1.3 for further discussion). This simple difference results in two quite dissimilar compounds.

The hydrazines, having no unpaired electrons, are diamagnetic and suitable for analysis using nuclear magnetic resonance (NMR) spectroscopy (see Section 1.6.2). The hydrazyls are paramagnetic due to their unpaired electron. They are best "seen" by using electron paramagnetic resonance (EPR) spectroscopy (see Section 1.6.3). The hydrazines range in colour from yellow to orange to red, and have a uv-visible electronic absorption between 300 and 400 nm. The colour of the hydrazyls ranges from dark plum (a red-purple) to dark violet (a black-purple). Their electronic spectra show one absorption band at approximately 520 nm, and one at approximately the wavelength of its corresponding hydrazine. The hydrazyls are usually somewhat light-sensitive, requiring "dark" storage, whereas the hydrazines are relatively light-insensitive and require no such special storage procedures.

1.2.2 Oxidizing Agents: PbO_2, MnO_4^-, and MnO_2

Traditionally, lead dioxide has been used to oxidize aromatic hydrazines to their corresponding hydrazyls [GR22, CDW61]. The oxidation usually is carried out in the presence of anhydrous sodium sulfate. The sulfate acts as a drying agent and blocks the reduction of the hydrazyl back to its precursor by H_2O, a by-product in the reduction of Pb(IV) to Pb(II) [GR22]:

$$PbO_2 + 2H^+ + 2e^- \rightleftharpoons PbO + H_2O,$$

The utilization of specially activated lead dioxide has been documented as a more efficient oxidant [CDW61].

The use of potassium permanganate to oxidize hydrazines to their corresponding hydrazyls was reported in 1986 [BW86]. Given that $KMnO_4$ can undergo photolytic decomposition, the oxidant is freshly ground prior to its use (to expose fresh surface area). The oxidation proceeds with or without the presence of small amounts of the phase-transfer catalyst tetra-*n*-butyl-ammonium bromide (TBAB). The addition of a drying agent is not necessary. Since it is reported that water is essential for the following half-reaction,

$$MnO_4^- + 4H^+ + 3e^- \rightleftharpoons MnO_2 + 2H_2O,$$

it is postulated [BW86] that if manganese dioxide is produced, then any water formed is unavailable to reduce the free radical because it has been taken up by MnO_2 or is in the coordination shell of any excess MnO_4^- that may be present. It is further theorized that a possible first step in oxidation by $KMnO_4$ involves the generation of the hydrazyl and hydrogen manganate anion ($HMnO_4^-$). The disproportionation (the change of a substance into two or more dissimilar substances typically by coincident oxidation and reduction) of the anion then follows. At the very least, the authors [BW86] suggest that the first step in the oxidation is a one-electron transfer to permanganate.

There have been no reports of the successful oxidation of aromatic hydrazines to hydrazyls by manganese dioxide. In fact, its failure was reported [BW86] alongside the successful oxidation by $KMnO_4$. The authors of the paper postulated that the manganese of $KMnO_4$, which is originally in the +7 oxidation

state, winds up at +4. Other reports [F76] suggest that, in the presence of activated manganese dioxide, symmetrical 1,2-disubstituted hydrazines dehydrogenate to yield azo compounds, and unsymmetrical 1,1-disubstituted hydrazines either produce tetrazenes by way of N—N coupling, or form hydrocarbons through nitrogen elimination and C—C coupling. The product seems to be dependent upon the kind of solvent employed, but none of the products are free radicals.

1.2.3 Reduction by, and Titration with, Thiosalicylic acid

Analysis by potentiometric titration of aromatic hydrazyls (in particular $DH_2\bullet$, see Section 1.3) with thiosalicylic acid (TSA) was reported in 1965 as an alternative to determination by reaction with hydroquinone. It is an accurate and easy method of analysis for $DH_2\bullet$, and takes advantage of the hydrazyl's ability to abstract hydrogen atoms from mercaptans [WA65].

TSA is a reducing agent. Solutions of TSA in acetone or ethanol are readily standardized acidimetrically. The end-point is easily determined by potentiometric titration. The use of the indicator curcumin, which gives a sharp colour change from yellow to orange, makes the standardization even more convenient [WA65].

Acetone and ethanol solutions of TSA react cleanly and quickly with $DH_2\bullet$. TSA and the reaction products are not intensely coloured and, as such, the intense purple colour of $DH_2\bullet$ (actually, it's disappearance) is used as an indicator. The conversion to yellow (orange), which corresponds to the

reduction of DH_2•, is taken as the end-point. Products of the reaction are 2,2-diphenyl-1-picryl hydrazine (DH_2-H) and 2,2'-dithiosalicylic acid, and no major side reactions were seen. This method works best with concentrations of DH_2• that range from *ca.* 1 x 10^{-6} M to 1 x 10^{-2} M; the optimal concentration being 1 to 5 x 10^{-3} M [WA65].

1.3 2,2-Diphenyl-1-picryl hydrazyl (DH_2•)

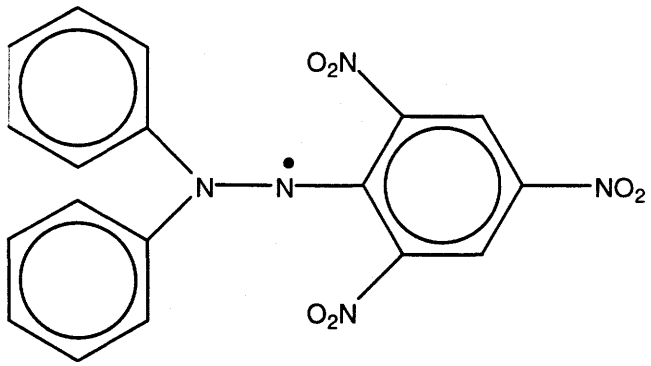

Figure 2: 2,2-Diphenyl-1-picryl hydrazyl

The well-documented free radical 2,2-diphenyl-1-picryl hydrazyl (DH_2•), where "picryl" represents the 2,4,6-trinitrophenyl group, was discovered and investigated during the 1920s by Stefan Goldschmidt [GR22]. The radical structure exhibits a magnetic moment brought about by the uncompensated spin motion of the odd electron [I58]. Subsequent paramagnetic susceptibility measurements and *ortho-para* hydrogen conversion have confirmed DH_2• to be an essentially 100 % free radical stable in various environments [B65]. As stated above, a free radical is an atom, or group of atoms, that has an odd number of valence electrons. The unpaired electron customarily makes the

atom or molecule chemically very reactive when compared to moieties with paired electrons.

Although a free radical, $DH_2\bullet$ is relatively stable even at room temperature and therefore is readily available commercially. One reference [BFMB61] describes the stability of $DH_2\bullet$ as "sterically conditioned", and indeed steric factors play a key role in the stabilization of $DH_2\bullet$. The picryl ring is at approximately 90 ° to the estimated plane of the two phenyl groups. The *ortho*-nitro groups of the picryl ring have no room for free rotation. Steric repulsions cause these nitro groups to twist away from coplanarity with the picryl ring [BFMB61, WBRW91]. The radical assumes a non-planar form, allowing conjugation throughout the molecule and decreasing the tendency for the central bond to dissociate [BFMB61].

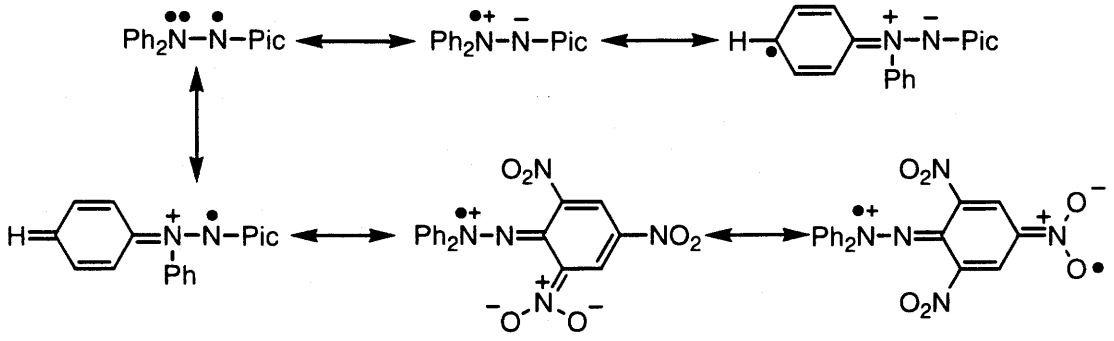

Figure 3: Some resonance structures of $DH_2\bullet$ [FHT68]

Also a key factor in the stabilization of $DH_2\bullet$ is the extended delocalization of the unpaired electron over the molecule shown in Figure 3. The canonical (accepted) forms that place the odd electron on N_1 contribute approximately 62 % to the resonance structure, those that place the odd

electron on N_2 about 26 %, and those that place the unpaired electron on any of the phenyl rings or their substituents about 10 % [FHT68].

$DH_2\bullet$ is quite stable as both a solid and in solution [FHT68, Y96]. Even at low temperatures, it does not tend to dimerize in either phase. It does not react with molecular oxygen ($\bullet O—O\bullet$) or with $NO\bullet$. As well, it will not disproportionate even with sustained heating. However, $DH_2\bullet$ is somewhat sensitive to light and should be stored accordingly. Ordinarily deep-violet, exposure to bright light will decrease the depth of colour. In some cases, this attribute can be used to accelerate reactions of a number of amines and phenols with $DH_2\bullet$ by photochemical means [FHT68]. Absorption bands at 320 and 520 nm in the visible-ultraviolet region of its electronic spectrum set it apart from its corresponding hydrazine (DH_2-H), which only absorbs at 320 nm. As such, the absorption band at 520 nm is generally recognized to be typical of $DH_2\bullet$ itself [Y96].

$DH_2\bullet$ is used extensively in electron paramagnetic resonance (EPR) spectrometry as a standard for free-radical work. In its powder form, it has an accurately known g factor, the effective Zeeman (correction) factor, of 2.0037 ± 0.0002 at room temperature. In a deoxygenated solution of benzene, in which it is readily soluble, it has a factor of 2.00354 ± 0.00003 at room temperature. As such, it is widely used as an EPR standard for the calculation of g values. As well, it is employed as a gauge for intensity, line width, concentration, and magnetic-field spacings [WBW94 pp. 68, 510-511].

In polymer chemistry, $DH_2\bullet$ is an acknowledged and generally useful radical scavenger. It is used to determine rates at which polymerization is initiated and at which chain-propagating radicals are formed. $DH_2\bullet$ is useful in the stabilization of polymers and monomers to light, heat and oxidation. It is also used to confirm the occurrence of polymerization [FHT68].

Another application that highlights the characteristics of the stable free radical is hydrogen-atom abstraction. In boiling chloroform, it readily dehydrogenates C—H bonds in dihydro -anthracenes, -benzenes, -napthalenes, and -pyridines, with third-order kinetics and fairly high activation energies (E_a = 6 to 8 kJ/mole). $DH_2\bullet$ more readily dehydrogenates complexes containing N—H bonds than C—H bonds, due to the greater ease of nitrogen to move between sp^3 (tetrahedral) and sp^2 (planar) configurations. Reactions with primary aromatic amines are of third-order kinetics and with secondary aromatic amines are of second-order kinetics. Hydrogen abstraction from O—H bonds occurs with second-order kinetics. In general, dehydrogenation by $DH_2\bullet$ of S—H bonds takes place more easily than from C—H, O—H, or N—H bonds. Reaction kinetics are second-order with an approximate activation energy of 3.5 kJ/mole [FHT68].

In-vitro determination of the level of antioxidants in mammalian blood, liver and brain samples by $DH_2\bullet$ was first reported in the mid-20^{th} century [B58, G63, GS64I, GS64II]. In chloroform and ethanol, $DH_2\bullet$ exhibits a strong uv-visible absorption band at 517 nm and gives a deep violet colour (no matter the solvent and at very low concentrations). The decolorization of $DH_2\bullet$ (the violet

colour fades and a yellow colour appears) in response to the addition of antioxidants in solution, as its odd electron becomes paired off, is a measure of the antioxidants present and can be followed spectrophotometrically [G63]. Blois [B58] reports that there is in fact, a pronounced stoichiometric relationship between the decolorization of $DH_2\bullet$ and the number of odd electrons that become paired off. $DH_2\bullet$ reacts quantitatively with molecules that have reversibly oxidizable groups to give results conforming to the mechanisms shown in Figure 4. These compounds include ascorbic acid, cysteine, glutathione, polyhydroxy aromatic molecules (e.g., hydroquinones), tocopherol, and certain aromatic amines (e.g., *p*-aminophenol). Thiol (S-H) groups of proteins were also oxidized, however, glucose, purines, pyrimidines, and aromatic molecules containing only single hydroxyl (HO) groups were not.

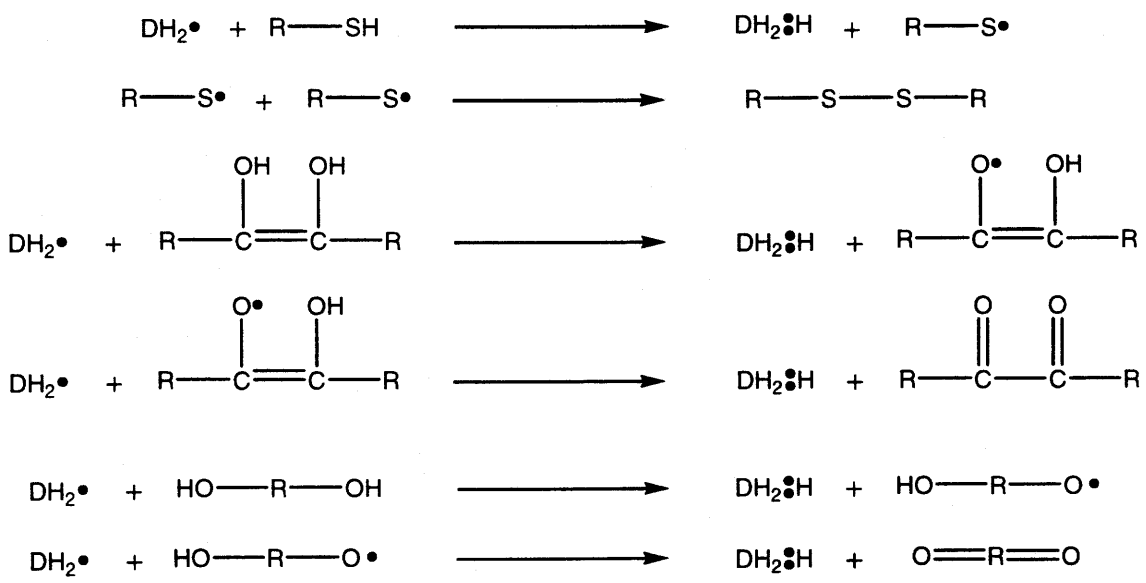

Figure 4: Stoichiometric relationship between $DH_2\bullet$ and some oxidizable groups [B58]

Today, the DH_2• assay is commonly used to measure the radical-scavenging (antioxidant) activity of compounds and/or extracts [BCB95, KvLdE2002, SHBB2002]. Reactions are carried out in organic (benzene, dioxane, ethanol, methanol) or organic-aqueous (50 % ethanol) solutions. Although insoluble in water, the typical intense dark-purple colour of DH_2• shows up well even at very low concentrations (to 10^{-4} M). A better assay would involve the water-soluble analogs of DH_2•. Their water-solubility precludes the need for organic or aqueous-organic solvents, and aqueous solutions are also highly coloured at equally low concentrations.

1.4 Some Analogs of DH_2• and its Diamagnetic Precursor

Since their introduction in the 1920s, DH_2-H and DH_2• have been the topic of many a research paper. A SciFinder Scholar [SciFS2000] search of the less-than-comprehensive concepts "diphenylpicryl hydrazine, diphenylpicryl-hydrazyl, and DPPH" (a commonly used acronym of DH_2•), resulted in 2,828 "hits". Some of the interest in these compounds is due to their reactivity with other molecules to give analogs, the stability of the free radical and its use in EPR, and the effect of substitution on the thermodynamic properties of intramolecular reorientation (see Section 1.6.2.1) and on spectral properties. Since a comprehensive review would turn out to be book-length, herein is presented a select-few examples of hydrazine and hydrazyl analogs.

One common and important reaction of DH_2• with halogens, NO_2•, and other free radicals is addition of the attacking species at either, or both, of the

para positions in the unsubstituted phenyl rings, resulting in an aryl-substituted picryl hydrazine (the "displaced" *para* hydrogen atom bonds with the lone electron) as shown in Figure 5 [WSK61]. The resultant hydrazines are then oxidized to the corresponding hydrazyls. In the case of NO_2•, both mono- and

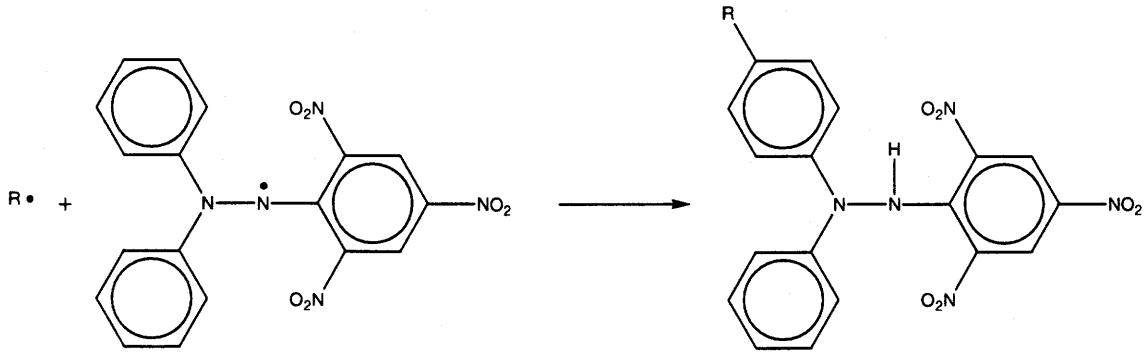

Figure 5: Substitution at the *para*-position of the unsubstituted phenyl

di- *para*-substituted picryl hydrazines/hydrazyls have been reported and corrected an earlier misconception that the product of the reaction with NO_2• is 2,2-diphenyl-1-hydroxy-1-picryl hydrazine [WSK61, BW86]. Some other species, besides halogens and nitro groups, which have been "placed" in the *para* position of the unsubstituted phenyl(s) include —OCH_3, —CH_3, —$COOCH_3$, and —C_6H_5 [CDW61].

An interesting study of bromo- and nitro- substitution reactions [CQRW83] revealed an unexpected mixture during the addition of bromine. At ice (0 °C) temperatures, during "fast addition of bromine" to DH_2-H and DH_2•, the expected mono- and di- substituted products were synthesized. However at higher temperatures, during "slow addition of bromine", the picryl-substituted products

2-(*p*-nitrophenyl)-2-phenyl-1-(2-bromo-4,6-dinitrophenyl) hydrazine and 2-(*p*-bromophenyl)-2-phenyl-1-(2-bromo-4,6-dinitrophenyl) hydrazine were formed. It was postulated that, in inert organic solvents, nitro groups, displaced from the picryl ring of $DH_2\bullet$ by Br•, reacted with $DH_2\bullet$ to form the compounds. This study added to the growing awareness that there are reactions in which one radical can replace another in aromatic compounds.[CQRW83].

Alkali salts of DH_2-H have also been reported [WJ62] in the scientific literature via reaction with alkali ethoxides (C_2H_5OM, where M represents an alkali atom). They are of the general form:

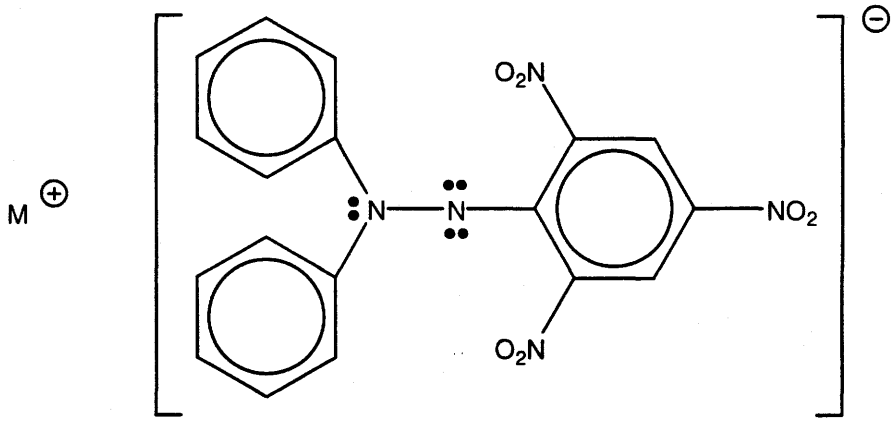

Figure 6: General form of alkali (2,2-diphenyl-1-picryl)hydrazinates

Lithium, potassium, sodium, rhubidium, and also quaternary ammonium salts of DH_2-H were synthesized and characterized. Concurrently, similar alkali salts of the nitrated mono- and di- *para* phenyl analogs of DH_2-H (mentioned above) were also reported. The alkali salts are diamagnetic (absence of EPR absorption) and sensitive to moisture. On the whole, they dissolve in polar organic solvents but are insoluble in nonpolar organic solvents [WJ62].

The synthesis of 2,2-dimethyl-1-picryl hydrazine (DMPH-H), by changing the "diphenyls" of DH_2-H to "dimethyls", has been reported [QWS2000]. However, DMPH-H is not oxidizable to the corresponding picryl hydrazyl. A difference in the hybridization of the "dimethyl/diphenyl" nitrogens is a main reason for this failure. In DMPH-H the nitrogen atom is sp^3 hybridized whereas in DH_2-H, the hybridization of the nitrogen atom in question is sp^2 with some sp^3 character [WBRW91, BNQRWZ99, QWS2000].

Many derivatives have also been reported by substitution in the "picryl" ring. Some of these include substitution of either an *ortho* or *para* NO_2• with H (to give 2,2-diphenyl-1-2,4- and 2,6-dinitrophenyl hydrazyl) [BFMB61, MIC61], and *para* NO_2• with COOH or bromine [KY*etal*63]. In these instances the hydrazines were oxidizable to the corresponding stable hydrazyls.

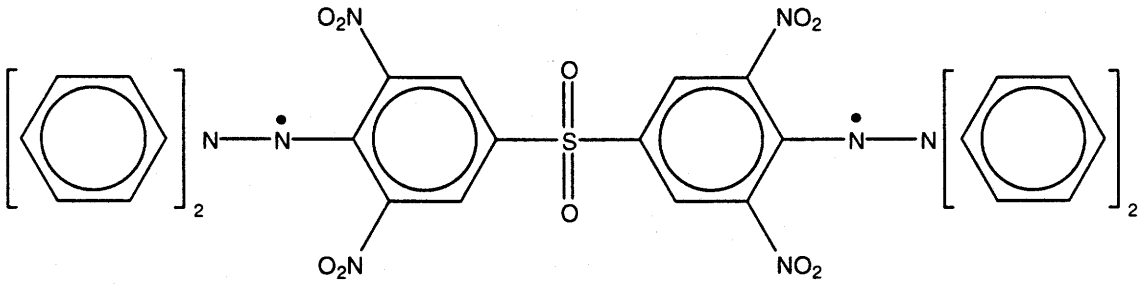

Figure 7: 1,1'-[sulfonylbis(2,6-dinitro-p-phenylene)]bis[2,2'-diphenylhydrazyl]

Finally, one particularly interesting derivative that has been reported [LO69] is the stable biradical 1,1'-[sulfonylbis(2,6-dinitro-p-phenylene)]bis[2,2-diphenyl hydrazyl] (44'BHS) shown in Figure 7. The biradical is offered as an appropriate standard for EPR by the grace of it's "great" stability over time, the

constancy and ease of its preparation, and it's characteristic EPR parameters which, in general, are independent of the method used for recrystallization [LO69]. Solubility of the biradical was not stated.

1.5 Water-soluble DH_2• Analogs

In 1953, the first stable water-soluble analog of DH_2•, the sodium salt of 2,2-diphenyl-1-(2,4-dinitro-6-sulfophenyl) hydrazyl (see Figure 8), was reported from a study to determine the effect of changes in the structure of the hydrazyl compound on the average position of the unpaired electron [J53]. While the

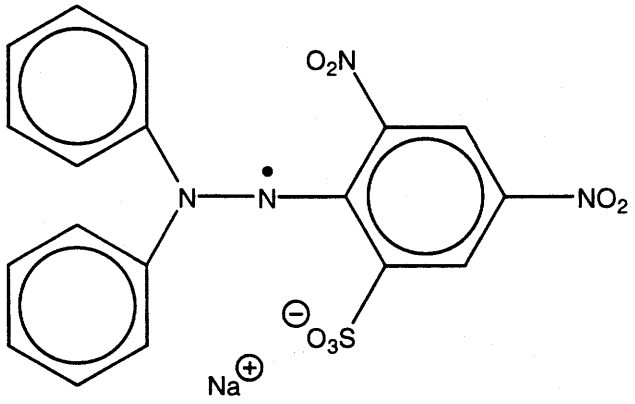

Figure 8: Sodium 2,2-diphenyl-1-(2,4-dinitro-6-sulfophenyl) hydrazyl

EPR spectrum was submitted, no properties (*i.e.*, solubility) or synthesis was given, nor has its synthetic procedure ever been reported. However, one can see that the derivative entails substitution of an *ortho* (relative to the picryl C—N bond) nitro group with a sodium-sulfonate group (SO_3Na).

Almost a decade later, in 1961, the synthesis of the potassium analog of the above salt was published in the scientific literature [IM62]. Concurrently, the *para* derivative, potassium 2,2-diphenyl-1-(2,6-dinitro-4-sulfophenyl) hydrazyl,

and 2,2-diphenyl-1-(2,6-dinitro-4-sulfophenyl) hydrazyl, the "protonated" (H^+) form (see Figure 9), were also reported [IM62]. Of course, the respective precursor sulfo-hydrazines were detailed as well. The physical properties of the sulfo derivatives were described; the chief among them were the stability and water-solubility of the compounds.

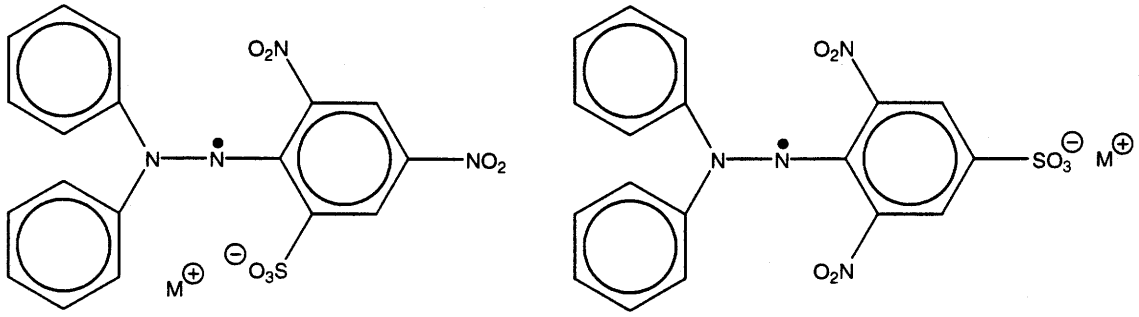

Figure 9: General form of the substituted picryl- *ortho* and *para* sulfo analogs of DH_2• (where M^+ can signify H^+, K^+, Na^+, etc.)

Very few references to these sulfo-derivatives have since been made. A 1963 study [KY*etal*63] of substituted diphenylpicryl hydrazyls was published in which the spin density distribution of both the *ortho* and *para* potassium sulfo-hydrazyl salts was determined by EPR in polycrystalline and liquid samples. EPR spectra of the two salts were also presented therein. In 1966, the electro-chemical generation of the potassium-*ortho* derivative was described [ILSV66]. Lastly, a study that put forward the suitability of employing the potassium-*ortho* salt for the examination of hydrogen abstraction in biological and pharmaceutical reactions was published in 1971 [DO71]. In order to identify the point of substitution, here on, substituted analogs of DH_2-H and DH_2• will be be designated as either substituted diphenyl, or substituted picryl.

While not much more was to be found about the substituted picryl sulfo-analogs of $DH_2\bullet$, in 1971 a Hungarian paper [PS71] was published in which was reported the synthesis of phenyl/diphenyl-substituted sulfo analogs (see Figure 10). (This and a few other Hungarian-language papers only recently became available to us and a select few were translated by Ms. Viorica Bondici.)

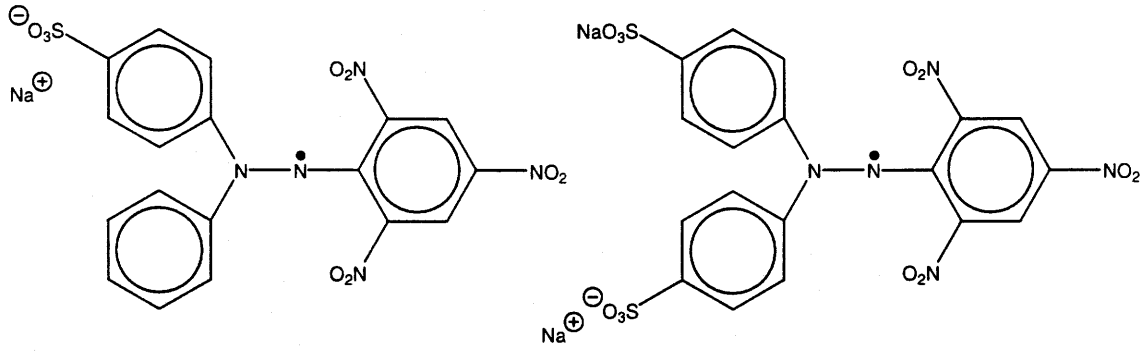

Figure 10: Sodium salts of *p*-sulfo- and *p,p'*-disulfo-2,2'-diphenyl-1-picryl hydrazyl

Both the *p*-sulfo- and *p,p'*-disulfo-2,2'-diphenyl-1-picryl hydrazyl sodium salts are readily soluble in water, but insoluble in non-polar solvents. In the synthetic paper, IR absorption parameters are presented for both the hydrazyls and the hydrazines [PS71]. The mono-sulfonate is more stable than the di-sulfonate. It was further investigated with regard to its reactivity with hydroxide ions (HO^-) in which EPR spectra, from pH studies, of the mono-sulfonate hydrazyl under acidic, basic and neutral conditions were presented [PM74]. As well, the formation of a hydroxy-derivative of the mono-sulfonate by reaction with aqueous NaOH was reported [PV74]. The hydroxyl group added to the "sulfonated" phenyl ring *meta* to the sulfo group.

More recently, the sodium salt of 2-phenyl-2-(*p*-sulfophenyl)-1-picryl hydrazyl (the mono-sulfonate) has been used to determine the radical-scavenging activity of sterically hindered phenol-dextran conjugates in water and water-dioxane mixtures [DAKB99, ADKB2000], and the influence cyclodextrins exert on the kinetics of the oxidation of amino acids and bovine serum albumin [IISL2001]. In 2000, an "optimized modified synthesis" was reported for the "mono- and di- sulfonated" picryl hydrazine and hydrazyl salts. Concurrently, the formation of supramolecular complexes between the mono and di-sulfonated picryl hydrazine and crown ethers or kryptands was reported, as well as the synthesis of several picryl hydrazine derivatives by initial reaction with the mono-sulfonate [ICB2000]. After reaction, the SO_3Na group of the mono-sulfonate was modified to $ClSO_2$, then to NH_2SO_2, or CH_3OSO_2. Attachment of larger molecules containing primary or secondary amino groups, such as found in amino acids, was also reported. Not all phenyl-substituted picryl hydrazines were oxidizable to the corresponding hydrazyls. Decomposition of some liquid solutions and solid product was also described. Spectral data for the compounds were also included, but the solubility of the compounds was not mentioned [ICB2000].

1.6 Tools of Investigation

Following are brief explanations of a number of tools routinely used in the investigation of organic compounds bound for biomedical research. For a more comprehensive description of each section, the reader is referred to books on

the respective topics, the individual references, as well as analytical chemistry, biochemistry, organic chemistry, and physics texts.

It may also be prudent to offer herein a generalized definition of the term spectroscopy. Spectroscopy is the measurement of energy that is absorbed or emitted when matter interacts with electromagnetic radiation. The types of spectroscopy are classified with respect to the range of frequencies (type of radiation) applied. All provide spectra that can be described according to the frequency, intensity, and shape of spectral bands or lines [L-BH69].

1.6.1 **Elemental Analysis (C, H, N and N, S)**

Basically, the objective of elemental analysis is to ascertain the elemental composition, as well as the purity, of organic molecules. Major components of organic compounds include carbon C, hydrogen H, nitrogen N, oxygen O, and sulfur S. Calculation of the molecular (chemical) structure is possible if the molecular mass and the percentage of each element in the compound are known. As such, techniques have been developed to analyse milligram samples of organic compounds to determine their elemental (C, H, N, O, S) percentages [KMOW98].

Fritz Pregl developed the technique behind elemental analysis while at the Universities of Innsbruck and Graz in Austria. In 1923 he was awarded the Nobel Prize in Chemistry "for his invention of the method of micro-analysis of organic substances". His methods still apply today augmented by modern instrumentation. Essentially, the technique consists of four steps:

1. disintegration of an accurately-weighed amount of a substance through rapid combustion (oxidation) in a stream of oxygen at sufficiently high temperatures (1000 °C to 1800 °C),
2. separation of the products of the reaction,
3. detection of very small amounts of gases that are produced during combustion of the sample, and
4. calculation of elemental percentages [KMOW98].

If the chemical structure of the sample under study is known beforehand, comparison of calculated and experimental percentages of the molecular elements will be an evaluation of the purity of the sample. The more closely experimental and calculated values are, the purer will be the sample.

1.6.2 Nuclear Magnetic Resonance (NMR) Spectroscopy

Nuclear magnetic resonance spectroscopy is one of the most powerful tools available to the research scientist. It is routinely used to study a variety of nuclei including ^{1}H, ^{13}C, ^{15}N, ^{19}F, and ^{31}P. Since carbon and hydrogen are major components of organic compounds, carbon-13 and proton NMR are most commonly used [W91]. NMR spectroscopy is routinely utilized for structural (chemical) elucidation, the study of chemical exchange and molecular dynamics, structural (three-dimensional) studies (e.g., proteins, DNA), drug design, and, in medicine in magnetic resonance imaging (MRI).

NMR is a phenomenon which arises when the nuclei of certain atoms, whose spin $I \neq 0$, are exposed to an external magnetic field. Because these

nuclei possess a spin angular momentum and an associated magnetic moment, they will align themselves either with the external field (lower energy level) or against the field (higher energy level). In the absence of an applied field, they assume random orientations. Nuclear magnetic resonance is based on these variations in the orientation of the nuclei with reference to the external magnetic field. Since the energy variance between the two spin states is small, a strong external magnetic field (> 14,000 gauss) is required, the stronger the magnetic field, the greater the energy difference [LC77, R86, W91].

In NMR, the transitions between the two energy levels are induced by the absorption of radio frequency radiation. If the correct combination of electromagnetic radiation and external magnetic field strength is applied, the nucleus will "flip" its spin. When this happens, the nucleus is described as being "in resonance" and the energy absorbed is recorded. The resonance frequency is given by, $\nu = \frac{\gamma B_0}{2\pi}$, where ν is the resonance frequency, γ is the gyromagnetic ratio (a constant dependent upon the magnetic moment associated with the nucleus of interest), and B_0 is the magnitude of the applied magnetic field [LC77, R86, W91].

As has been shown, the frequency whereupon a given nucleus attains resonance is proportional to the magnitude of the external field and the nuclear gyromagnetic ratio. A third factor must also be taken into consideration, that of the environment of the nucleus itself. Circulating electrons that generate small magnetic fields in opposition to the applied field surround nuclei in organic compounds. This electron "cloud" partially shields the nucleus from the external

magnetic field so that the effective field at the shielded nucleus is slightly less than that which has been applied. The electron density around each nucleus varies in relation to the sort of nuclei and bonds in the molecule. The opposing field, and therefore the effective field, at each nucleus, even of the same type, will differ in different parts of the molecule. As such, each distinctive nucleus will resonate at a different field. This phenomenon is called the chemical shift (δ), and is measured as the difference (in parts per million) between the resonance frequency of the nucleus and a standard. In ^{1}H-NMR spectroscopy, the standard often used is tetramethylsilane (TMS) [LC77, R86, W91].

1.6.2.1 Dynamic NMR

In general, molecules of the type RNHPic, where Pic = picryl and R ≠ H, undergo intramolecular reorientation, Figure 11, due to hindered internal rotation about the amino-nitrogen picryl-ring-carbon bond [BTW98]. The two spin-bearing nuclei $H_{(A)}$ and $H_{(B)}$ are of the same type, but their magnetic environments are different. In part, this is due to an intramolecular hydrogen bond between the amino proton and one of the two adjacent *ortho*-nitro groups on carbons 2 and 6 of the picryl ring (refer to Figure 5) that causes the *ortho*-nitro groups to be at different orientations relative to the ring. As conformation interchange occurs, $H_{(A)}$ and $H_{(B)}$ exchange magnetic environments and hence ^{1}H-NMR resonance frequencies. Each nucleus will be in each environment (separately) for a mean environmental lifetime (τ) that is a function of temperature and is dependent upon the kinetics of the exchange. As such, the

rate constant of the exchange process ($k_T = \tau^{-1}$) may be extracted from the NMR line shape. Analysis of a series of line shapes at varying temperatures will yield the kinetic parameters of the restricted internal rotation [TW90, BTW98, BNQRWZ99].

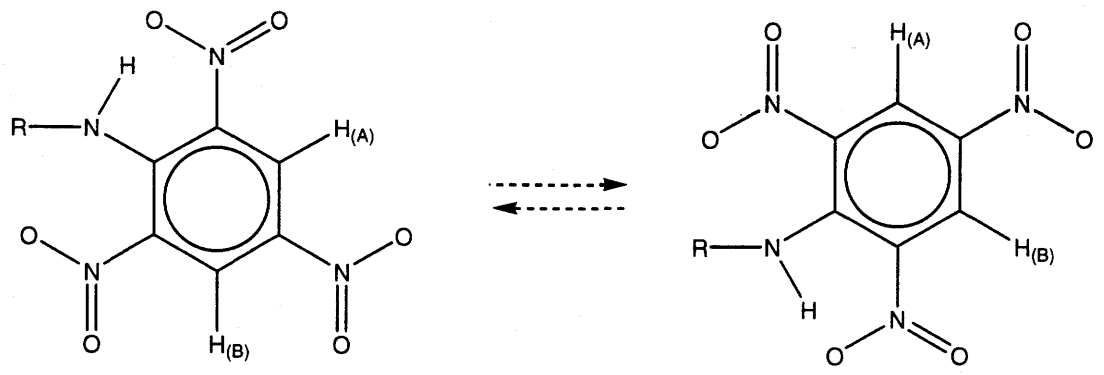

Figure 11: Conformation Interchange for molecules of the type RNHPic

The NMR line shapes of the picryl protons will range from a single sharp peak at high temperature to two doublets at low temperature. These line shapes correspond respectively to a very rapid exchange (short τ) and a very slow exchange (long τ) of magnetic environments. Spectral data (e.g., chemical shift, line widths) taken from a series of line shapes between these two temperatures are used in a computer program such as WINDNMR [RWin97] to simulate those line shapes [TW90, BTW98]. This is done by varying the rate parameter k until a "best-fit-by-eye" match between the simulated and experimental spectra is reached.

Using the simulated rate parameters and the corresponding experimental temperatures, an Arrhenius plot is constructed (the natural logarithm of the rate

parameter k against the reciprocal of absolute temperature T^{-1}) from which the molar activation energy and the frequency factor can be determined (linear-regression analysis). Subsequently, the pseudo-thermodynamic activation kinetic parameters enthalpy, entropy, and Gibbs free energy changes can be calculated [S82]. Gibbs free energy, the parameter least susceptible to systematic errors [TW90], is a measure of the energy required for intramolecular reorientation to take place. From this parameter we may postulate which factors hinder rotation and to what extent. A more comprehensive description of this topic, as well as the previous studies this method is based on, can be found in TW90 and BTW98.

1.6.3 Electron Paramagnetic Resonance (EPR) Spectroscopy

Electron paramagnetic resonance spectroscopy is a form of absorption spectroscopy, in which molecules that contain unpaired electrons absorb microwave radiation. Species that contain unpaired electrons include free radicals, transition complexes, transition-metals ions, lanthanide ions, and triplet-state molecules. EPR is a tool used to gain insight into the identity, structure, and dynamics of paramagnetic compounds.

EPR is analogous in many respects to NMR. In both techniques, an applied external magnetic field causes splitting of spin-degenerate energy levels (the Zeeman effect). The transitions between Zeeman levels are then recorded [G90]. Normally, samples are positioned in a resonating cavity between the poles of a magnet, then irradiated by monochromatic microwave energy, as the

magnetic-field strength is scanned. The microwaves are generated by a klystron tube, a well-known low-noise vacuum tube [WBW94]. Without an applied external field, the unpaired spin of the electron is free to adopt any and all orientations as regards direction in space, with equal probability. When a strong (> 100 gauss) magnetic field **B** is applied to a paramagnetic sample, the unpaired electron's spin will "align" itself either parallel or antiparallel to the magnetic field vector direction, resulting in two distinct energy states (Zeeman levels) of the electron. This occurs because the charge of the electron and spin angular momentum consequently impart a magnetic moment. Transitions between these two discrete energy levels are brought about by irradiation with an electromagnetic beam (the microwaves) that results in an EPR signal. When the energy difference (ΔU) of the two spin states corresponds to the energy of the microwave radiation, absorption (i.e., resonance) occurs. Since the precise magnetic field at which resonance takes place depends upon the environment neighbouring the electrons, valuable information about that environment can be obtained. The energy equation for resonance to occur is: $\Delta U = h\nu = g_e \beta_e B + \ldots$, where $h\nu$ is the microwave energy, g_e is the Zeeman splitting constant for a free electron, β_e is the Bohr magneton, and B is the magnitude of the applied magnetic field that satisfies the condition of resonance [C64, G90, WBW94].

A single unpaired electron has a spin $S = \frac{1}{2}$. When the single electron is located in proximity to a magnetic nucleus of an isotope whose spin $I \neq 0$, it may interact with its neighbour's nuclear-dipole moment. This results in splitting

of the resonance (hyperfine splitting) and gives rise to the EPR spectrum [G90, WBW94].

1.6.3.1 The Hydroxyl Radical

As has been explained (see Section 1.1), the production of ROS/RNS is a normal and important characteristic of aerobic respiration. One of the more biologically important and, chemically, the most reactive species generated is the hydroxyl radical HO•. Hydroxyl radicals are formed in cells as by-products of the consecutive monovalent reduction of dioxygen (•O—O•) in cellular metabolism, and by exposure to ionizing radiation or other agents that generate free radicals. The cytotoxic effects of oxygen in animals, micro-organisms, and plants living in an oxygenic atmosphere is primarily due to HO• [HG99].

The HO• molecule is short-lived and, once formed, indiscriminately attacks all biomolecules in its immediate vicinity, often at diffusion-limited rates – in other words, limited chiefly by how fast HO• can diffuse from its site of generation to a molecule less than a few nanometres away [HG99]. Hydroxyl radicals pass through membranes with ease and cannot be kept out of cells. They react with all types of biologically important molecules (e.g., lipids, nucleic acids, proteins, sugars) and are involved in numerous cellular disorders (e.g., inflammation, cell death) [CS99, HG99].

The HO• molecule is formed as a result of disabling the superoxide anion ($O_2^{\bullet -}$) to hydrogen peroxide (H_2O_2). Termed Fenton chemistry, peroxide readily reacts with ferrous iron (Fe^{2+}) or other transition-metal ions to produce hydroxyl radicals.

$$Fe^{2+} + H_2O_2 \longrightarrow Fe^{3+} + HO\bullet + HO^-.$$

Ferric iron (Fe^{3+}) can be cycled back to ferrous iron through oxidation by $O_2^{\bullet -}$ thereby making available more Fe^{2+} to react with yet another H_2O_2 molecule.

$$Fe^{3+} + O_2^{\bullet -} \longrightarrow Fe^{2+} + O_2.$$

Thus, even trace amounts of transition-metal ions have the potential to generate large quantities of HO•. Combining the above-two reaction schemes gives what is called the iron-catalyzed Haber-Weiss reaction:

$$H_2O_2 + O_2\bullet^- \longrightarrow HO\bullet + HO^- + O_2.$$

Since H_2O_2 and $O_2^{\bullet -}$ are ubiquitously formed from O_2 as by-products of cellular metabolism, they are potentially available in all aerobic cells [CS99].

EPR cannot directly detect radicals such as HO• because they have such relatively short half-lives. As such, the method of spin trapping is employed to stabilize these short-lived molecules allowing for their detection by EPR.

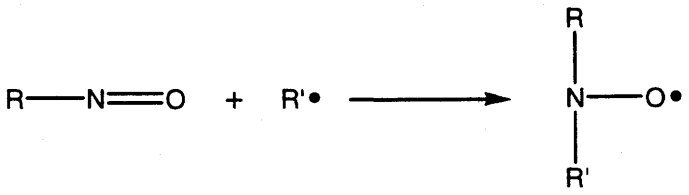

Figure 12a: Spin-adduct due to nitroso spin traps

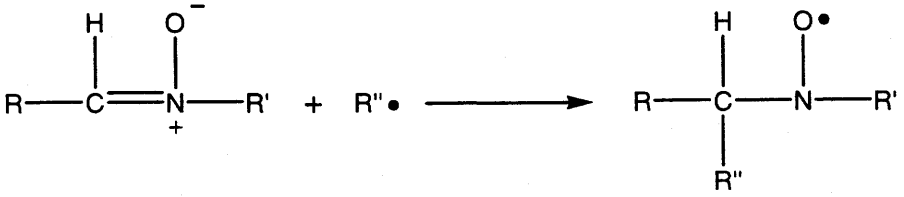

Figure 12b: Spin-adduct due to nitrone spin traps

Basically, spin trapping works by allowing the radical to react with the "trap" to produce a more stable, or long-lived, radical known as a spin adduct. Radical reactions with nitroso and nitrone spin traps most often produce nitroxide radicals (Figure 12a and 12b). However, for oxygen-radical trapping nitrones are more commonly used as they tend to result in more stable spin-adducts than nitroso spin traps. Two examples of nitrone traps are α-phenyl-*tert*-butylnitrone (PBN) and 5,5-dimethylpyrroline-*N*-oxide (DMPO) shown in Figure 13 [KS95, HG99].

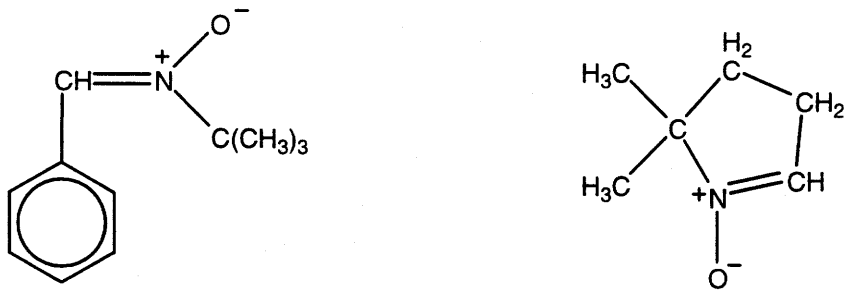

Figure 13: The spin traps PBN (left) and DMPO (right)

1.6.4 X-ray Crystallography

The experimental technique routinely used to determine the three-dimensional structure molecules that range from the large, such as proteins and DNA, to the very small, is single-crystal x-ray diffraction or, in other words, x-ray crystallography. The knowledge of precise molecular structures is a fundamental necessity for drug design and for functional studies, based on structure, that assist in the discovery and development of beneficial therapeutic compounds. The only component required is one "perfect" crystal.

X-ray diffraction from crystals gives us much of our knowledge about the internal structure of crystals – about the intramolecular, as well as intermolecular, angles and distances. Crystals have the ability to diffract x-rays. When x-rays are passed into a crystal, the x-rays are scattered by the interaction with the electrons associated with the atoms or ions that make up the crystal. This scattering gives rise to "diffraction patterns" which are determined by the relative positions and "scattering powers" of each atom or ion in the crystal. The number of electrons in an atom or ion determines the intensity of its diffraction pattern, with heavier species scattering more efficiently. A crystal is aligned in a diffractometer, the diffraction pattern measured, then the crystal is realigned at a new angle and the procedure is repeated several times. These patterns provide the organizational data about the components of the molecule [KMOW98]. Thus, high purity of the crystal is essential for accurate determination of a molecule's structure. The presence of contaminant molecules would interfere with the crystal's "pure" structure (size and geometry) and "contaminate" the overall diffraction pattern.

The math behind the analysis and refinement of this data is highly complex and time-consuming. However, "high-tech" computer software that is freely shared amongst crystallography research groups has made data manipulation much easier. Nonetheless, considerable expertise is still required to operate that software properly and attain meaningful data.

1.7 Hypothesis and Objectives

Numerous diseases that afflict living organisms have been linked to cellular/biomolecular damage caused by reactive nitrogenic and oxygenic species, many of which are free radicals. In response, a stable water-soluble free radical able to react with other free radicals could, in theory, act as a free-radical scavenger *in vivo* and detect, decrease or eliminate harmful free-radical activity. Towards this goal, we propose to synthesize picryl-substituted, water-soluble analogs of the stable free radical $DH_2\bullet$. In order for biomedical use, the end product needs to be free of harmful contaminants (pure).

The objectives of this research are:

- Preparation of picryl-substituted sulfohydrazine salts
    - Substitution at the *ortho* position on the picryl ring
        - Synthesis of the K^+ salt and the H^+ ("acid") form
        - Ample supply and detailed description of synthesis
        - Synthesis of other salts (e.g., Na^+, Li^+, Ag^+, ...)
    - Substitution at the *para* position on the picryl ring
        - Synthesis of the K^+ salt and the H^+ ("acid") form
        - Ample supply and detailed description of synthesis
        - Synthesis of other salts (e.g., Na^+, Li^+, Ag^+, ...)
- Preparation of picryl-substituted sulfohydrazyl salts
    - Substitution at the *ortho* position on the picryl ring
        - Synthesis of the K^+ salt and the H^+ ("acid") form

        - Ample supply and detailed description of synthesis
        - Synthesis of other salts (e.g., Na^+, Li^+, Ag^+, ...)
    - Substitution at the *para* position on the picryl ring
        - Synthesis of the K^+ salt and the H^+ ("acid") form
        - Ample supply and detailed description of synthesis
        - Synthesis of other salts (e.g., Na^+, Li^+, Ag^+, ...)
- Characterization of the compounds synthesized
    - Melting points
    - Elemental analysis
    - Uv-visible light spectroscopy
    - Confirmation of structure and purity by crystallography
    - NMR for the diamagnetic sulfohydrazine salts (spectra and interpretation)
    - EPR for the paramagnetic sulfohydrazyl salts (spectra and interpretation)
- Toxicity studies of the compounds synthesized
- Reactions of the compounds synthesized

2. EXPERIMENTAL

2.1 Materials

Acetone, Fisher Scientific, HPLC grade/uv cut-off 330 nm

Calcium Carbonate, Aldrich Chemical Company, Inc., powder, 99 + %, A.C.S. reagent

Celite 545, diatomaceous earth, FisherChemicals, Fisher Scientific, Fair Lawn NJ, U.S.A., not acid washed

Chloroform, Aldrich Chemical Company, Inc., 99+ % A.C.S. HPLC grade

Chloroform, BDH Inc, A.C.S. reagent

Ortho-chloronitrobenzene, Aldrich Chemical Company, Inc., 99+ %

Para-chloronitrobenzene, Aldrich Chemical Company, Inc., 99 %

Diethyl ether, EM Science, anhydrous ether, absolute, A.C.S. reagent

1,4-Dioxane, Aldrich Chemical Company, Inc., 99 + %, A.C.S. reagent

1,4-Dioxane, Aldrich Chemical Company, Inc., 99.9 % HPLC grade

2,2-Diphenylhydrazine hydrochloride, Aldrich Chemical Company, Inc., 97 %

Dowex® 50WX8-100 ion-exchange resin, Aldrich Chemical Company, Inc., Dowex-50W-hydrogen, strongly acidic resin

95% Ethanol, Commercial Alcohols, Inc.

Fuming sulfuric acid, Aldrich Chemical Company, Inc., A.C.S. reagent, free SO_3 = 18.0 – 24.0 %

Hydrochloric acid, Aldrich Chemical Company, Inc., A.C.S. reagent

4,4'–Methylenebis(N,N-dimethyl)-aniline (Arnold's Base), Aldrich Chemical Company, Inc., 98 %

Nitric acid, BDH Inc., A.C.S. reagent

Nitric acid, red fuming, Alfa Aesar, A.C.S. fuming, 90 % assay

Potassium periodate, Aldrich Chemical Company, Inc., 99+ %

Potassium permanganate, A.C.S. reagent grade

289 Pulp, Schleicher & Schuell, Keene NH, U.S.A., ash-free analytical filter paper

Sodium hydroxide, pellets, BDH Inc.,97 %, analytical reagent

Sodium sulfate, EM Science, anhydrous granular, A.C.S. reagent

Perdeuterated solvents for NMR:

All from Aldrich Chemical Company Inc., Milwaukee WI, U.S.A.:

Acetic-d_3 acid-d, 99.9 atom % D

Acetone-d_6, 100.0 atom % D

Acetonitrile-d_3, 99.95 atom % D

Deuterium oxide, 99.9 atom % D

Dichloromethane-d_2, 99.5 atom % D

Dimethyl-d_6 sulfoxide, 100.0 atom % D

Dimethyl-d_6 sulfoxide, 99.9 atom % D

Methyl-d_3 alcohol-d, 99.95 atom % D

Methyl-d_3 alcohol-d, 99.8 atom % D

Pyridine-d_5, 100.0 atom % D

Tetrahydrofuran-d_8, 99.5 atom % D

Solvents for EPR (not already listed):

From Aldrich Chemical Company Inc., Milwaukee WI, U.S.A.:

Anisole, 99.7 %, anhydrous

Benzaldehyde, redistilled, 99.5 + %

Benzene, 99.9 + %, HPLC grade

Ethyl trichloroacetate, 97 %

N,N-Dimethylformamide, 99.9 + %, HPLC grade

Nitrobenzene, 99 + %

Phenetole, 99 %

Pyridine, 99.8 %, anhydrous

Tetrahydropyran, 99 %, anhydrous

Toluene, 99.8 %, anhydrous

Others:

Acetone, EM Science, Merck KGaA, Darmstadt, Germany, HPLC grade

Acetonitrile, PIERCE, Rockford IL, U.S.A., silylation grade

Water, deionized distilled

2.2 Synthesis and Purification Procedures

The synthetic procedure, gathered from scientific literature published over more than half a century (1891 to 1962) and modified until the end products could be consistently reproduced, is as follows. The details are presented herein.

The modification to $DH_2\bullet$ is at the "picryl" ring, where a nitro group (NO_2), either in the *ortho* or *para* position relative to the hydrazino-nitrogen picryl-ring-carbon bond, is replaced by a sulfo group (SO_3^-). To synthesize the modified picryl ring, we start with chloronitrobenzene, either the *ortho* or *para* form. It is readily available and relatively inexpensive. Chloronitrobenzene has a nitro group which we will keep and a chloride ion, a good leaving group. Sulfonation followed by nitration will add a sulfo group and the second nitro group, respectively. The modified "picryl" ring is then ready to be attached to the diphenylhydrazine backbone by nucleophilic aromatic substitution. Subsequent oxidation of the resultant "sulfo-hydrazine" yields the corresponding "sulfo-hydrazyl".

2.2.1 **Potassium 2-Chloro-3,5-dinitrobenzenesulfonate**

2.2.1.1 Sulfonation of *p*-Chloronitrobenzene

2-Chloro-5-nitrobenzenesulfonic acid was prepared by the sulfonation of *p*-chloronitrobenzene according to the procedure of Fischer [F1891], and Ullmann and Juengel [UJ09]. In a round-bottom flask set in an ice bath, *p*-chloronitrobenzene (8.1 g, 51.3 mmole) was carefully added to fuming H_2SO_4 (20 mL, 0.4 mole H_2SO_4; with 20%, 93.4 mmole SO_3). Once the addition was complete, the flask was removed from the ice bath, heated to and maintained at 160 °C in a glycerol bath, and refluxed with stirring for six (6) hours. It was then left to cool overnight with stirring.

The cooled dark-brownish-red mixture was poured onto approximately 23 g of ice. The resulting dark-brown solid was filtered with suction and washed with a small portion of 6.0 M aqueous HCl. The product was allowed to dry and 13.65 g of the crude acid was recovered. The crude acid was recrystallized in 10% HCl, and 6.8 g (55 %yield) of the pure acid was recovered.

The melting point of the pure acid is 117 – 119 °C. ^{1}H NMR δ in DMSO-d_6 are 8.61 ppm (1H, d), 8.16 ppm (1H, dd), 7.70 ppm (1H, d).

2.2.1.2 Nitration of 2-Chloro-5-nitrobenzenesulfonic Acid

Potassium 2-chloro-3,5-dinitrobenzenesulfonate was prepared according to the procedure of Ullmann *et al.* [UEWKH09]. In a round-bottom flask set in an ice bath, crude 2-chloro-5-nitrobenzene-sulfonic acid (6.0 g, 25.3 mmole) was slowly added to fuming H_2SO_4 (15.0 mL, 0.29 mole H_2SO_4; with 20 %, 0.07 mole SO_3) with stirring. In a separate flask also on ice, fuming H_2SO_4 (4.2 mL, 0.08 mole H_2SO_4; with 20 %, 0.02 mole SO_3) was added drop-wise to HNO_3 (4.2 mL, 0.095 mole). The mixture was then added drop-wise to the round-bottom flask. The round-bottom flask was transferred to a glycerol bath and the temperature was slowly raised to 96 °C with stirring. After 5 hours, the heat was removed and the solution was allowed to cool overnight.

The cooled pale-yellow solution was poured onto approximately 110g ice. An aqueous, saturated KCl solution (45 mL) was added to the mixture and potassium 2-chloro-3,5-dinitrobenzenesulfonate precipitated out of solution. The shiny white crystals were vacuum-filtered, washed with ice-cold saturated (aq) KCl, then with a small amount of ice-cold distilled H_2O and set aside to dry. The yield was 96 % (3.9 g).

The solid does not melt below 300 °C but a colour change begins at 285 °C. ^1H NMR δ in DMSO-d_6 are 8.91 ppm (1H, d), 8.78 ppm (1H, d).

2.2.2 Potassium 4-Chloro-3,5-dinitrobenzenesulfonate

Potassium 4-chloro-3,5-dinitrobenzenesulfonate was prepared as follows, according to the procedure of Rabinowitz and Wagner [RW51]. In a round bottom flask set in an ice bath, fuming H_2SO_4 (20.0 mL, with 20 %, 0.09 mole SO_3) was added drop-wise to *o*-chloronitrobenzene (7.878 g, 0.05 mole) with stirring. The flask was removed from the ice bath, allowed to sit at room temperature for 20 minutes, then transferred to a glycerol bath that had been preheated to 100 °C. The flask was refluxed with stirring for two (2) hours, then removed from heat, placed back in an ice bath, and chilled well.

In a separate flask, also set in an ice bath, fuming H_2SO_4 (6.0 mL, with 20 % SO_3) was added to red fuming HNO_3 (6.0 mL). Upon completion, the mixture was slowly added to the above chilled solution while still on ice. Additional fuming H_2SO_4 (5.5 mL, with 20% SO_3) was then added drop-wise. The mixture was removed from the ice bath and allowed to sit at room temperature for one hour. It was then placed in a preheated glycerol bath (100 °C) and refluxed with stirring for sixteen (16) hours. The solution was removed from the heat, chilled in an ice bath then poured over approximately 150 g crushed ice to quench the reaction.

An aqueous KCl solution (15 mL, 4.0 M) was added to the mixture and potassium 4-chloro-3,5-dinitrobenzenesulfonate precipitated out of solution. The shiny white crystals were vacuum-filtered, washed with ice-cold (aq) KCl and set on a watchglass to dry. The yield was 87 % (13.94 g). The solid begins to decompose at 290 °C. ^{1}H NMR δ in DMSO-d_6 is 8.45 ppm (2H, s).

2.2.3 1,1-Diphenylhydrazinium 2,2-Diphenyl-1-(2,6-dinitro-4-sulfo)phenyl Hydrazine (DPH-DP4SH)

DPH-DP4SH was prepared according to the procedure that Ikrina and Matevosyan [IM62] used to produce 2,2-diphenyl-1-(2,6-dinitro-4-sulfophenyl) hydrazine, as follows: potassium 4-chloro-3,5-dinitrobenzene-sulfonate (8.00 mmole) was added to 25.00 mL of distilled H_2O in a round-bottom flask along with a magnetic stir bar. The round-bottom flask was attached to a reflux condenser and set in a glycerol bath. The mixture was refluxed in air with stirring while the glycerol bath temperature was gently raised to 100 °C. IM62 used "the boiling water bath"; the use of an oil bath at 100 °C reproduced the necessary reaction temperature. As the temperature of the oil bath approached 70 °C, the solid dissolved to give a light-yellow solution. 1,1-Diphenylhydrazine (24.00 mmole) was added to 100.00 mL 95 % ethanol, mixed and then added to the hot solution. IM62 refers simply to "alcohol". The reaction was refluxed with stirring for 10 hours while the temperature of the glycerol bath was maintained at 100 °C. The heat was then reduced to the lowest setting and the mixture was cooled overnight. The cooled reaction mixture was removed from the glycerol bath, rotary-evaporated to almost dryness, and the product extracted with excess chloroform (reagent grade, not dried). The resultant mixture was filtered and the solution rotary-evaporated to dryness. IM62 removed the solvent by distillation.

The product was crystallized from hot 95 % ethanol. The resultant bright-orange needle-like crystals were vacuum-filtered, rinsed with ice-cold 95 % ethanol, set on a watchglass to dry, and placed on the lab bench away from direct light. The yield was 29 %. The solid decomposes at 157-159 °C. No literature melting point is available for this product. However, IM62 reported a melting point (decomposition) of 161-162 °C for the product that was obtained from the synthetic procedure that was followed.

2.2.4 Potassium 2,2-Diphenyl-1-(2,6-dinitro-4-sulfo)phenyl Hydrazine (K-DP4SH)

K-DP4SH was prepared according to the procedure of Ikrina and Matevosyan [IM62], as follows: potassium 4-chloro-3,5-dinitrobenzenesulfonate (11.00 mmole) was added to 20.00 mL of distilled H_2O in a round-bottom flask equipped with a magnetic stir bar. The round-bottom flask was attached to a reflux condenser and set in a glycerol bath. The mixture was refluxed in air with stirring while the glycerol bath temperature was raised to 100 °C. IM62 used "the boiling water bath"; the use of an oil bath at 100 °C reproduced the suggested reaction temperature. As the temperature of the oil bath approached 70 °C, the solid dissolved to give a light-yellow solution.

1,1-Diphenylhydrazine (25.00 mmole) was added to 20.00 mL of 1,4-dioxane (reagent grade), mixed, and added to the hot solution. To this mixture were added 25.00 mmole calcium carbonate (substituted for chalk [IM62]). The reaction was allowed to reflux with stirring for 24 hours while the temperature of the glycerol bath was maintained at 100 °C. The reaction mixture was then removed from the glycerol bath and immediately gravity-filtered while hot to remove the calcium carbonate. The filtered solution was set aside to recrystallize. The dark-red needle-like crystals of K-DP4SH that evolved were filtered off, rinsed with chilled dioxane, and set on a watchglass to dry. The yield was 29 %. The solid decomposes at 160 - 165.5 °C.

In order to improve the crystal quality for x-ray diffraction studies, K-DP4SH was further purified in two separate procedures. K-DP4SH was dissolved in minimal amounts of either hot distilled H_2O or hot 95% (aq) dioxane. In order to prolong the cooling time (as opposed to sitting out at room temperature) each solution was placed in separate preheated Dewar flasks. The Dewar flasks were capped and K-DP4SH was allowed to slowly recrystallize from each solution.

Dirty-yellow quartz-like crystals of K-DP4SH evolved from H_2O. The solid decomposed at 173.5-175 °C. IM62 reported a melting point (decomposition) of 225-227 °C for K-DP4SH recrystallized from water. The crystals were not suitable for x-ray diffraction, but the calculated CHN composition for K-DP4SH • H_2O compares well with the CHN composition found experimentally (see Section 3.2).

Bright orange/red needle-like crystals of K-DP4SH suitable for x-ray diffraction studies evolved from 95% dioxane (see Section 3.3). The solid decomposes at 178-179 °C. IM62 reported a melting point (decomposition) of 209-210 °C for K-DP4SH recrystallized from dioxane.

2.2.5 Potassium 2,2-Diphenyl-1-(2,4-dinitro-6-sulfo)phenyl Hydrazine (K-DP6SH)

K-DP6SH was prepared according to the procedure of Ikrina and Matevosyan [IM62], as follows: potassium 2-chloro-3,5-dinitrobenzene sulfonate (11.00 mmole) was added to 20.00 mL of distilled H_2O in a round-bottom flask equipped with a magnetic stir bar. The round-bottom flask was attached to a reflux condenser and set in a glycerol bath. The mixture was refluxed in air with stirring while the glycerol bath temperature was raised to 100 °C. IM62 used "the boiling water bath"; the use of an oil bath at 100 °C reproduced the required reaction temperature. As the temperature of the oil bath approached 70 °C, the solid dissolved to give a light-yellow solution.

To this mixture were added 22.00 mmole anhydrous calcium carbonate (substitute used for chalk [IM62]). 1,1-Diphenylhydrazine (22.00 mmole) was mixed with 20.00 mL of 1,4-dioxane (reagent grade) and added to the above solution. The reaction solution was allowed to reflux with stirring for 24 hours while the temperature of the glycerol bath was maintained at 100 °C. The reaction mixture was then removed from the glycerol bath and immediately gravity-filtered while hot to remove the calcium carbonate.

Unlike K-DP4SH, K-DP6SH did not crystallize from the filtered and cooled reaction mixture as reported by IM62. After cooling, the reaction mixture needed to be rotary-evaporated to force the solid product out of solution (super-saturation). The dark-red/orange powder of the potassium salt was isolated by

vacuum-filtration, rinsed with chilled 1,4-dioxane, set on a watchglass to dry, and placed on the lab bench away from direct light. The yield was 45 %. The solid decomposes at 183 – 189 °C.

K-DP6SH was purified further by slow recrystallization from distilled H_2O. K-DP6SH was dissolved in the minimum amount of hot solvent. The solution was then placed in a preheated Dewar flask, capped, and allowed to slowly cool, in air. Dark red/burgundy-coloured, shiny needle-like crystals suitable for x-ray diffraction evolved (see Section 3.3). The solid decomposes at 192-193.5 °C. IM62 reported a melting point (decomposition) of 187-188 °C for K-DP6SH recrstallized from water.

2.2.6 1,1-Diphenylhydrazinium 2,2-Diphenyl-1-(2,6-dinitro-4-sulfo)phenyl Hydrazyl (DPH-DP4SH•)

DPH-DP4SH• was prepared according to the procedure Ikrina and Matevosyan [IM62] used to synthesize 2,2-diphenyl-1-(2,6-dinitro-4-sulfophenyl) hydrazyl as follows. The reaction was carried out in the absence of overhead fluorescent lighting and in the dark as much as possible. DPH-DP4SH (2.5 mmole) was dissolved in 250.00 mL chloroform (HPLC grade) with stirring. An excess of MnO_2 (two to three times the mass of the hydrazine), and an approximately equal mass of anhydrous Na_2SO_4, were then added and the solution was allowed to oxidize with stirring for 90 minutes. IM62 used PbO_2 as the oxidizing agent and allowed the oxidation to proceed for two hours.

The dark-purple reaction mixture was vigorously filtered (twice) to separate the radical solution from the Na_2SO_4 and unreacted MnO_2. The filtered reaction solution was rotary-evaporated to approximately $\frac{1}{8}^{th}$ of its initial volume. The dark-purple solution was treated with excess diethyl ether (≈ 500 mL) and DPH-DP4SH• was forced out of solution. The black-purple precipitate was then separated from the solution by vacuum-filtration, rinsed with diethyl ether, and set in the cupboard on a watchglass to dry. It takes repeated precipitation from chloroform solution by diethyl ether to purify the free radical. The yield was 53 %. The solid decomposes at 173.5 – 176 °C. No literature melting point is available for this product. However, the product of this synthetic procedure reported by IM62 changed at 120 °C and vigorously decomposed at 157 °C.

2.2.7 **Potassium 2,2-Diphenyl-1-(2,6-dinitro-4-sulfo)phenyl Hydrazyl (K-DP4SH•)**

K-DP4SH• was prepared according to the procedure of Ikrina and Matevosyan [IM62], as follows. The reaction was carried out in the absence of overhead fluorescent lighting and in the dark as much as possible. In an Erlenmeyer flask equipped with a magnetic stir bar, 3.2 mmole of K-DP4SH were dissolved in 125 mL acetone at room temperature. An excess of MnO_2 (two to three times the mass of K-DP4SH) was then added and the solution was allowed to oxidize with stirring for two hours. IM62 used dioxane as the solvent and PbO_2 as the oxidizing agent. They also initially heated the solution and allowed the oxidation to proceed over three hours as it cooled.

The blue/purple reaction mixture was vigorously filtered (twice) to separate the radical solution from unreacted MnO_2. The filtered reaction solution was rotary-evaporated to approximately $\frac{1}{8}^{th}$ of its initial volume. The dark-purple solution was treated with excess diethyl ether (≈ 500 mL) and K-DP4SH• was forced out of solution. The dark-purple precipitate was then separated from solution by vacuum-filtration, rinsed with diethyl ether, and set in the cupboard on a watchglass to dry. It takes repeated precipitation from acetone solution by diethyl ether to purify the free radical. The yield was 74 %. The solid decomposes at 195 – 197 °C. IM62 reported a change in product at 110 °C, and vigorous decomposition at 120 °C.

2.2.8 Potassium 2,2-Diphenyl-1-(2,4-dinitro-6-sulfo)phenyl Hydrazyl (K-DP6SH•)

K-DP6SH• was prepared according to the procedure of Ikrina and Matevosyan [IM62], as follows. The reaction was carried out in the absence of overhead fluorescent lighting and in the dark when possible. In an Erlenmeyer flask equipped with a magnetic stir bar, K-DP6SH (2.15 mmole) was dissolved in 50 mL of a 1:1 (by volume) mixture of 1,4-dioxane (HPLC grade, not dried) and distilled H_2O at room temperature with stirring. An excess of MnO_2 (two to three times the mass of K-DP6SH) was then added and the solution was allowed to oxidize with stirring for one hour. IM62 used dioxane alone as the solvent and initially heated the solution. As well, PbO_2 was used as the oxidizing agent, and the oxidation proceeded over two hours as the solution cooled.

The red/purple reaction mixture was vigorously filtered (twice) to separate the radical solution from unreacted MnO_2. The filtered reaction solution was rotary-evaporated to dryness. The residue was dissolved in a minimal amount of 97 % (aq) dioxane. The dark-purple solution was treated with excess diethyl ether (≈ 600 mL) and K-DP6SH• was forced out of solution. More diethyl ether is required for the *ortho* salt than for the two *para* salts. If an insufficient amount is used, the K-DP6SH• sticks to the walls of the flask. The dark-red/purple precipitate was then separated from solution by vacuum-filtration, washed with diethyl ether, and set in the cupboard on a watchglass to dry. It takes repeated precipitation from 97 % (aq) dioxane solution by diethyl ether to purify the free

radical. The yield was 62 %. The solid decomposes at 201 – 203 °C. IM62 reported a change in product at 115 °C and rigorous decomposition at 155 °C.

2.2.9 **1,1-Diphenylhydrazine (DPH)**

1,1-Diphenyl hydrazine was prepared according to the procedure of Arbuzov and Valitova [AV57], as follows:

1,1-Diphenylhydrazine hydrochloride (20.05 g, 0.09 mole) was treated with 60.0 mL of warm 25 % (aq) sodium hydroxide solution. The mixture was stirred for one hour at low heat allowing most of the base (dirty blue curds) to float to the top. The mixture was transferred to a separatory funnel and the oily mixture was extracted with 3 x 50 mL portions of diethyl ether. The combined diethyl ether portions were transferred to a clean separatory funnel and washed with 50 mL portions of distilled H_2O until the aqueous layer was neutral to litmus (no alkaline reaction). The washed ether extract was dried over sodium sulfate and filtered. The solvent was removed by rotary evaporation to give 1,1-diphenylhydrazine. The resultant liquid product was used without further purification. The yield was 86 %.

2.2.10 **Manganese Dioxide (MnO_2)**

MnO_2 was prepared according to the procedure of McKenzie [M71], as follows. In a large Erlenmeyer flask (4 L) equipped with a large magnetic stir bar, 1.0 mol (≅158 g) $KMnO_4$ was dissolved in 2½ L distilled, deionized H_2O. In the fume hood, the mixture was slowly heated with stirring to almost the boiling point.

Gradually, drop-wise with stirring, 2 mol (≅ 200 g or 170 mL) concentrated HCl were added to the hot solution. There was no colour change. However, chlorine gas evolved from the mixture and bubbled out of solution, thereby necessitating the procedure to be performed in the fume hood. Once the HCl had been added (after ≅ 15 minutes), the mixture was stirred for an additional 10 minutes. It was then cooled overnight in the fume hood.

The solid MnO_2 was separated from solution by vacuum-filtration using a 0.1 μm nitrocellulose filter. The chocolate-brown solid was washed with distilled deionized water until the filtrate gave a negative response to a 10 % (aq) silver nitrate solution (precipitation of white silver chloride did not occur). This is a very lengthy procedure and it took about five days to rinse clean the very large amount of solid obtained.

The solid was placed on watchglasses and set in the cupboard, away from light but in air, to dry. It was then pulverized with mortar and pestle, placed in brown-glass bottles, and stored in the dark.

2.3 Inorganic Component Assays

2.3.1 Potassium Assay

2.3.1.1 Sodium Tetraphenylboron

In neutral solutions or in the presence of acetic acid, potassium forms a white solid complex upon the addition of sodium tetraphenylboron $Na[B(C_6H_5)_4]$. An arrow (↓) in the following reactions indicates the formation of a precipitate.

$$K^+ + [B(C_6H_5)_4]^- \longrightarrow K[B(C_6H_5)_4] \downarrow$$

The precipitate is mostly insoluble in water but soluble in acetone and in strong acids and bases. Ammonium, caesium, rubidium and thallium(I) ions will interfere with the assay [S79].

Preparation of the reagent entails dissolving 3.42 g of sodium tetraphenylboron in water (distilled) and then dilution to 100 mL giving a solution of approximately 0.1 M. If the solution is cloudy, it must be filtered. The solution can be kept for up to two weeks [S79].

2.3.2 Manganese(II) Assay

2.3.2.1 Arnold's Base

A solution of Arnold's base (tetramethyl-diamino-diphenylmethane) in chloroform is employed as a sensitive assay to detect small amounts of manganese as permanganic acid, which oxidizes Arnold's base to an intensely blue colour. Permanganic acid is formed by the addition of saturated (aq) potassium periodate, KIO_4 [S79].

$$2\ Mn^{2+} + 5\ IO_4^- + 3\ H_2O \longrightarrow 2\ MnO_4^- + 5\ IO_3^- + 6\ H^+$$

A drop of the sample in solution is placed on a spot plate. Next one drop of saturated (aq) potassium periodate and two drops of Arnold's base in chloroform (1 % solution) are added. A deep-blue colour will form in the presence of Mn(II) [S79].

2.3.2.2 Sodium Hydroxide Solution

Addition of sodium hydroxide (NaOH) solution to manganese(II) compounds initially results in a white precipitate of manganese(II) hydroxide, which is insoluble in excess reagent.

$$Mn^{2+} + 2\ OH^- \longrightarrow Mn(OH)_2 \downarrow$$

On exposure to air, the precipitate quickly oxidizes and turns brown as hydrated manganese dioxide, $MnO(OH)_2$, is produced [S79].

$$Mn(OH)_2 \downarrow + O_2 + H_2O \longrightarrow MnO(OH)_2 \downarrow + 2\ OH^-$$

2.4 NMR Instrumentation

The 300 MHz NMR spectra were obtained on a Bruker AMX 300 spectrometer (Bruker Analytik GmbH, Rheinstetten, Germany) and the data was processed with the accompanying software, UXNMR version 970101.3.

The 500 MHz spectra were obtained on a Bruker Avance 500 spectrometer (Bruker Analytik GmbH, Rheinstetten, Germany) with a Spectrospin Ultra Shield magnet system. The accompanying software packages XWINNMR and XWINPLOT version 2.0 were used to process the

data and plot the spectra. Temperature control for the low temperature 500 MHz spectra was accomplished with the Bruker Variable Temperature Unit, BVT3000.

NMR samples were prepared using perdeuterated solvents. For storage, solvents were added to appropriate molecular sieves and placed in a dessicator with Drierite. Perdeuterated solvents used in the pseudothermodynamic experiments (see Sections 1.6.2.1 and 3.5) were of the highest purity available and were used immediately upon opening. NMR experiments were carried out using 5 mm o.d. NMR sample tubes from Wilmad Labglass, Buena NJ, U.S.A.. All experiments were carried out in air.

2.5 EPR Instrumentation

The electron paramagnetic resonance studies were performed using a modified Bruker ESP-300 X-band field-swept spectrometer (resonant frequency ca. 9.5 GHz) equipped with a Bruker ER-4107 WZ high-sensitivity resonator (Bruker, Karlsruhe, Germany). EPR investigations of in-air solutions were carried out in small-diameter (1 mm i.d.) glass capillary tubes supplied by Kimble Products. For ease of positioning in the spectrometer, these tubes were placed inside larger (3 mm i.d.) quartz tubes. For solutions from which dissolved di-oxygen was to be removed, pyrex sample tubes (~1 mm i.d) were custom-made (by Mr. Rick Elvin) for attachment to a vacuum system. In such experiments, each solution was degassed at pressures between 10^{-3} and 10^{-5} mbar for at least six freeze-pump-thaw cycles, before being sealed under vacuum

conditions. Mr. David F. Howarth prepared all the degassed samples. Unless stated otherwise, all EPR measurements were made at room temperature.

Most of the solvents were obtained from Aldrich Chemicals and most classified as having high-pressure liquid chromatography (HPLC) purity. When HPLC-grade solvents were unavailable, either spectroscopic grade or those classified with purity greater than 99 % were used. Where required, solvents were further dried as prescribed [LLP99] Tetrahydrofuran and dimethyl-formamide were distilled prior to use. The usual concentrations of the salt solutions used in the EPR studies were estimated to be 10^{-3} M. More dilute solutions (~10^{-5} M) were used in certain experiments to further reduce inter-molecular electron-spin exchange. All solutions were shielded from bright light.

EPR data collection was achieved with software supplied by Bruker. Appropriate calibration procedures were followed to ensure at least six-digit accuracy in both the microwave frequencies and the magnetic-field values. The spectra were analyzed and plotted by using the WINEPR, version 2.11, software supplied by Bruker. Mr. D.F. Howarth performed the EPR spectral simulations, from which the EPR parameters were then obtained, for the sulfo-hydrazyl salts using the computer program EPR-NMR [MW2001]. An analytical procedure was developed by Dr. Z. Zimpel to automate the spectral-fitting process and to obtain an estimation of the "quality" of each simulated spectrum.

2.6 Elemental Analysis Instrumentation

Elemental analyses were performed by Mr. Ken Thoms using a Perkin Elmer 2400 CHN Elemental Analyzer (1987) from Perkin Elmer, Instrument Division, Norwalk, CT, U.S.A.. Samples were dried under vacuum for approximately 12 hours then stored over phosphorous pentoxide in a glass dessicator.

2.7 Crystallography Instrumentation

The x-ray diffraction data sets for the potassium salts were obtained by Dr. Bob MacDonald, Department of Chemistry, University of Alberta, Edmonton, Alberta, using a Bruker (1997) SMART/CCD X-ray diffractometer with the SAINT data processing program, Bruker AXS Inc., Madison, Wisconsin, USA.

The structures were solved and refined by Dr. J. Wilson Quail, Department of Chemistry, University of Saskatchewan, Saskatoon, Saskatchewan using SHELXLS97 [S97a] to solve the structures and SHELXL97 [S97a] to refine the structures.

The x-ray diffraction data for the diphenylhydrazinium salt was obtained by Dr. J. Wilson Quail using a Nonius CAD4 X-ray diffractometer, with the CAD-4 EXPRESS [EN92] data acquisition program. Data were processed (by Dr. Quail) with Xtal 3.7 [HBO2000]. The structure was solved with SHELXLS97 [S97a] and refined with SHELXL97 [S97a] (by Dr. Quail.)

Crystals of the pure sulfo-hydrazines were dried under vacuum then over phosphorous pentoxide prior to their analysis.

2.8 Ultraviolet-visible Spectroscopy Instrumentation

The ultraviolet-visible light spectra were obtained using a Beckman Coulter DU 640 spectrophotometer, Beckman Instruments Inc., Fullerton CA, U.S.A.. The data was processed using MS Excel 2000 for the PC. Standard rectangular UV/semi-micro optical-glass cuvettes (spectrophotometer cells) with a 10 mm light path length were used. The cuvettes were purchased from VWR Scientific Products, West Chester, PA, U.S.A..

2.9 External Testing of the Sulfo- Hydrazines and Hydrazyls

2.9.1 National Institute of Neurological Disorders and Stroke

National Institute of Neurological Disorders and Stroke
Preclinical Pharmacology Section, Epilepsy Branch
Division of Convulsive, Infectious and Immune Disorders
Rockville, MD, U.S.A.

The compounds will be evaluated for pathological symptoms and neurotoxicity in mice as well as in rats. MES (maximal electroshock seizures) and scPTZ (convulsions induced by the subcutaneous administration of pentylenetetrazole) screens will be used to evaluate the compounds for anticonvulsant activity, which is a good indicator of the compounds' ability to penetrate the central nervous system.

2.9.2 **Rega Institute for Medical Research**

Rega Institute for Medical Research

Laboratory of Experimental Chemotherapy

Leuven, BELGIUM

The compounds will be evaluated towards murine L1210, human Molt 4/C8, and CEM T-lymphocyte cells for antineoplastic activity. The compounds will also be examined to determine if they are, themselves, cytotoxic.

3. RESULTS AND DISCUSSION

3.1 The Synthetic Procedures

The general forms of the *ortho* and *para* sulfonated diphenylpicryl hydrazines and hydrazyls are shown in Figures 14 and 15. The potassium salts of both the *ortho* and *para* versions of the sulfonated hydrazines and hydrazyls have been synthesized. An unexpected diphenylhydrazinium (DPH^+) salt, in lieu of the protonated acid (H^+), form that had been the goal, has also been synthesized. The cation is shown in Figure 16. Only the *para* DPH^+ salt of

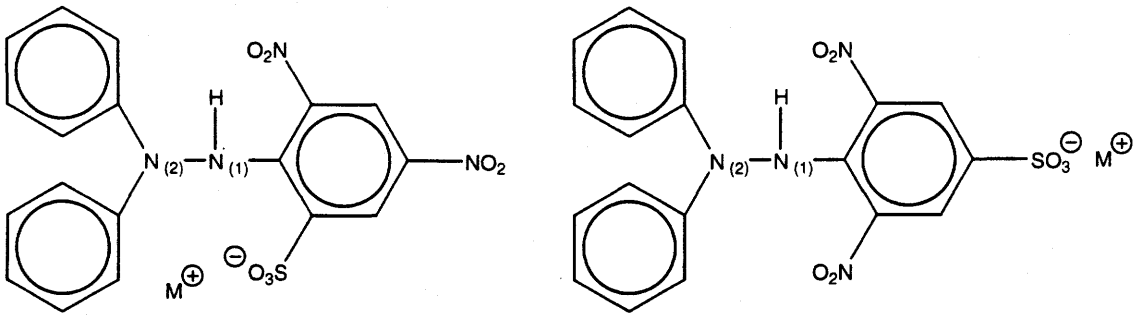

Figure 14: The sulfonated diphenylpicryl hydrazines (where $M^+ = K^+, DPH^+, Na^+, Li^+$, etc.)

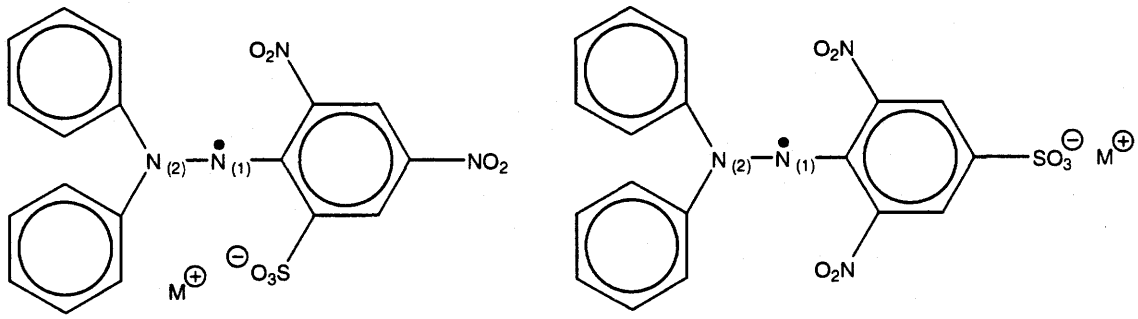

Figure 15: The sulfonated diphenylpicryl hydrazyls (where $M^+ = K^+, DPH^+, Na^+, Li^+$, etc.)

the sulfonated hydrazine and corresponding hydrazyl have been prepared. Attempts at synthesizing the *ortho* DPH^+ salt in an analogous synthetic procedure have not been successful.

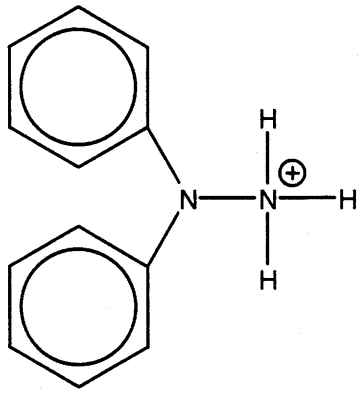

Figure 16: The 1,1-diphenylhydrazinium cation

Synthesis of the *para*-sulfo diphenylpicryl hydrazine salts [IM62]

The reaction schemes for the synthesis of the *para* sulfonated salts are shown in Figure 17. The reactions are sensitive to the solvent ratios. Optimal volume ratios are: H_2O : 1,4-dioxane at 1:1 (for the K^+ salt) and H_2O : 95 % ethanol at 1:4 (for the DPH^+ salt). In the synthesis of K-DP4SH, it seems that the calcium carbonate, used as a substitute for chalk, should be added to the reaction solution before the DPH:dioxane mixture (see Section 2.2.4). When added after, recrystallization did not occur. For the synthesis of all the sulfonated picryl hydrazine salts (both *ortho* and *para*), an oil bath heated to ≈ 100 °C was used in lieu of a water bath.

The ^1H NMR spectra of K-DP4SH crystals that evolved from the reaction mixture revealed no impurities except those associated with solvent molecules

trapped in the crystal matrix, in this case, dioxane. When the crystals were powdered, the intensity (area under the curve) of the solvent peak (dioxane) was markedly decreased. ^{1}H NMR spectra of DPH-DP4SH showed no such solvent peak(s). An apparent "double set" of diphenyl proton peaks was our first clue as to the nature of the synthesized salt. As already stated, the objective of that reaction had been the synthesis of the "acid" form of the sulfonated picryl hydrazine as reported in the literature [IM62]. Since subsequent repetition of the synthetic procedure has always resulted in the DPH^+ salt, we assume the authors of the synthesis may have been mistaken in the identification of their product.

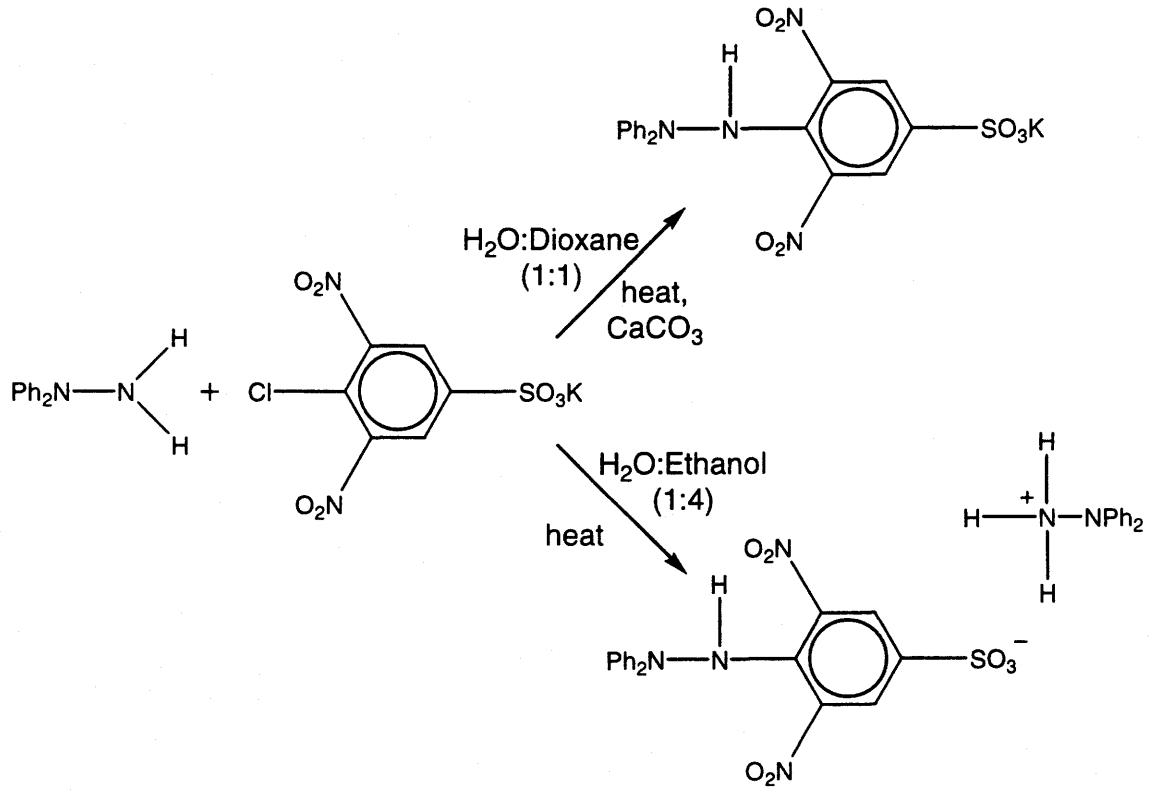

Figure 17: Synthesis of the *para* sulfonated diphenylpicryl hydrazine salts

Synthesis of the *ortho*-sulfo diphenylpicryl hydrazine salt [IM62]

The reaction scheme for the synthesis of the *ortho* sulfonated salt is shown in Figure 18. As with the *para*-hydrazines, the ratio of solvent volumes is crucial and must be maintained (H_2O : 1,4-dioxane at 1:1). However, in this synthesis, it seems that the calcium carbonate must be added to the reaction solution after the DPH:dioxane mixture (see Section 2.2.5). When added before, recrystallization did not occur. The mass ratio of ortho-sulfonate to DPH had to be reduced from 1:2.5 to 1:2.0 to make the reaction work. This greatly facilitated the separation of product from any remaining DPH.

The ^1H NMR spectra of K-DP6SH crystals (evolved from the reaction mixture) dissolved in perdeuterated DMSO (dimethylsulfoxide) revealed no impurities except those associated with solvent (water) trapped in the crystal matrix. When the crystals are powdered, the intensity (area under the curve) of the water peak was markedly decreased.

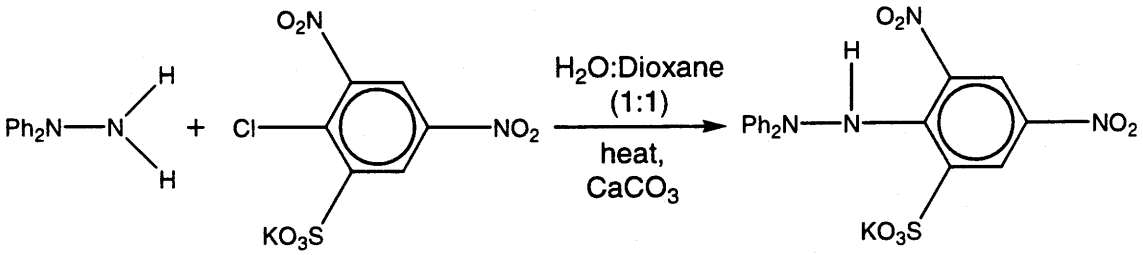

Figure 18: Synthesis of the *ortho* sulfonated diphenylpicryl hydrazine salt

The synthesis of both potassium salts is identical save for the starting potassium chloro-sulfonate (4-chloro-3,5-dinitrobenzenesulfonate for the *para* version, 2-chloro-3,5-dinitrobenzenesulfonate for the *ortho* version). Both

procedures are detailed in the literature [IM62]. However, while the synthesis is given for the protonated H^+ *para* hydrazine sulfonate, no details are given for an analogous synthesis of the *ortho* form, nor is it reported to have been produced. Nevertheless, we attempted to synthesize the H^+ (or DPH^+) salt of the *ortho* picryl hydrazine in a procedure identical (except for the starting chloro-sulfonates) to that given for the protonated *para* "salt". Neither the H^+ nor the DPH^+ salt was produced by this synthesis. The proton NMR spectra of the reaction solution revealed that the end result was mostly a mix of the starting materials and the solvents used in the synthesis.

For attempts at producing sodium salts of the sulfonated hydrazines and hydrazyls, sodium salts of 2-chloro- and 4-chloro- 3,5-dinitrobenzenesulfonate were synthesized by replacing KCl with NaCl. Then in procedures analogous to those used to produce the potassium salts, we tried to synthesize the corresponding sodium salts. We were able to obtain a very crude sodium salt of the *ortho* sulfonated diphenylpicryl hydrazine (reported to have been analyzed by Jarrett [J53]) however, the *para* synthesis was unsuccessful. The crude sodium *ortho* sulfonated hydrazine was oxidized to the corresponding hydrazyl by addition of MnO_2, water, and dioxane. Although obtained in solution, the sodium *ortho* sulfonated hydrazyl decomposed (reduced) during removal of the solvent by rotary evaporation and could not be isolated in "solid" form. The synthesis of the sodium salt was inconsistent, and requires further adjustment to improve repeatability and to obtain a pure salt.

Crystals for x-ray crystallography

Appropriate crystals (for x-ray diffraction) of DPH-DP4SH evolved easily from a hot 95 % (aq.) ethanol solution set aside at room temperature to cool (see Section 2.2.3). While the potassium salts in their respective crystallization solutions (hot dioxane for the *para* salt, hot distilled H_2O for the *ortho* salt) evolved crystals upon cooling at room temperature, the crystals were either too small or too disordered to be adequate for x-ray diffraction. However, when the cooling process was slowed down, well-ordered and suitable crystals evolved for each of the potassium-sulfonated hydrazines out of their respective solvent systems. As such, thanks to Dr. J. Wilson Quail who obtained the x-ray diffraction data, processed them, and refined them, we have the crystal structures of DPH-DP4SH, K-DP4SH, and K-DP6SH (see Section 3.3).

Synthesis of the sulfonated diphenylpicryl hydrazyl salts [IM62]

Rather than using the oxidant lead dioxide as prescribed in the literature [IM62], we used manganese dioxide to oxidize the sulfonated picryl hydrazine salts to their corresponding hydrazyls. In fact, when oxidation by PbO_2 of any of the precursor salts was attempted, the reactions were unsuccessful and the hydrazyls were not synthesized. On the other hand, when using PbO_2 from the same batch, oxidation of DH_2-H to DH_2• proceeded rapidly. It should be noted that the PbO_2 was a few years old and a newer batch may have the oxidizing power to synthesize the sulfonated hydrazyls.

Besides change in the oxidant, some of the solvent systems were also altered. DPH-DP4SH was oxidized to DPH-DP4SH• in a like manner (chloroform and sodium sulfate, both anhydrous) as that prescribed in the literature [IM62] for the oxidation of "H-DP4SH" to "H-DP4SH•", the reported "protonated" salts of the *para* sulfonated picryl hydrazine and hydrazyl. In the literature [IM62], both the *ortho* and *para* potassium salts, in analogous procedures, are oxidized in dioxane. The solution is heated prior to addition of the oxidant, then allowed to cool during the oxidation. For the potassium salts, we found that, when using MnO_2, oxidation did not occur if the solvent was only dioxane. However when a small amount of water was added, oxidation did take place but the compounds were unstable, hard to isolate, and reaction solutions quickly decomposed (in a matter of hours). We also tried 100 % water, but that led to no oxidation. As such, we determined that the best solvent system for the oxidation of the *ortho* potassium salt was water and dioxane in a one-to-one ratio by volume. The *para* salt can also be oxidized in a like manner, but it was determined that a better product is synthesized by using acetone as the solvent of oxidation. We also found that heating was unnecessary to the success of the oxidations.

Since we hope to use these stable water-soluble free radicals for biomedical applications, it is very important that they be "ultra pure" (free from harmful contaminants). Early batches of the sulfonated diphenylpicryl hydrazyls were found to contain manganese (CHN analysis, manganese (II) assay, melting points). So a rigorous filtration method employing Celite 545 and filter

paper pulp was devised. Recent CHN analysis (see Section 3.2) indicates that the vigorous filtration has improved the quality of the free radical solids (all of which are fine powders) but, to date, we have been unable to obtain crystals of any quality.

Melting points of the more efficiently filtered solids are lower than those determined for initial batches. Early batches had decomposition temperatures above the range of the melting point apparatus (>> 300 °C) indicating the presence of manganese dioxide (decomposes >> 300 °C). More recently, melting points (decomposition) of the various salts were determined to be: DPH-DP4SH• at 174 to 176 °C, K-DP4SH• at 195 to 197 °C, and K-DP6SH• at 201 to 203 °C. Further purification may be necessary and the best solvent system for recrystallization must still be determined for all the sulfonated diphenylpicryl hydrazyl salts.

Lastly, we were able to improve the synthetic yields by keeping the ratio (by mass) of manganese dioxide to each of the hydrazine precursors between 4 to 1 and 3 to 1. As well, rotary evaporation of the reaction solutions was carried out in the absence of fluorescent lighting, and at lower temperatures (15 to 20 °C). The hydrazyl salts seem to be particularly sensitive to light during the rotary evaporation stage. Their entire synthesis was carried out either shaded from, or in the absence of, fluorescent lighting. These procedures also improved the "quality" of the products.

3.2 Elemental Analysis (CHN)

The elemental composition of the sulfonated picryl hydrazine and hydrazyl salts, calculated as percentages of carbon, hydrogen, and nitrogen present, is summarized below in Table 1. Confirmation (if any) of molecular composition by x-ray crystallography is indicated.

As already stated, while crystals of the sulfonated picryl hydrazines have been obtained, crystals of the respective picryl hydrazyls have not been acquired. We have seen that DPH-DP4SH crystallizes without solvent molecules trapped in its crystal structure (see Section 3.3 for further discussion). K-DP4SH crystallizes with 1,4-dioxane, in a ratio of 2 to 3, trapped in its crystal structure, as does K-DP6SH with H_2O in a ratio of 1 to 1. This is reflected in the experimental CHN percentages in Table 1.

Although not adequate for crystallography, crystals of K-DP4SH crystallized from distilled H_2O were also obtained (see Section 2.2.1). Elemental analysis of those "water" K-DP4SH crystals yielded experimental values C = 44.39 %, H = 2.92 %, and N = 11.40 %. Calculated values of K-DP4SH with one molecule of H_2O included in its crystal structure are C = 44.44 %, H = 3.11 %, and N = 11.52%. From these data we assume that, when crystallized from water, K-DP4SH, like K-DP6SH, also traps water in a ratio of 1 to 1.

Even though we have so far been unable to obtain crystals of the sulfonated picryl hydrazyl salts, elemental analysis of these compounds does provide a basis for speculation as to their structural composition. We know that DH_2-H is a clathrate-forming compound [WBRW91] and traps molecules of the solvent used for its recrystallization. As already shown, the potassium picryl

hydrazine sulfonates also trap solvent molecules upon crystallization. So we may assume the hydrazyl salts may do the same.

While DPH-DP4SH crystals are "solventless", CHN analysis (Table 1) indicates DPH-DP4SH• has solvent in its powder "matrix". Otherwise, since the mass of only one hydrogen atom differentiates the two, a "bare" free radical would have the same CHN percentages as its "bare" precursor molecule. DPH-DP4SH• does not; it has carbon ≈ 48 %, while DPH-DP4SH has carbon ≈ 59 %. Since DPH-DP4SH• is crystallized from chloroform/diethyl ether, and having tried various combinations of solvent and free radical, we think that chloroform may crystallize with DPH-DP4SH.

CHN analyses of the potassium hydrazyl salts also differ from their precursor hydrazines. It is feasible that the change in the *ortho* salt may be a change in the ratio of solvent (in this case, water) to product as indicated in Table 1. Less likely is the change indicated in the *para* salt of the hydrazyl compared to its respective hydrazine. However, after having calculated the percentages of numerous elemental composition combinations, the numbers indicate that the potassium *para* hydrazyl salt, unlike its diamagnetic precursor molecule, traps water, not dioxane, in its powder "matrix". X-ray crystallography can confirm or correct these theories and the attainment of crystals of each of the synthesized salts is still in progress.

Table 1: Summary of elemental (CHN) analysis of the sulfo picryl hydrazine and hydrazyl salts

DPH-DP4SH Confirmed by crystallography			
	% Calculated	% Experimental (two trials)	
Carbon	58.63	58.48	58.61
Hydrogen	4.26	3.92	4.08
Nitrogen	13.67	13.58	13.49
K-DP4SH : 1,4-dioxane (2:3) Confirmed by crystallography			
	% Calculated	% Experimental (two trials)	
Carbon	47.99	47.53	47.44
Hydrogen	4.20	3.97	4.02
Nitrogen	9.33	9.20	9.29
K-DP6SH : H_2O (1:1) Confirmed by crystallography			
	% Calculated	% Experimental (two trials)	
Carbon	44.44	44.22	44.27
Hydrogen	3.11	2.83	2.82
Nitrogen	11.52	11.33	11.20
DPH-DP4SH• : chloroform (2:3) Not confirmed by crystallography			
	% Calculated	% Experimental (two trials)	
Carbon	47.73	48.59	47.44
Hydrogen	3.37	2.92	2.59
Nitrogen	10.60	10.52	10.88
K-DP4SH• : H_2O (3:2) Not confirmed by crystallography			
	% Calculated	% Experimental (two trials)	
Carbon	45.09	44.93	45.23
Hydrogen	2.80	2.81	2.76
Nitrogen	11.68	11.46	11.51
K-DP6SH• : H_2O (1:2) Not confirmed by crystallography			
	% Calculated	% Experimental (two trials)	
Carbon	42.94	43.81	42.58
Hydrogen	3.20	3.41	2.33
Nitrogen	11.13	11.18	10.76

3.3 X-ray Crystallography

The crystal structures of the following were determined by x-ray crystallography at low temperatures (193 ± 2 K for the potassium salts and 150 ± 2 K for the diphenylhydrazinium salt).

DPH-DP4SH (*para*), $C_{30}H_{26}N_6O_7S$, was crystallized from 95% (aq) ethanol. DPH-DP4SH (Figure 19) crystallizes in the triclinic space group p_-1, with a = 5.7938(8) Å, b = 15.805(4) Å, c = 16.849(4) Å, α = 69.54(2)°, β = 83.940(16)°, γ = 87.348(17)°, Z = 2, wR2(F^2) = 0.1418, based on all 5814 independent (unique) reflections.

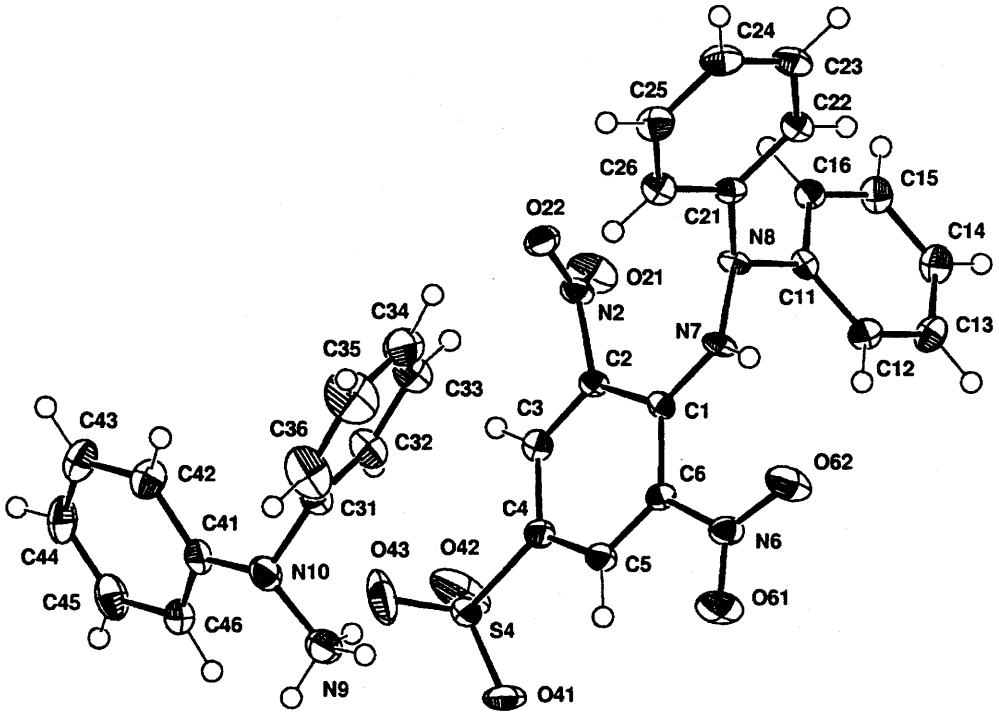

Figure 19: A general ORTEPII [J76] view of DPH-DP4SH

K-DP4SH (*para*), $C_{24}H_{25}KN_4O_{10}S$, was crystallized from 95% (aq) dioxane. K-DP4SH (Figure 20) crystallizes in the monoclinic space group $P2_1/c$, with a = 24.911(2) Å, b = 5.8875(5) Å, c = 18.0156(15) Å, $\alpha = 90°$, $\beta = 99.64(1)°$, $\gamma = 90°$, Z = 4, $wR2(F^2) = 0.0906$, based on all 5298 independent (unique) reflections.

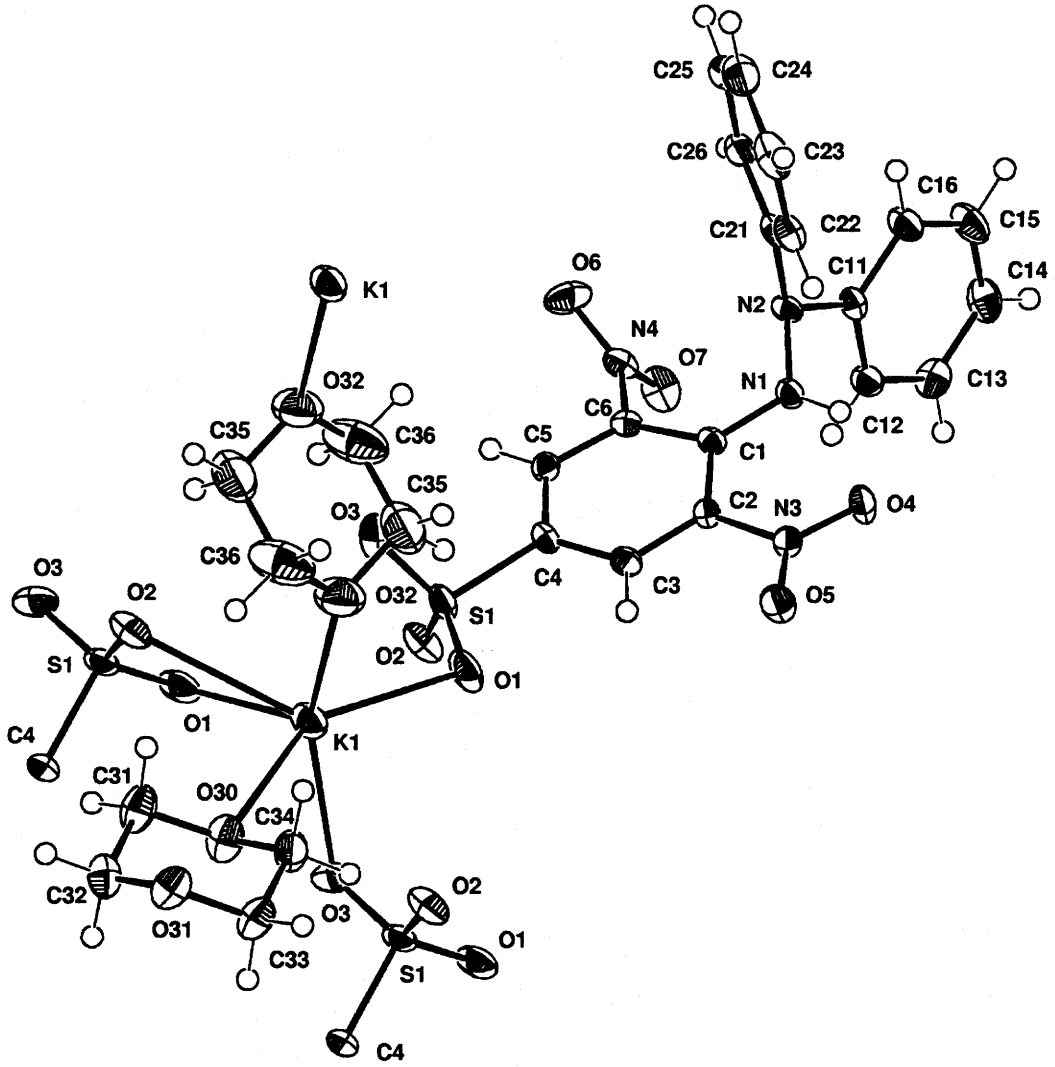

Figure 20: A general ORTEPII [J76] view of K-DP4SH

K-DP6SH (*ortho*), $C_{18}H_{15}KN_4O_{8.076}S$, was crystallized from doubly-distilled H_2O. K-DP6SH (Figure 21) recrystallizes in the monoclinic space group $P2_1/c$, with a = 14.1374(9) Å, b = 8.7410(10) Å, c = 16.6082(11) Å, $\alpha = 90°$, $\beta = 90.600(10)°$, $\gamma = 90°$, Z = 4, $wR2(F^2) = 0.1172$, based on all 4187 independent (unique) reflections.

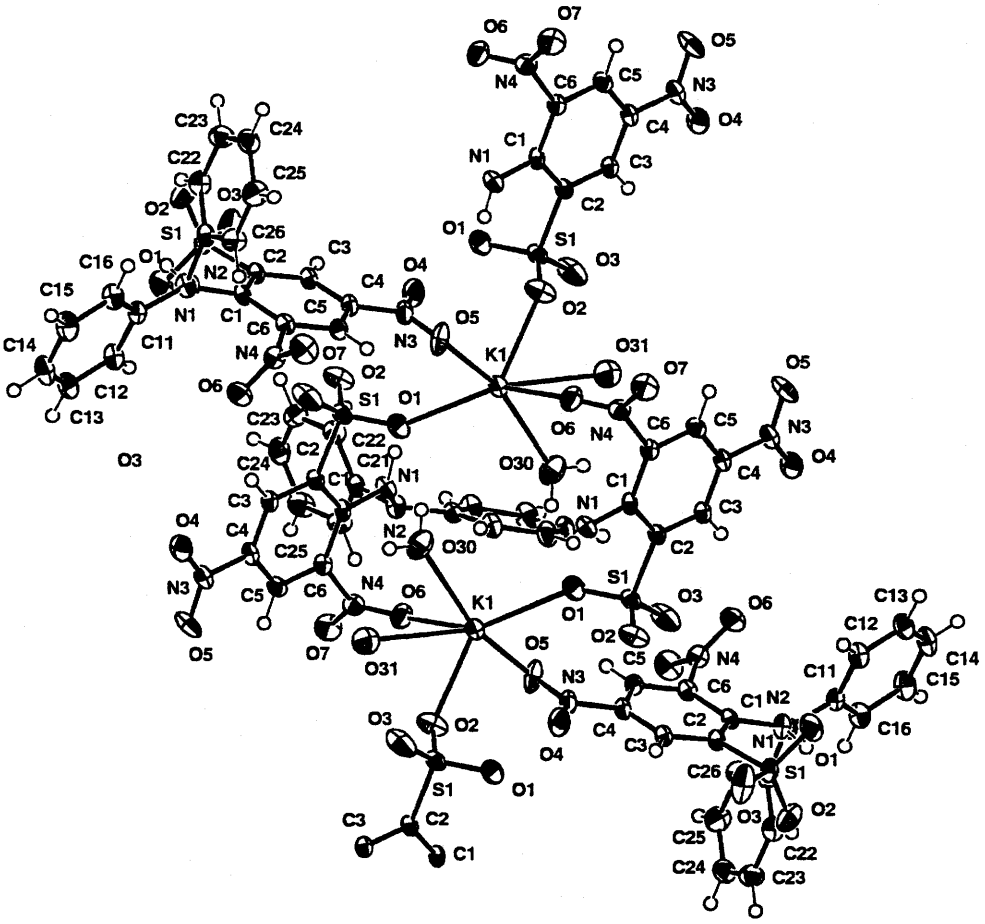

Figure 21: A general ORTEPII [J76] view of K-DP6SH

The general ORTEPII [J76] views of the hydrazines are drawn with non-hydrogen ellipsoids (a model for thermal/vibrational motions) placed at the 50 % probability level. For clarity, the H atoms are depicted as small "open" spheres (O)of arbitrary size.

There are no solvent molecules trapped in the DPH-DP4SH structure (Figure 20) and no large cavities exist in the lattice. However, both K-DP4SH (Figure 21) and K-DP6SH (Figure 22), like DH_2-H [WBRW91], crystallize with interstitial clathrate solvent molecules. Each K-DP4SH cavity contains one-and-a-half guest molecules (1,4-dioxane); each K-DP6SH cavity contains one guest molecule (H_2O). Guest molecules in both structures reflect the solvent used for crystallization, 95% (aq) dioxane and distilled H_2O respectively.

Table 2: Assignments of referenced atoms within the crystal structures

Crystal	DPH-DP4SH	K-DP4SH	K-DP6SH
"diphenyl" nitrogen	N8	N2	N2
"picryl" nitrogen	N7	N1	N1
"*ortho*" nitrogen	N2, N6	N3, N4	N4
- attached oxygen	O21 & 022, O61 & O62	O4 & O5, O6 & O7	O6 & O7
"*ortho*" sulfur	---	---	S1
- attached oxygen	---	---	O1, O2, O3

In DPH-DP4SH, the bond angles for N8 were found to be 113.8(3), 119.9(3), and 110.8(3) °. These are consistent with a trigonal N atom with sp^2 (and some sp^3) hybridization. The angles for the equivalent atom in K-DP4SH (N2) were found to be 112.44(15), 119.42(15), and 114.73(15); in K-DP6SH (N2) were found to be 113.89(16), 120.94(16), and 114.67(17). As such, the potassium salts show the same geometry as DPH-DP4SH and all three compare well to DH_2-H. The bond angles for the equivalent N atom, which is described as having sp^2 hybridization with some sp^3 character, in DH_2-H are 115.2(4), 123.9(4), and 113.9 ° [WBRW91]. Thus, the sulfo-hydrazines share this structural similarity with DH_2-H.

The structures of the *para* salts have an intramolecular hydrogen bond between the H atom on the "picryl nitrogen" and one of the O atoms on one of the *para* nitro groups. In the potassium *para* salt, the hydrogen bond is to O4 of N3 or O7 of N4; in the diphenylhydrazinium *para* salt, the bond is to O62 of N6 or O22 of N2 (for discussion of the intramolecular reorientation of molecules such as these, see Section 1.6.2.1). However, the potassium *ortho* salt has an intramolecular hydrogen bond from the equivalent H atom to an O atom (O1) of the *ortho* sulfo group (S1). The hydrogen bond does not appear to bond with any of the O atoms of the *ortho* nitro group. Even so, in all the salts, regardless if the bond is to an O atom of a nitro group or of a sulfo group, this intramolecular hydrogen bond results in the formation of a six-membered ring, a structure common to all picryl hydrazines [WBRW91 ,BNQRWZ99]. The effect for the *para* salts (DPH^+, K^+) is that the planes of the [N3, N6] nitro groups are very close [–7.6(5), –2.2(3) °] to the planes of the picryl ring. The same can be said for the planes of the [N2, N4] nitro groups with torsion angles of [173.4(3), 179.85(17) °]. This is like the coplanar situation in DH_2-H [WBRW91]. The situation is very similar in the potassium *ortho* salt, where the plane of the sulfo group (S1) is also very close [–172.71(16) °] to the plane of the picryl, as is the plane of the nitro group [N4, 167.94(18) °].

The potassium *para* salt, like DH_2-H, has no further hydrogen bonding to H1. However, H1 of the potassium *ortho* salt also shows intermolecular hydrogen bonding with O4 and N3 on an adjacent molecule, resulting in a three-centre (bifurcated) hydrogen atom. As well, the H atoms of the guest water molecule participate in extensive intermolecular hydrogen bonding to O atoms of the sulfo groups in adjacent molecules and to the picryl nitrogen (N1). H30A bonds to O1 and N1 (in the same molecule) and to the O atom of an adjacent water molecule resulting in a four-centre (trifurcated) hydrogen atom. The diphenylhydrazinium *para* salt also exhibits extensive inter- and intramolecular hydrogen bonding from H7, from the H atoms of the diphenylhydrazinium cation (H9A, H9B, H9C), and from select H atoms of the picryl ring and the diphenyl rings of both the cation and the anion.

The potassium salts also both exhibit extensive intermolecular bonding from the K atom to O atoms of nitro and sulfo groups of adjacent molecules as well as to O atoms of the guest molecule (H_2O in the case of the *ortho* salt, dioxane in the case of the *para* salt. K atoms, which have a positive charge, like the negative charges of O atoms. As a result, the negatively charged O atoms form a cage around the positively charged K atoms.

For the reader's convenience, the crystal data is presented as tables in Appendix A4. Crystal data for DPH-DP4SH begins with Table A3, page 167 in the appendices. Crystal data for K-DP4SH begins on page 177 with Table A10, and that for K-DP6SH on page 187 with Table A17.

3.4 Ultraviolet-Visible Light Spectroscopy

The ultraviolet-visible light absorption spectra of DH_2-H in 100 % ethanol (EtOH) and of the sulfo-picryl hydrazine salts in distilled water and 100 % EtOH are presented in Figure 22. Similar spectra of DH_2• in 100 % EtOH and of the sulfo-picryl hydrazyls in 100 % EtOH and in distilled H_2O are presented in Figure 23. Table 3 summarizes the absorptions found in Figures 22 and 23. A comparison of K-DP4SH in "wet" (solvent used as shipped by distributor) EtOH (Figure 22b, 395 nm) and "dry" (solvent dried as prescribed in LLP99) EtOH (Figure 22c, 394 nm) showed very little difference (1 nm) in absorption. As such, further hydrazine spectra were obtained without rigorous "drying" of the organic solvents. A similar comparison for K-DP4SH• did show a difference so, EtOH was dried as prescribed in LLP99 and used for the hydrazyl spectra.

Table 3: Summary of Uv-vis absorptions (in air, at room temperature) for Figures 22 and 23 (experimental absorptions of DH_2-H and DH_2• are in agreement with literature values [CDW61])

Compound	Wavelength (λ, nm)		
	In 100 % EtOH		In distilled H_2O
DH_2-H	321.0		Not soluble
DPH-DP4SH	396.0		387.0
K-DP4SH	395.0		388.0
K-DP6SH	321.0, 350.0		331.0
DH_2•	331.0, 523.0		Not soluble
DPH-DP4SH•	310.5, 325.0, 364.0, 513.5		315.5, 326.5, 359.0, 520.5
K-DP4SH•	313.0, 329.0, 360.0, 508.0		312.0, 326.5, 359.0, 520.5
K-DP6SH•	325.5, 348.5, 527.0		337.0, 537.5

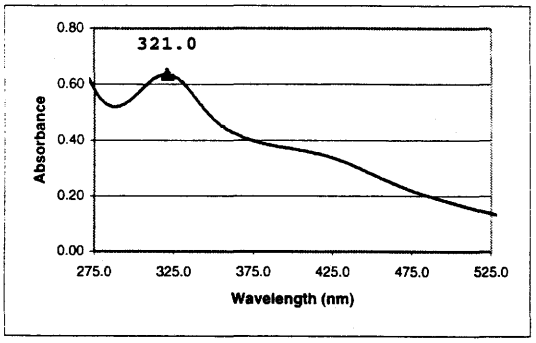

a) DH_2-H in EtOH (not dried)

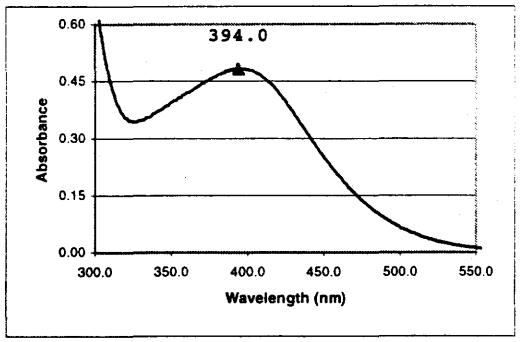

b) K-DP4SH in EtOH (dried)

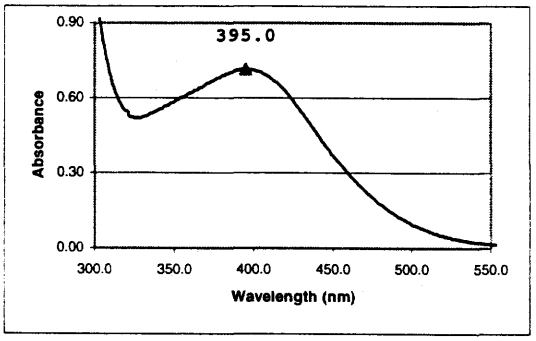

c) K-DP4SH in EtOH (not dried)

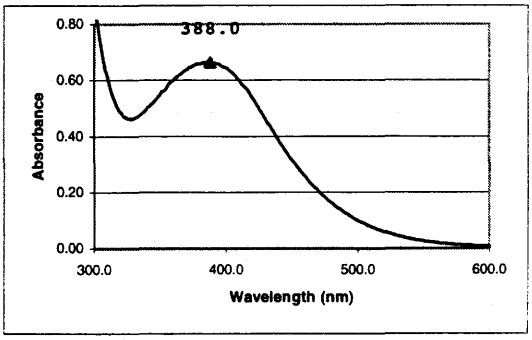

d) K-DP4SH in distilled H_2O

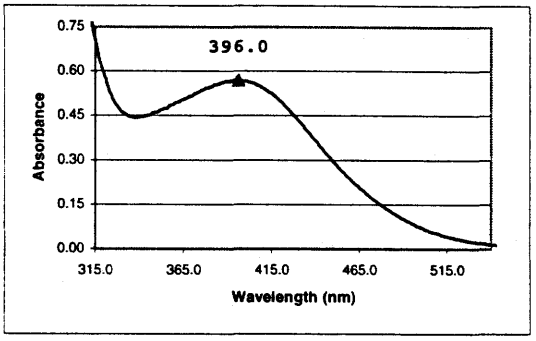

e) DPH-DP4SH in EtOH (not dried)

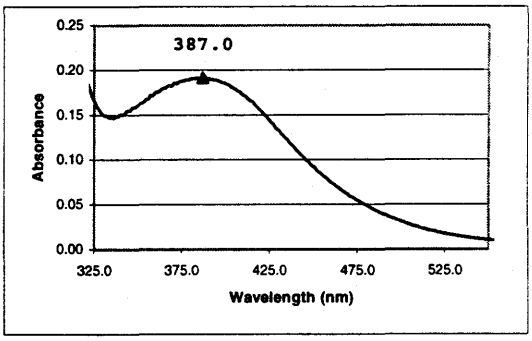

f) DPH-DP4SH in distilled H_2O

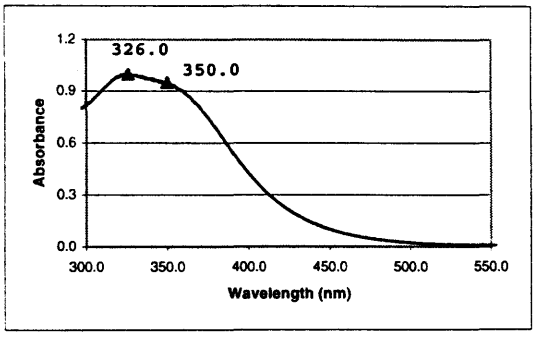

g) K-DP6SH in EtOH (not dried)

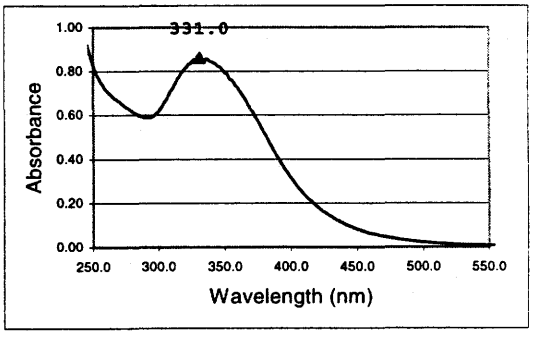

h) K-DP6SH in distilled H_2O

Figure 22: Uv--vis spectra of DH_2-H and of the synthesized sulfo-picryl hydrazine salts (in air, at room temperature)

As can be seen from Figure 22, the absorptions of the sulfonated hydrazine salts in the ultraviolet-visible light spectrum are similar to those of DH_2-H. The diamagnetic species have one broad band between 300 and 400 nm. In 100 % EtOH, the *para* sulfonated hydrazine salts absorb at a much higher wavelength (396 nm for the DPH^+ salt, 395 nm for the K^+ salt) than DH_2-H (321 nm) in the same solvent. In distilled water, both of the *para* sulfonates experience a hypsochromic shift (shift to shorter wavelengths). On the other hand, the *ortho* sulfonated hydrazine salt in 100 % EtOH appears to have two absorptions in the region where DH_2-H (in the same solvent) absorbs. The lower absorption of the *ortho* salt (321 nm) is similar to that for DH_2-H, the other absorption (350 nm) is only slightly longer. In distilled water, the *ortho* sulfonate gives a single absorption at 331 nm.

As seen in Figure 23, the paramagnetic species generally have two areas at which they absorb, one in the "hydrazine" region and one above 500 nm, both of which are typical of the picryl hydrazyls. However, the sulfonated salts in EtOH have multiple absorptions between 300 and 400 nm (the *para* salts have three absorptions, the *ortho* salt has two), while $DH_2\bullet$ in EtOH has but a single absorption. In water, the *para* hydrazyls still exhibit three absorptions at lower wavelengths, but the *ortho* hydrazyl has but one (337.0 nm), very close to the wavelength of the $DH_2\bullet$ absorption (331.0 nm) in the same region.

All paramagnetic species, the sulfo hydrazyl salts in EtOH and in water as well as $DH_2\bullet$ in EtOH, each has just one absorption above 500 nm. This absorption is indicative of the extended conjugation found these free-radical

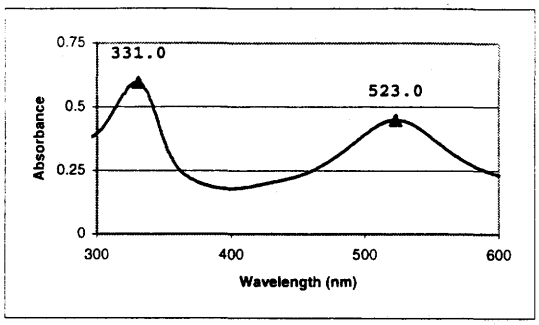

a) $DH_2\bullet$ in EtOH (dried)

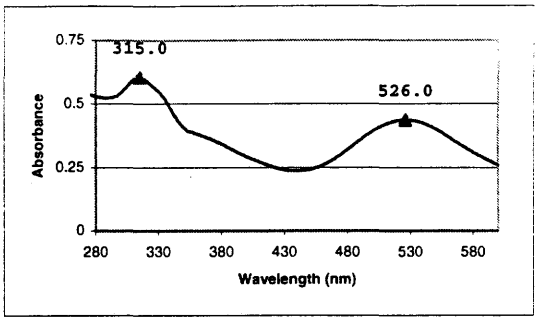

b) DPH-DP4SH• in EtOH (not dried)

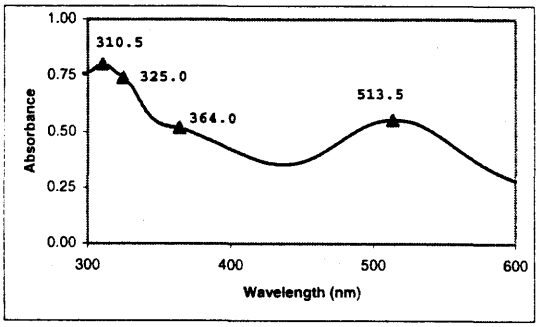

c) DPH-DP4SH• in EtOH (dried)

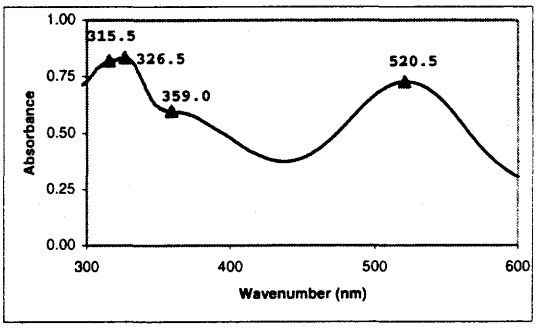

d) DPH-DP4SH• in H_2O

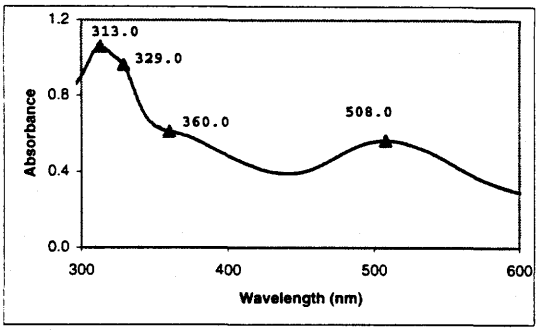

e) K-DP4SH• in EtOH (dried)

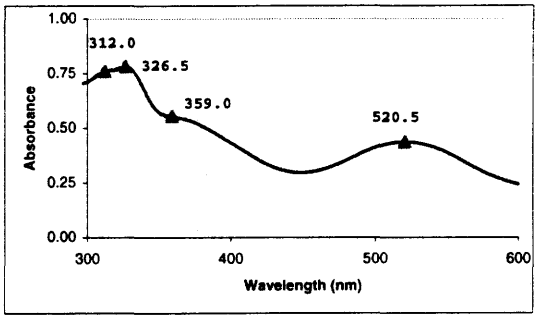

f) K-DP4SH• in H_2O

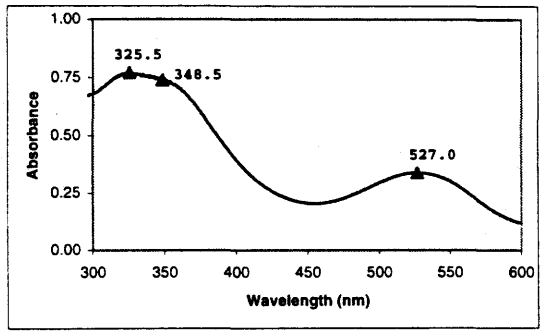

g) K-DP6SH• in EtOH (dried)

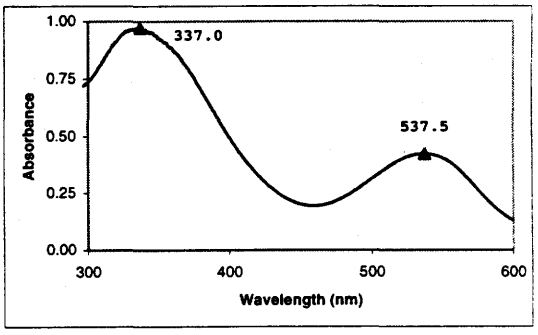

h) K-DP6SH• in H_2O

Figure 23: Uv-vis spectra of $DH_2\bullet$ and of the synthesized sulfo-picryl hydrazyl salts (in air, at room temperature)

molecules. In EtOH, the *para* substituted hydrazyls absorb at a much lower wavelength (DPH^+ salt at 513.5 nm, the K^+ salt at 508.0 nm) than $DH_2\bullet$ (523.0 nm), while the *ortho* substituted hydrazyl absorbs at a slightly lower wavelength (527.0 nm) than $DH_2\bullet$. In water, the absorption of *para* salts (both salts absorb at 520.5 nm) is still lower, but closer to the absorption of $DH_2\bullet$ in EtOH, while the absorption of the *ortho* salt is much higher (537.5 nm). Nevertheless, as is the case for $DH_2\bullet$, the reduction of the picryl hydrazyl sulfonates to their respective hydrazine salts can be easily followed spectrophotometrically. An improvement upon $DH_2\bullet$ is that the reduction of the sulfonated hydrazyls can be followed even in purely aqueous solutions.

3.5 Nuclear Magnetic Resonance Spectroscopy

Proton NMR spectra

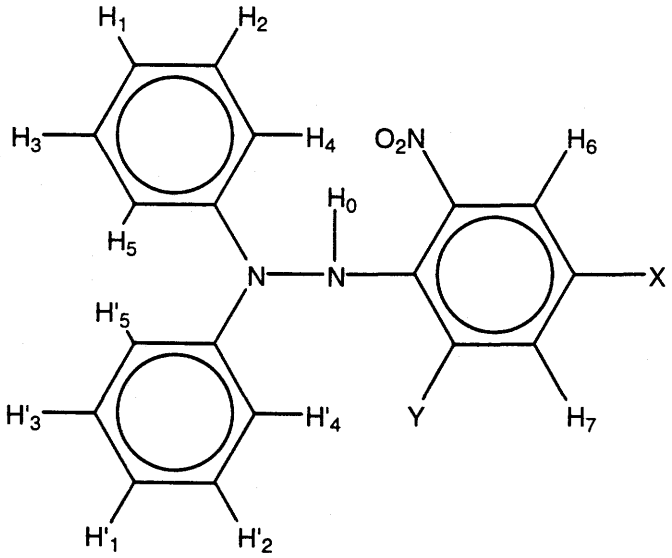

Figure 24: Proton (^{1}H) assignments for the sulfonated diphenylpicryl hydrazine salts

The protons in the sulfonated diphenylpicryl hydrazine molecules have been assigned labels (shown in Figure 24) to facilitate discussion of their ^{1}H-NMR spectra. The "substituents" X and Y represent the interchangeable sites of sulfonation (*ortho* or *para*), where $X \neq Y = NO_2$ or SO_3M (M = K or DPH). The two picryl protons remain in the *meta* position (relative to the picryl C – hydrazine N bond) regardless of the form (*ortho* , *para*) or type (M^+) of sulfonated salt. They have been labelled H_6 and H_7. H and H' (H-prime) are used to distinguish one set of diphenyl protons from the second set of diphenyl protons. The hydrazinic proton is designated as H_0.

Figures 25, 26, and 27 show characteristic 500 MHz ^1H NMR spectra of the sulfonated diphenylpicryl hydrazine salts in perdeuterated dimethylsulfoxide (DMSO). The upper spectrum (b) of each figure is an inset of the lower spectrum (a) and shows an expanded view of the region in which the protons of the sulfonated hydrazine salts (shown in Figure 24) resonate. The spectrum of DPH-DP4SH was acquired at 333.0 K (for reasons discussed later); the spectra of the potassium salts at 298.0 K. Table 4 lists the relevant chemical shifts.

Table 4: ^1H NMR chemical shifts (δ) for the sulfonated diphenylpicryl hydrazine salts

Molecule	δ - H_0	δ - H_6	δ - H_7	δ of the diphenyl protons	
	ppm from trimethylsilane (TMS)				
K-DP6SH T = 298.0 K	9.67	8.48 8.47	8.45 8.45	7.35 7.34 7.33	7.13 7.11 7.10
K-DP4SH T = 298.0 K	10.21	8.11		7.3232 7.3083 7.2921	7.12 7.10 7.09 7.07
DPH-DP4SH T = 333.0 K	9.96	8.13		twice the multiplets due to protons from cation (DPH^+)	

Besides the absorptions listed in Table 4, the spectrum of K-DP6SH shows a peak for DMSO (the solvent used) at 2.50 ppm and a large HOD (water) peak at 3.34 ppm (see Figure 25a). Unless dried vigorously, perdeuterated solvents, even if stored over molecular sieves, tend to contain a

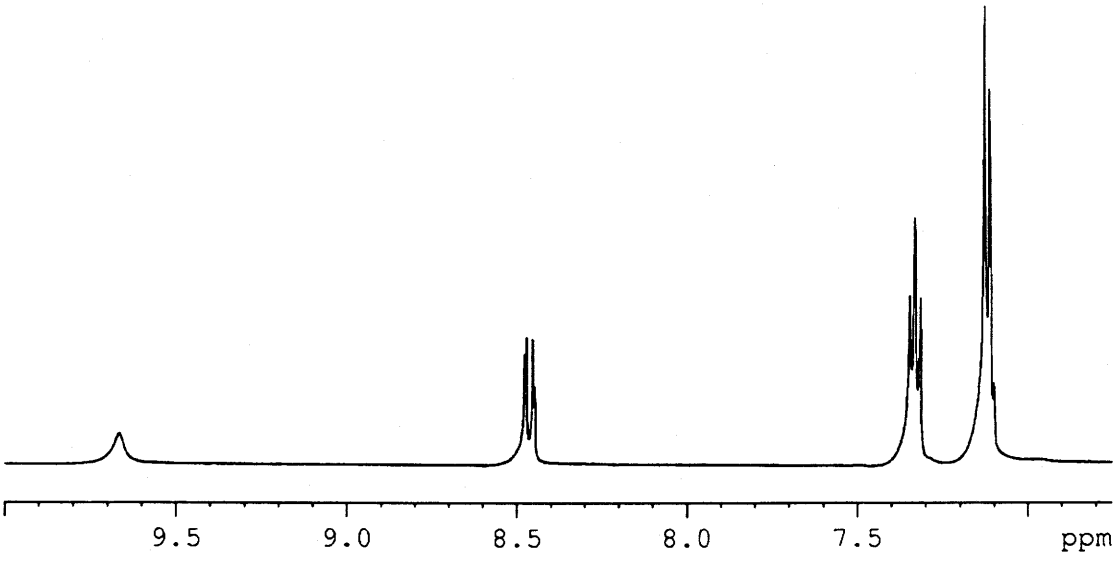

b) Close-up of the "*ortho* sulfonated diphenylpicryl hydrazine" region

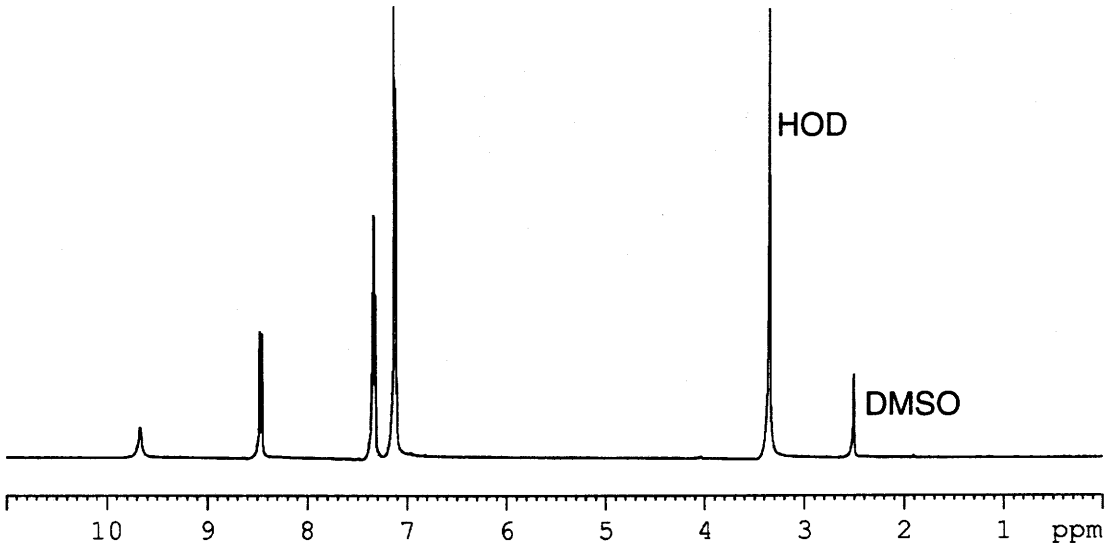

a) The full spectrum

Figure 25: 500 MHz ^{1}H NMR spectrum of K-DP6SH in DMSO-d6 (in air, at room temperature, at 500.23 MHz, ppm from TMS)

certain amount of water. We have seen that K-DP6SH traps water in its crystal matrix. As such, both DMSO and the hydrazine contribute to the HOD peak.

Although hard to see in Figure 25, the picryl peaks, whose associated protons are *meta* to each other, are a pair of doublets with a coupling constant (J_{ab}) of 2.63 Hz, which is typical of *meta* coupling. In the *ortho* sulfonated hydrazine (i.e., K-DP6SH) the picryl protons are inequivalent, H_6 being flanked by two nitro groups while H_7 is flanked by a sulfo group and a nitro group. Since the nitro groups exert a more deshielding influence on adjacent protons than the sulfo group, H_6 (8.48 and 8.47 ppm) absorbs downfield from H_7 (8.45 and 8.45 ppm). The hydrazinic proton (H_0), the most deshielded of all the protons, absorbs at 9.67 ppm. The pair of multiplets between 7.0 and 7.5 ppm is caused by the diphenyl protons. These are discussed below.

The spectrum of K-DP4SH (Figure 26) also shows a peak for DMSO at 2.50 ppm. This time, the large HOD peak at 3.33 ppm is due mostly to water contaminating the perdeuterated solvent (as explained above). One additional "solvent" peak distinguishes the *para* potassium salt from both the other two (as we shall see). The protons associated with the dioxane molecules contained within the crystal matrix of K-DP4SH absorb at 3.56 ppm.

Looking at their structure, one would assume that, in the *para* form of the sulfonated salt, the picryl protons H_6 and H_7 would be equivalent and their absorption would be a single sharp peak. They are both flanked by a nitro and a sulfo group, and they occupy the *meta* positions in the ring. However, because of hydrogen bonding between the hydrazinic proton H_0 and an oxygen of one of

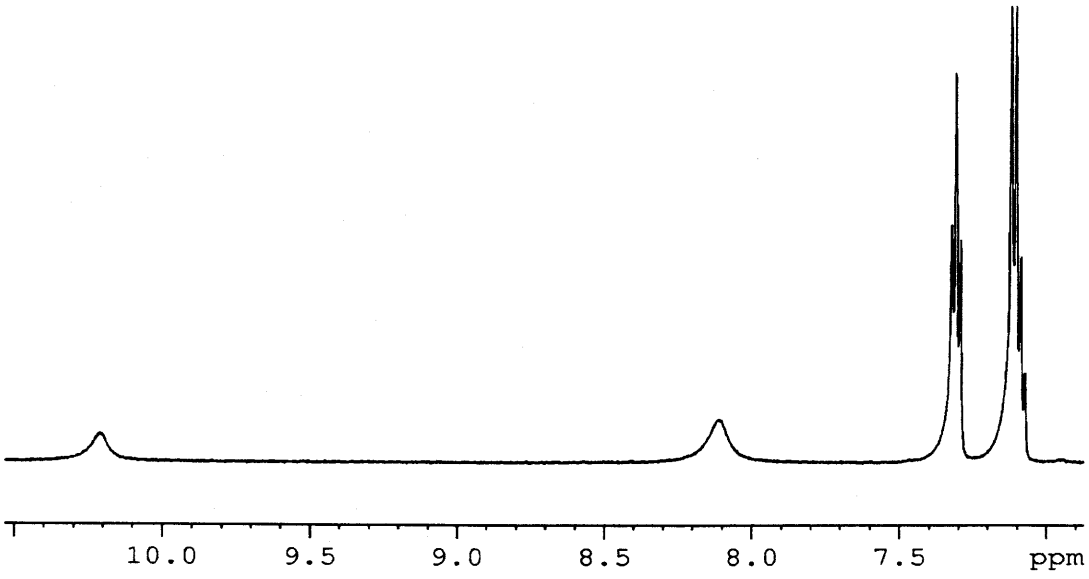

b) Close-up of the "*para* sulfonated diphenylpicryl hydrazine" region

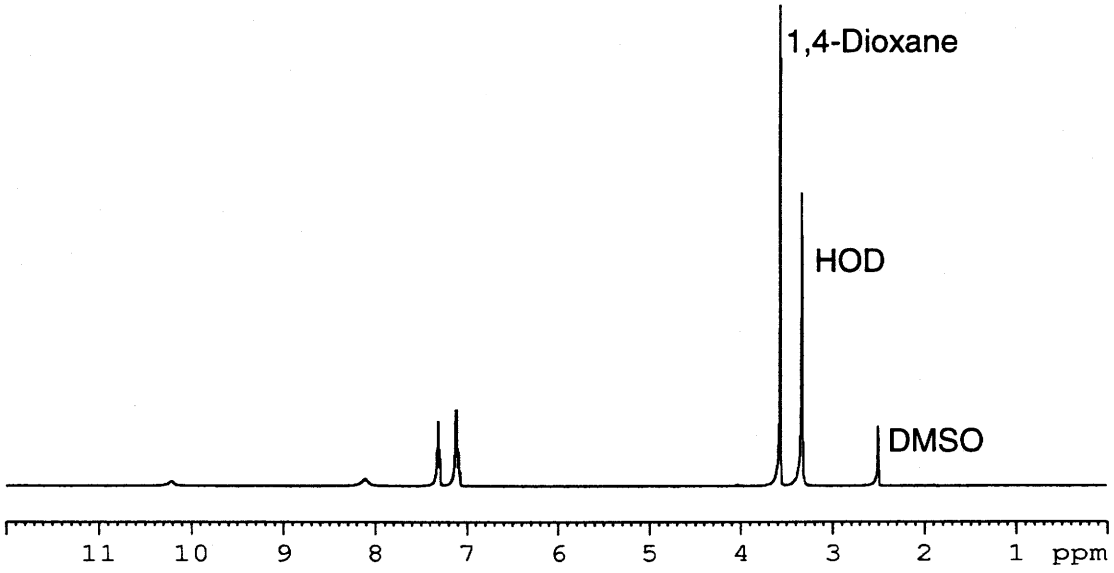

a) The full spectrum

Figure 26: 500 MHz ^{1}H NMR spectrum of K-DP4SH in DMSO-d6 (in air, at room temperature, at 500.23 MHz, ppm from TMS)

the *ortho* nitro groups (see Section 3.3), they are inequivalent. Furthermore, the molecule undergoes intramolecular reorientation (see Section 1.6.2.1) as the hydrogen bond interchanges between the two *ortho* nitro groups. As a result and dependent upon the solvent, most room-temperature ^{1}H NMR spectra of the *para* sulfonated salts show only a "small" averaged single peak for the picryl protons as shown in Figure 26. At lower temperatures, the absorption resolves into two peaks, as exhibited by the *ortho* sulfonated salts that may, or may not, show coupling. As the sample is taken above room temperature, the single peak increases in height (see Figure 27). In K-DP4SH, the average picryl proton absorption is at 8.11 ppm. The hydrazinic proton in this salt (10.21 ppm) is more deshielded than in the *ortho* salt (9.67 ppm) as a result of hydrogen bonding to the oxygen in the nitro groups rather than in the sulfo group as is the case for the *ortho* salt (see Section 3.3). The pair of multiplets between 7.0 and 7.5 ppm is due to the diphenyl protons. These are discussed below.

The spectrum of DPH-DP4SH (Figure 27) was acquired at 333.0 K in order to show the increased intensity of the averaged chemical shift of the picryl protons, and the extra diphenyl multiplets present in this salt. Since there are no solvent molecules trapped within its crystal matrix (see Section 3.3), the peak at 2.50 ppm is due to DMSO. There is a very broad shallow HOD-absorption centred at 5.0 ppm.

The chemical shift due to the picryl protons (now "equivalent " at this temperature) is seen at 8.13 ppm. At room temperature, the peak is at $\approx$ 8.12 ppm and resembles the equivalent peak for the *para* potassium salt. The

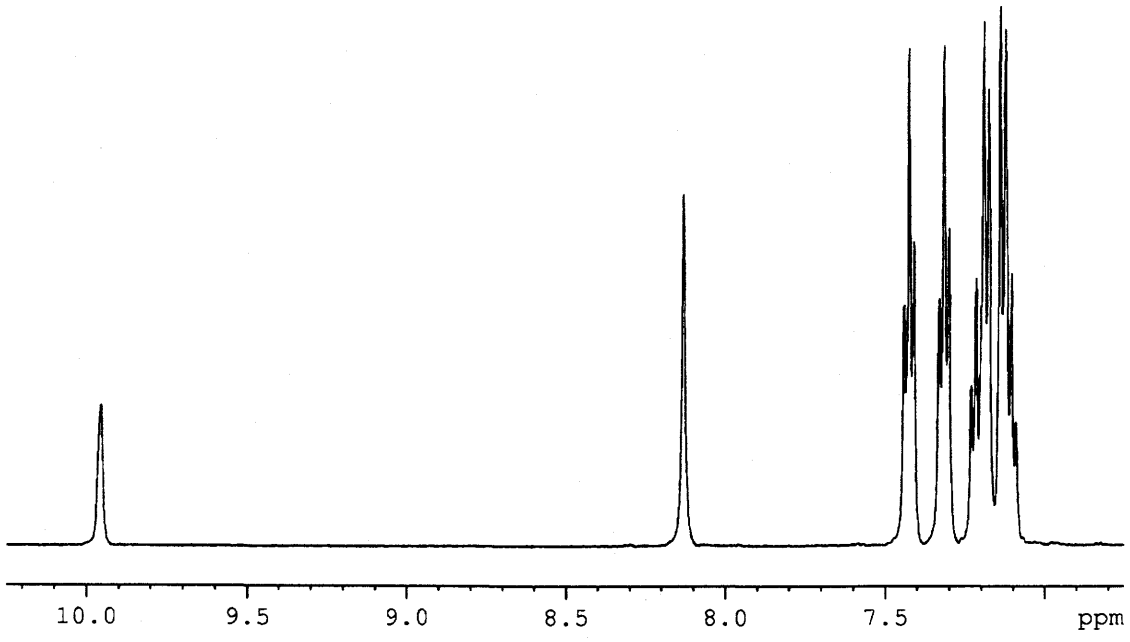

b) Close-up of the "*para* sulfonated diphenylpicryl hydrazine" region

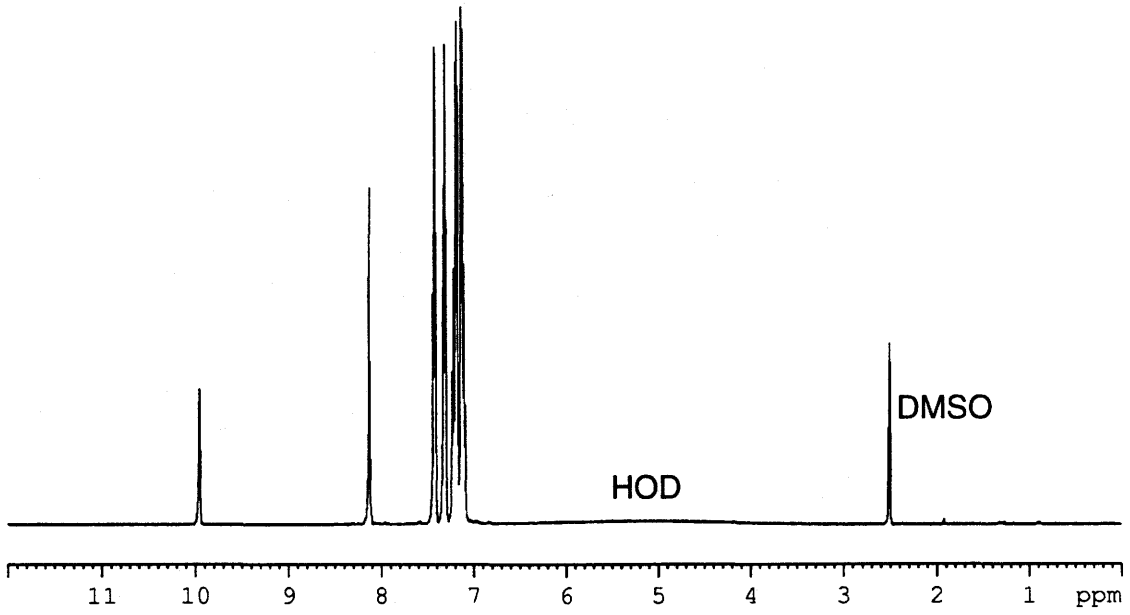

a) The full spectrum

Figure 27: 500 MHz ^{1}H NMR spectrum of DPH-DP4SH in DMSO-d6 (in air, at T = 333 K, at 500.23 MHz, ppm from TMS)

chemical shift due to the hydrazinic proton at this higher temperature is more intense, and seems to be more shielded (9.96 ppm) than its room-temperature counterpart (≈ 10.23 ppm). Between 7.0 and 7.5 ppm, there seems to be twice as many peaks attributable to the diphenyl protons in the DPH^+ salt as compared to the K^+ salts. This apparent "doubling" of the multiplets is caused by the additional diphenyl protons found in the diphenyl-hydrazinium cation, which we assume absorb more downfield than those in the sulfonated diphenyl hydrazine.

Simulation of the diphenyl protons in ^1H NMR spectroscopy

As explained in Appendix A3, the only way to determine the coupling constants and chemical shifts of the diphenyl protons in diphenylpicryl hydrazine molecules accurately is to simulate their ^1H NMR spectra. This was first done for DH_2-H (see Appendix A3). The reason that their absorptions are so complex is that each proton in the phenyl ring is not equivalent (a five-spin system) and experience *ortho*, *meta*, and *para* coupling to each other. If the diphenyl *ortho* and *meta* protons were equivalent to each other (there are two of each), we would have a three-spin system and a much simpler splitting pattern. Luckily, the diphenyl protons of one phenyl ring are equivalent to their counterparts in the other phenyl ring and only one "set" of chemical shifts must be determined. In the case of the DPH^+ salt, there is a second set of chemical shifts attributable to the cation's diphenyl protons that do not overlay the set of diphenyl proton chemical shifts of the main molecule (the anion). One way to assign which set

belongs to the cation and which set belongs to the anion, would be to substitute deuterium atoms for the diphenyl hydrogen atoms in either the anion or the cation. At this time, we assume that the diphenyl protons in the cation absorb downfield (more deshielded) from the "anionic" diphenyl protons.

The simulated ^1H NMR spectra for the potassium salts of the sulfohydrazines were based on experimental spectra acquired at 300 MHz and 500 MHz in both perdeuterated water and DMSO. Data acquired in this manner are summarized in Tables 5, 6, and 7. Simulated and experimental spectra are given in Figures 28 to 33. For an explanation as to how the data were determined and their interpretation, refer to Appendix A3.

Table 5 shows that, as with DH_2-H (see Appendix 3), the *meta* diphenyl protons are consistently more deshielded than either the *ortho* or *para* diphenyl protons. In perdeuterated dichloromethane (CD_2Cl_2), the *ortho* diphenyl protons in DH_2-H are the most shielded of the protons in the diphenyl rings. However, in the solvents employed, this is the case only for K-DP6SH in DMSO-d6. A direct comparison in CD_2Cl_2 was not possible as the potassium sulfohydrazines are not soluble in dichloromethane. For K-DP6SH in D_2O, as well as for K-DP4SH in D_2O and in DMSO-d6, the *para* diphenyl proton is the most shielded of the protons in the diphenyl rings. Even so, the chemical shifts of the *ortho* protons are very close to the chemical shift of the *para* proton. This can be attributed to the shielding influence of the nitrogen attached to the diphenyl rings. The nitrogen is an electron-donating moiety and has the greatest influence on the *ortho* protons of the diphenyl rings. The shielding of the *para* proton is due to its

Table 5: Resonant frequencies (chemical shifts) of the diphenyl protons in the potassium sulfohydrazines as determined by the simulation of their ^{1}H-NMR spectra, 300 MHz and 500 MHz, in air at room temperature

Solute			K-DP6SH (*ortho*)			K-DP4SH (*para*)		
Solvent			D_2O		DMSO-d6	D_2O		DMSO-d6
Spectrometer Frequency (MHz)			300.14	500.23	300.14	500.13	500.13	500.23
Temperature (K)			298.0	300.0	298.0	278.0	298.0	300.0
para -proton	resonant frequency (ppm)	V1	7.08	7.10	7.11	6.80	7.11	7.10
meta - H1		V2	7.26	7.28	7.30	6.97	7.28	7.31
meta - H2		V3	7.26	7.28	7.30	6.97	7.28	7.31
ortho - H1		V4	7.13	7.15	7.06	6.86	7.15	7.13
ortho - H2		V5	7.13	7.15	7.06	6.86	7.14	7.13
coupling constants (Hz)		J12	7.84	7.74	7.09	8.14	7.71	7.94
		J13	8.04	8.04	7.69	8.34	8.16	8.04
		J14	1.05	1.05	0.45	1.25	1.63	1.05
		J15	0.87	0.87	1.17	0.37	0.18	0.77
		J23	0.48	1.08	0.65	1.28	0.62	0.78
		J24	7.90	7.90	8.25	8.30	8.40	7.90
		J25	1.04	1.04	0.84	1.14	1.14	1.04
		J34	0.44	0.44	0.99	0.44	0.74	0.44
		J35	8.18	8.18	7.83	8.08	8.57	8.28
		J45	1.80	1.80	0.45	1.80	1.82	1.80
Width of spectrum (Hz)			105.00	135.00	126.00	210.00	210.00	229.00
Wa (Hz)			1.65	1.50	1.75	2.10	2.05	2.50

position in the ring. Bond-wise, it is the furthest removed from other atoms in the molecule. In this very limited study, it seems that the resonant frequencies of the protons in the diphenyl rings are greatly influenced by the solvent used. As such, it may be that the chemical shifts of these protons may correlate with Kamlet-Taft solvatochromic parameters (see Section 1.6.2.1). Further studies in other perdeuterated solvents are needed to confirm or refute any correlation that

may have been observed so far. As is seen below, the ^{1}H-NMR chemical shifts of the picryl protons, as well as EPR parameters, experimentally determined were relatively insensitive to the H-bonding characteristics of the solvents used. It would be interesting to see if the same holds true for the diphenyl protons.

Table 6: Comparison of actual and simulated "apparent" ^{1}H-NMR chemical shifts (δ) of the diphenyl protons of K-DP6SH (in air, at room temperature)

Solute	**K-DP6SH (*ortho*)**								
Solvent	**D_2O**						**DMSO-d6**		
Spectrometer Frequency (MHz)	300.14		% difference	500.23		% difference	300.14		% difference
Temperature (K)	298.0			300.0			298.0		
"Apparent" chemical shifts (Hz)	actual	simulated		actual	simulated		actual	simulated	
	2187.80	2188.2	-0.019%	3650.49	3650.8	-0.008%	2198.91	2198.8	0.005%
	2179.96	2180.0	-0.002%	3642.39	3642.6	-0.006%	2191.15	2191.2	-0.002%
	2172.19	2172.0	0.009%	3634.63	3634.4	0.006%	2183.61	2183.3	0.014%
	2143.15	2143.2	-0.002%	3579.44	3579.4	0.001%	2139.98	2139.6	0.018%
	2134.74	2134.7	0.002%	3571.54	3571.2	0.010%	2132.86	2132.3	0.026%
	2125.18	2125.6	-0.020%				2122.34	2122.0	0.016%
	2117.70	2117.8	-0.005%	3559.56	3559.6	-0.001%	2114.34	2113.7	0.030%
				3552.23	3551.9	0.009%			
				3544.86	3544.3	0.016%			

Tables 6 and 7 compare the "apparent" chemical shifts between the experimental and simulated ^{1}H-NMR spectra of K-DP6SH (Table 6) and K-DP4SH (Table 7). Refer to appendix A3 for an explanation of "apparent"

chemical shifts. As can be seen by the % difference, the values of "apparent" chemical shifts of the simulated ^{1}H-NMR spectra agree well with the values of the "apparent" chemical shifts seen in the corresponding experimental spectra. The percentage differences between the experimental and simulated "apparent" chemical shifts range from approximately 0.001% to 0.03%. As such, we are believe that the actual chemical shifts of the diphenyl protons presented in Table 5 are representative of their actual resonant frequencies.

Table 7: Comparison of actual and simulated "apparent" ^{1}H-NMR chemical shifts (δ) of the diphenyl protons of K-DP4SH (in air, at room temperature)

Solute	K-DP4SH (*para*)								
Solvent	D_2O						DMSO-d6		
Spectrometer Frequency (MHz)	500.13		% difference	500.13		% difference	500.23		% difference
Temperature (K)	278.0			298.0			300.0		
"Apparent" chemical shifts (Hz)	actual	simulated		actual	simulated		actual	simulated	
	3492.88	3493.0	-0.003%	3648.22	3648.8	-0.016%	3666.41	3666.3	0.003%
	3484.64	3484.9	-0.007%	3640.96	3640.9	0.002%	3658.62	3658.5	0.003%
	3477.06	3476.5	0.016%	3633.70	3633.5	0.006%	3650.73	3650.2	0.015%
	3434.09	3434.1	0.000%	3577.10	3577.8	-0.020%	3568.73	3569.0	-0.008%
	3425.70	3425.2	0.015%	3568.90	3568.7	0.006%	3560.58	3561.0	-0.012%
				3564.81	3564.9	-0.003%	3552.80	3553.5	-0.020%
	3408.75	3408.7	0.001%	3557.05	3557.3	-0.007%	3545.42	3545.4	0.001%
	3401.35	3400.8	0.016%	3549.52	3548.9	0.017%			
	3392.72	3392.7	0.000%						

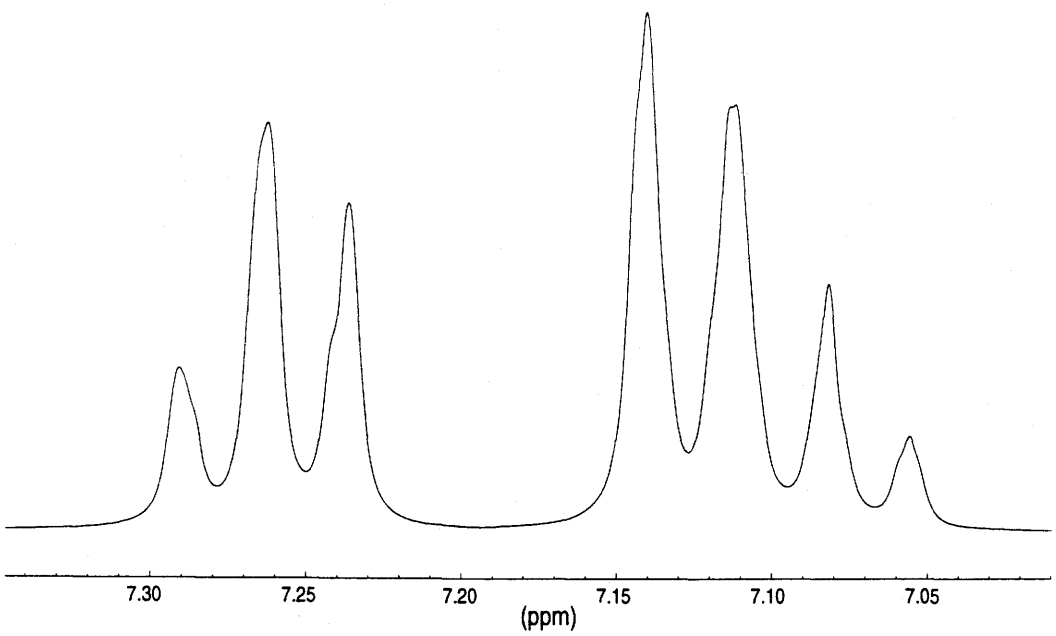

b) Simulated spectrum

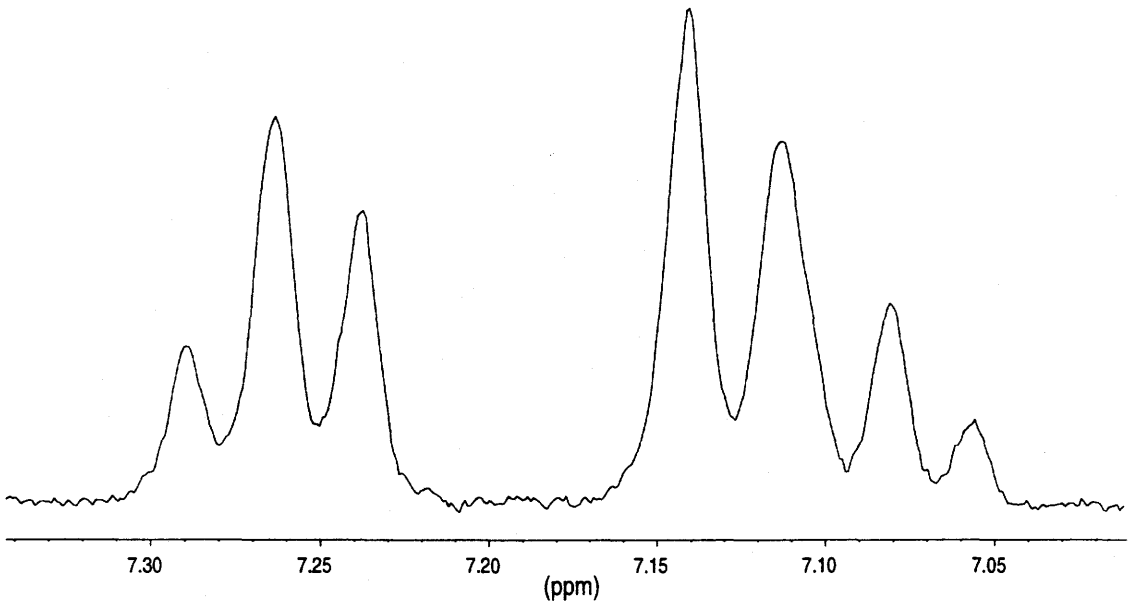

a) Experimental spectrum

Figure 28: Experimental and simulated spectra showing the chemical shifts of the diphenyl protons of K-DP6SH in D_2O at 300.14 MHz, in air, at room temperature

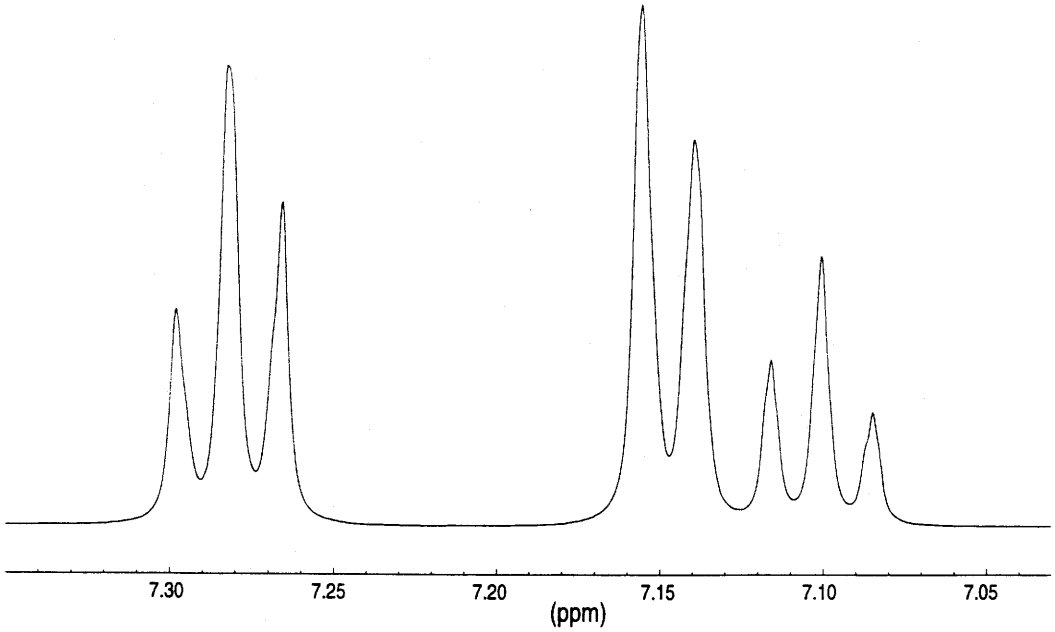

b) Simulated spectrum

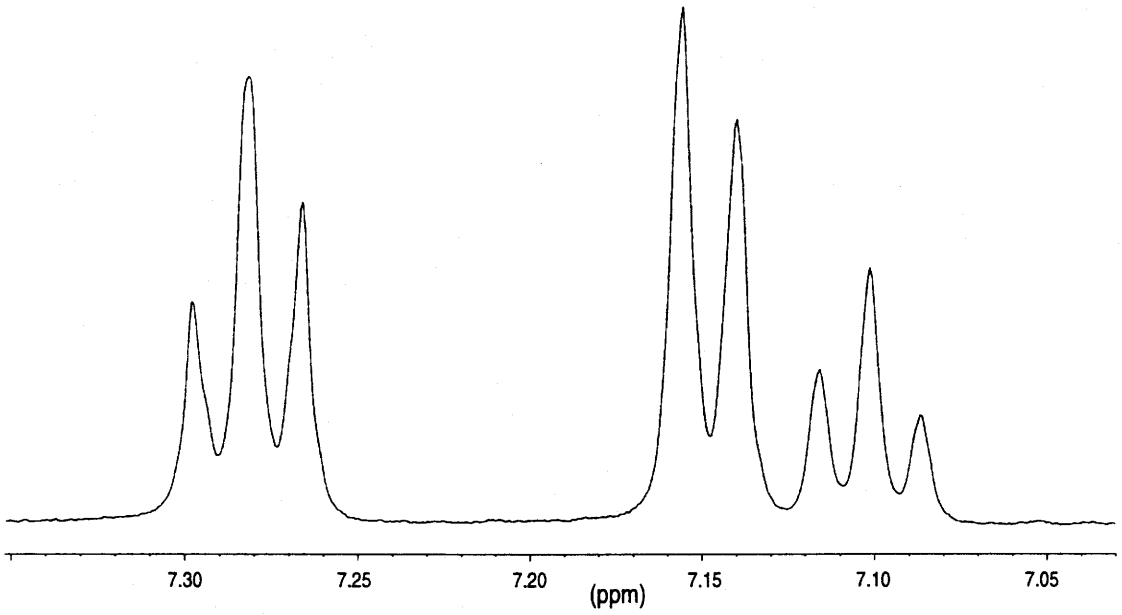

a) Experimental spectrum

Figure 29: Experimental and simulated spectra showing the chemical shifts of the diphenyl protons of K-DP6SH in D_2O at 500.23 MHz, in air, at room temperature

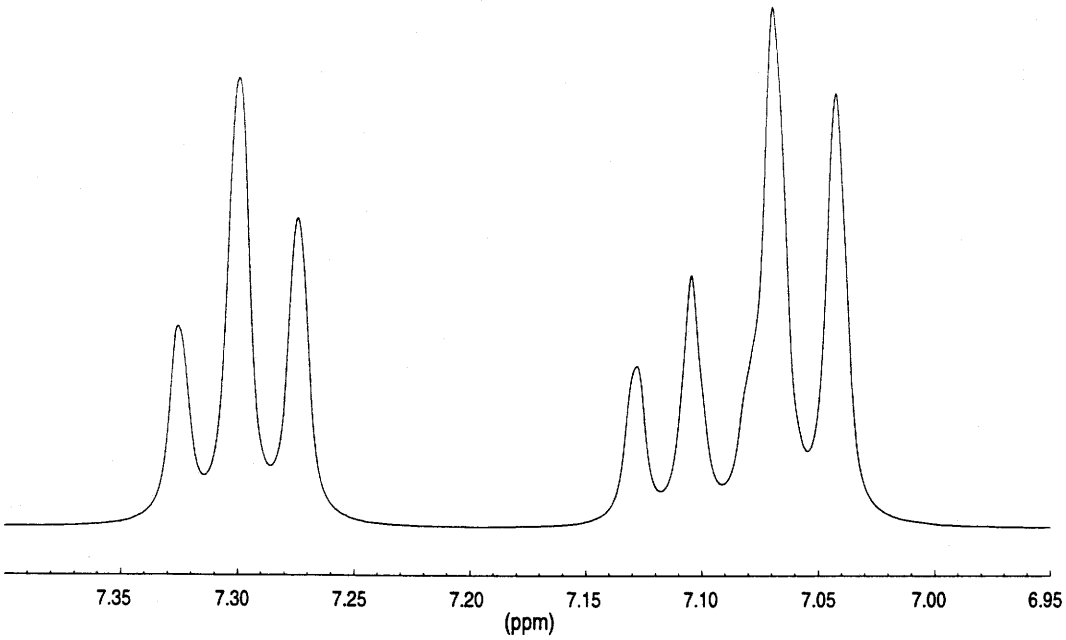

b) Simulated spectrum

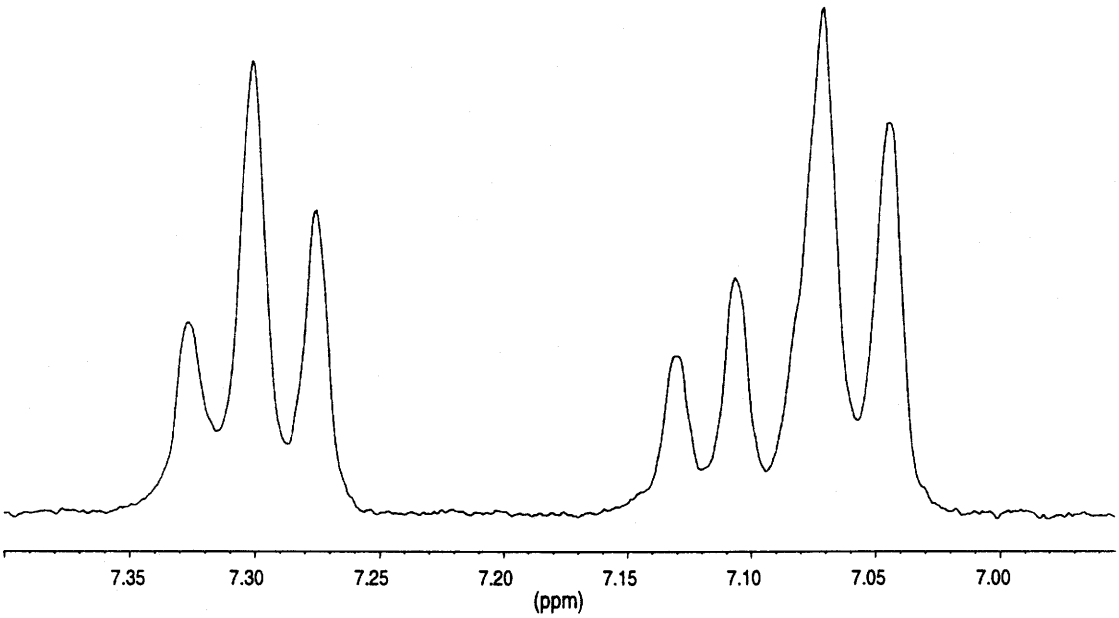

a) Experimental spectrum

Figure 30: Experimental and simulated spectra showing the chemical shifts of the diphenyl protons of K-DP6SH in DMSO-d6 at 300.14 MHz, in air, at room temperature

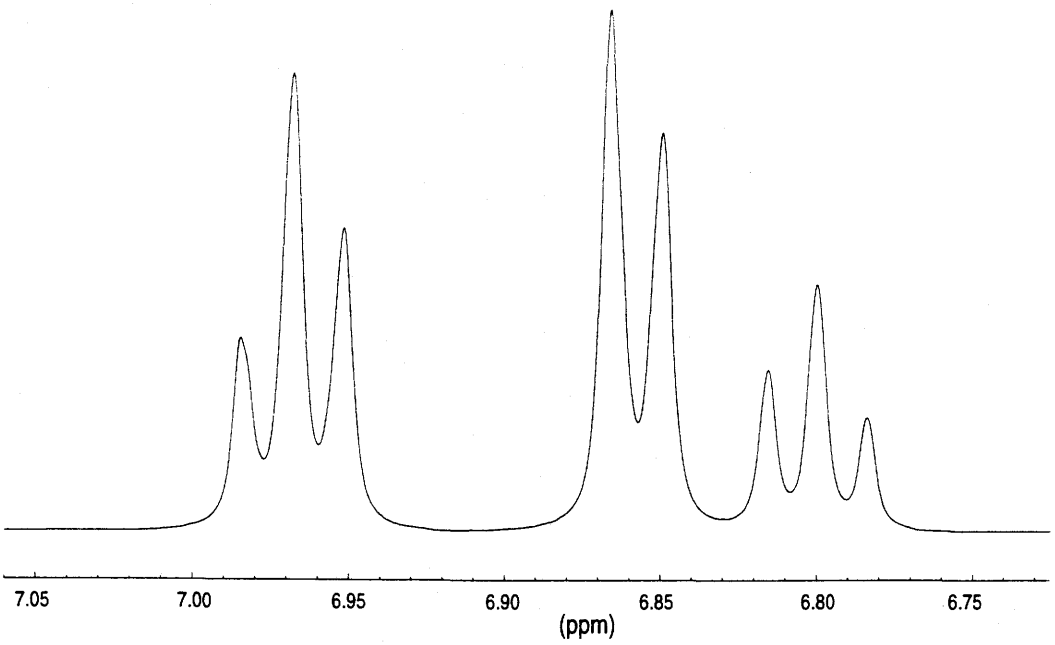

b) Simulated spectrum

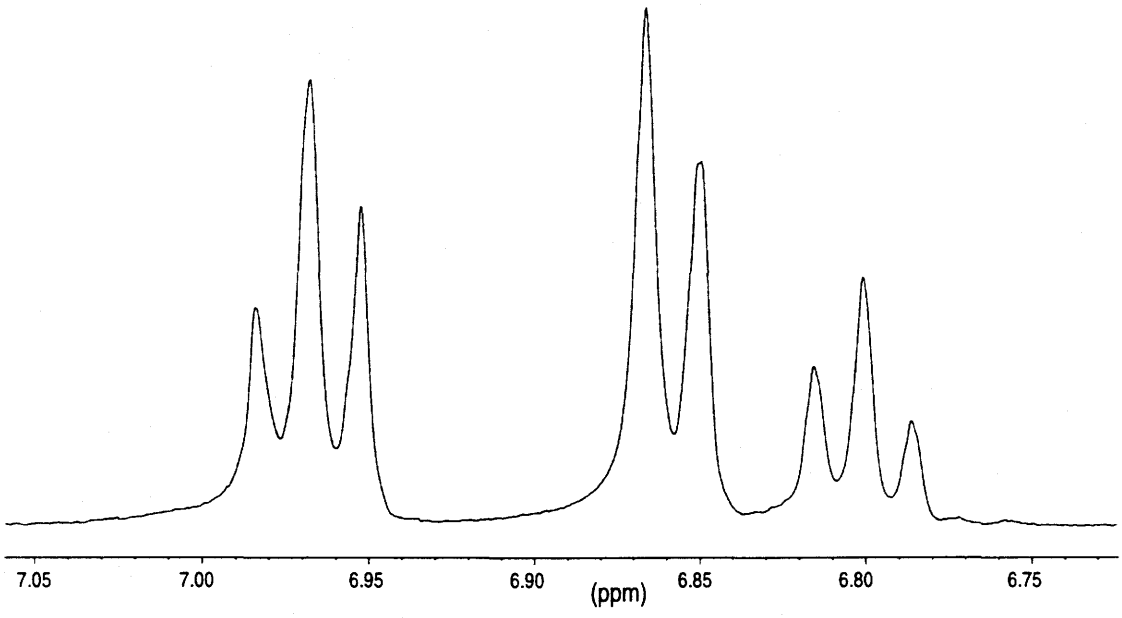

a) Experimental spectrum

Figure 31: Experimental and simulated spectra showing the chemical shifts of the diphenyl protons of K-DP4SH in D_2O at 500.13 MHz, in air, at 278 K

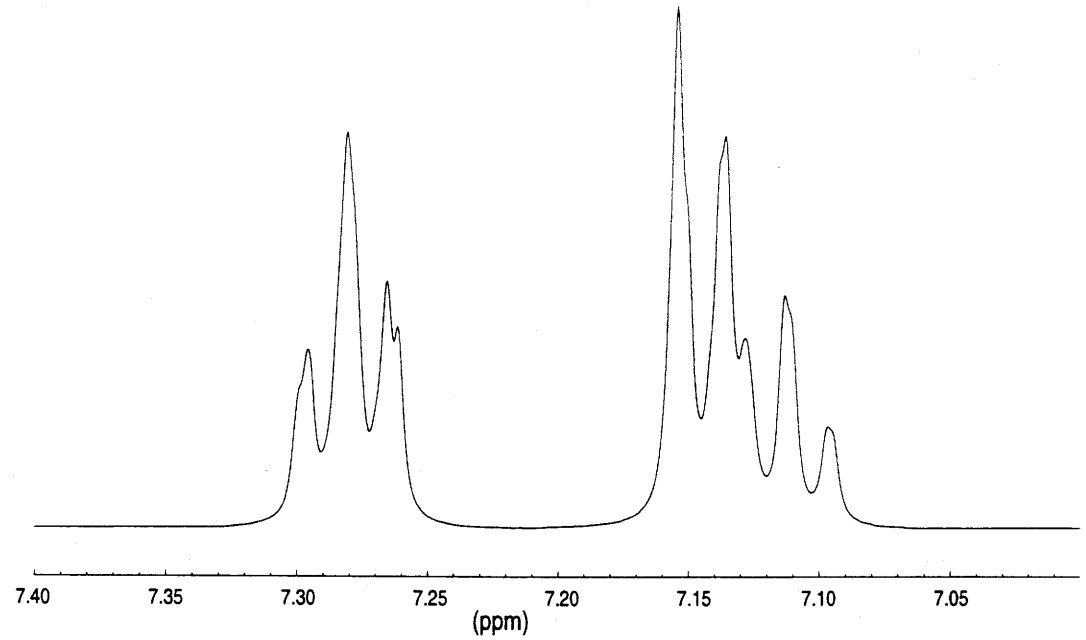

b) Simulated spectrum

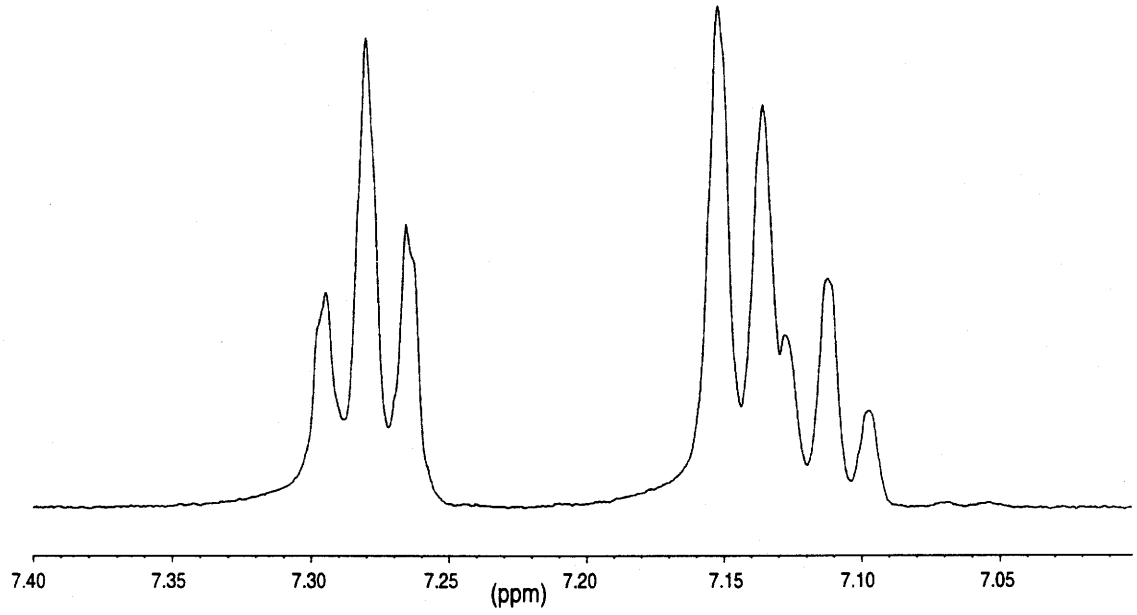

a) Experimental spectrum

Figure 32: Experimental and simulated spectra showing the chemical shifts of the diphenyl protons of K-DP4SH in D_2O at 500.13 MHz, in air, at 298 K (room temperature)

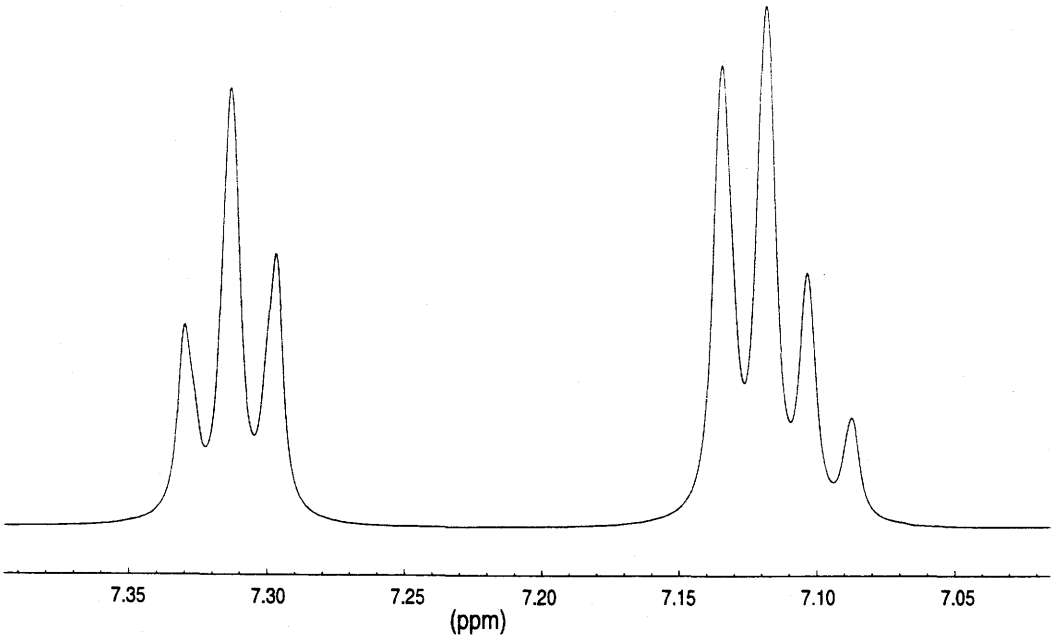

b) Simulated spectrum

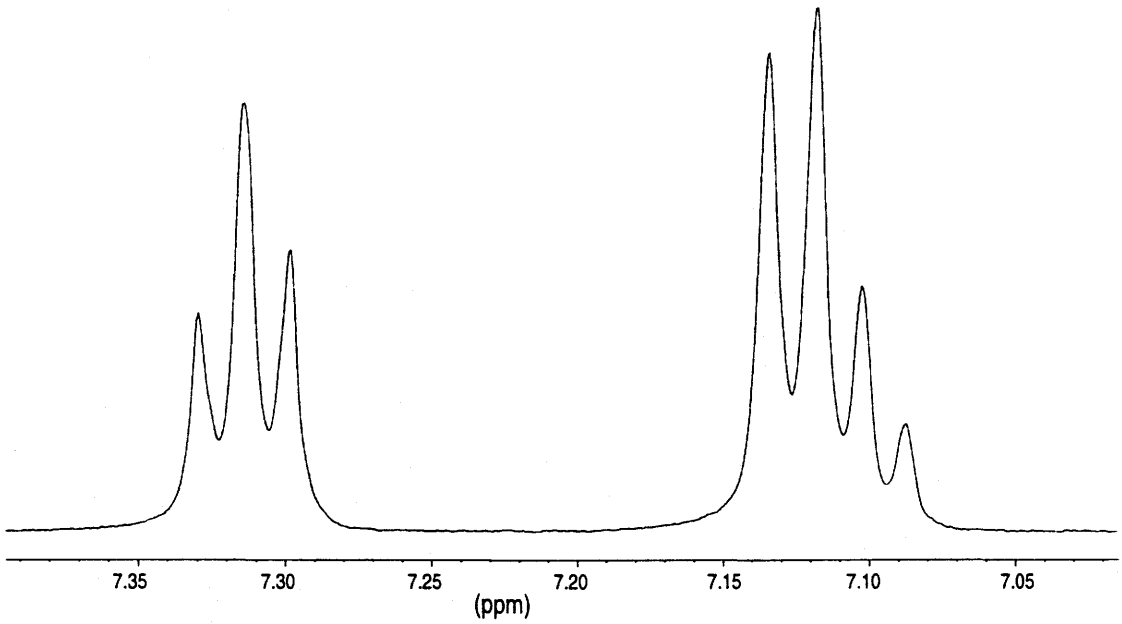

a) Experimental spectrum

Figure 33: Experimental and simulated spectra showing the chemical shifts of the diphenyl protons of K-DP4SH in DMSO-d6 at 500.13 MHz, in air, at room temperature

Carbon-13 NMR spectra

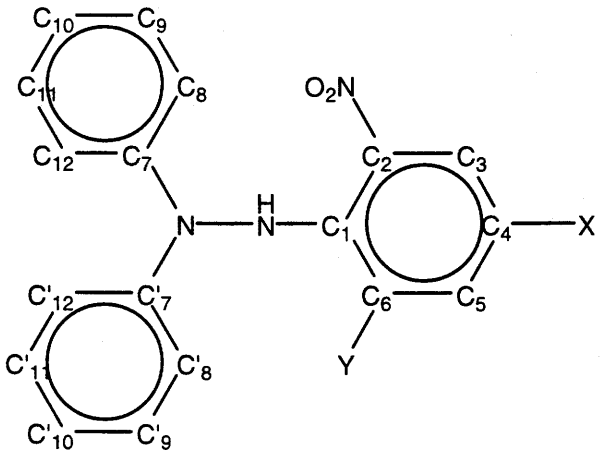

Figure 34: Carbon (^{13}C)assignments for the sulfonated diphenylpicryl hydrazine salts

The carbons in the sulfonated diphenylpicryl hydrazine molecules have been assigned labels (shown in Figure 34) to facilitate discussion of their ^{13}C-NMR spectra. The "substituents" X and Y represent the interchangeable sites of sulfonation (*ortho* or *para*), where $X \neq Y = NO_2$ or SO_3M (M = K or DPH). All told, there are eighteen carbons in each of the "unsolvated" molecules. These do not necessarily correlate to eighteen separate chemical shifts. While the protons of the unsubstituted phenyl ring were all non-equivalent, there are only four distinct carbons in the ring no matter the form of the hydrazine salts. These are C7, C8 = C12 (equivalent and give rise to one abosrption, C9 = C11, and C10. As with the protons, C-carbons for one phenyl ring are equivalent to their respective C'-carbons in the other phenyl ring.

Figures 35, 36, and 37 show characteristic 500 MHz ^{13}C NMR spectra of the sulfonated diphenylpicryl hydrazine salts in perdeuterated DMSO. The

upper spectrum (b) of each figure is an inset of the lower spectrum (a) and shows an expanded view of the region in which the carbons of the sulfonated hydrazine salts (shown in Figure 34) resonate. The ^{13}C spectrum of K-DP6SH was acquired at room temperature (298.0 K), those for the *para* salts were obtained at 333.0 K to show the "time-averaged" picryl-carbon peaks.

Assignment of the ^{13}C chemical shifts for each sulfonated hydrazine salt was greatly facilitated by the acquisition of spectra using three separate NMR techniques. These are: the "attached proton test" (APT), an NMR technique which differentiates between ipso carbons (no H atoms attached) and carbons with only one hydrogen attached; gradient-enhanced proton-detected heteronuclear multiple-quantum coherence spectroscopy (HMQC [HJ91, RVMGCZ92, WLKB93]), which shows short range (one-bond) proton-carbon correlation; and sensitivity-enhanced detection of heteronuclear multiple-bond connectivity by 2D multiple quantum NMR (HMBC [BS86, WLKB93, RVMGCZ92]), which shows long range (two- and three-bond) proton-carbon correlation. For more information about these NMR techniques, please refer to the indicated references as well as RVMGCZ92 and WLKB93. Table 5 lists the ^{13}C chemical shifts determined for each salt. Please note that although C-prime (C') carbons are not listed, they have the same chemical shift as their respective "C" counterparts.

The ^{13}C spectrum of K-DP6SH is shown in Figure 35. C_8 to C_{12} ($C_8 \equiv C_{12}$, $C_9 \equiv C_{11}$) of the diphenyl rings as well as C_3 and C_5 of the picryl ring each has one bonded hydrogen and correlate to the five upfield chemical shifts

between 120 and 130 ppm. The only absorbance more upfield is the chemical shift for DMSO at ≈ 40 ppm. No other solvent peak shows up, water molecules have no carbon atoms. We determined that the most deshielded carbon was C_7, and the remaining four peaks (the peak at ≈ 137 ppm is actually two peaks) correlate to the remaining four picryl carbons. See Table 5 for chemical shifts for each assigned carbon. All in all, there are 10 distinct carbons in K-DP6SH, which is reflected, in its carbon-13 spectrum.

Table 8: ^{13}C NMR chemical shifts (δ) for the sulfonated diphenylpicryl hydrazine salts

Carbon Assignment	K-DP6SH T = 298.0 K	K-DP4SH T = 333.0 K	DPH-DP4SH T = 333.0 K
	Chemical shift in ppm		
C_1	134.74	138.04	137.98
C_2	137.42	≈ 139.5	139.62
C_6	137.37		
C_3	125.34	127.49	127.49
C_5	122.98		
C_4	142.52	138.25	138.27
C_7	146.87	147.17	147.08
C_8, C_{12}	125.14	125.02	125.07
C_9, C_{11}	129.96	129.68	129.69
C_{10}	120.57	120.87	120.88

The spectra for the *para* sulfonated diphenylpicryl hydrazine salts are shown in Figures 36 (K^+ salt) and 37 (DPH^+ salt). Their spectra are quite similar

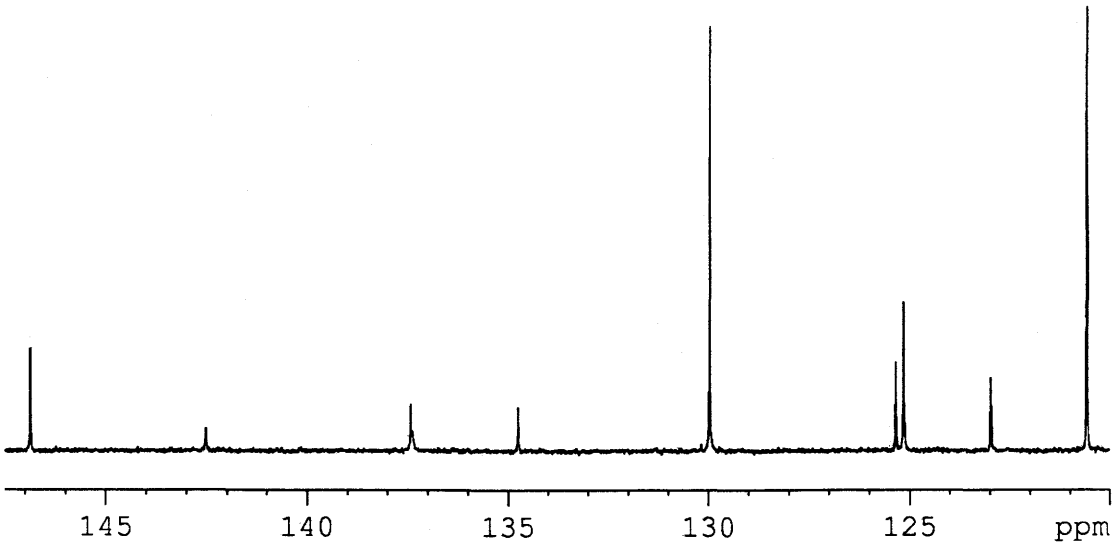

b) Close-up of the "*ortho* sulfonated diphenylpicryl hydrazine" region

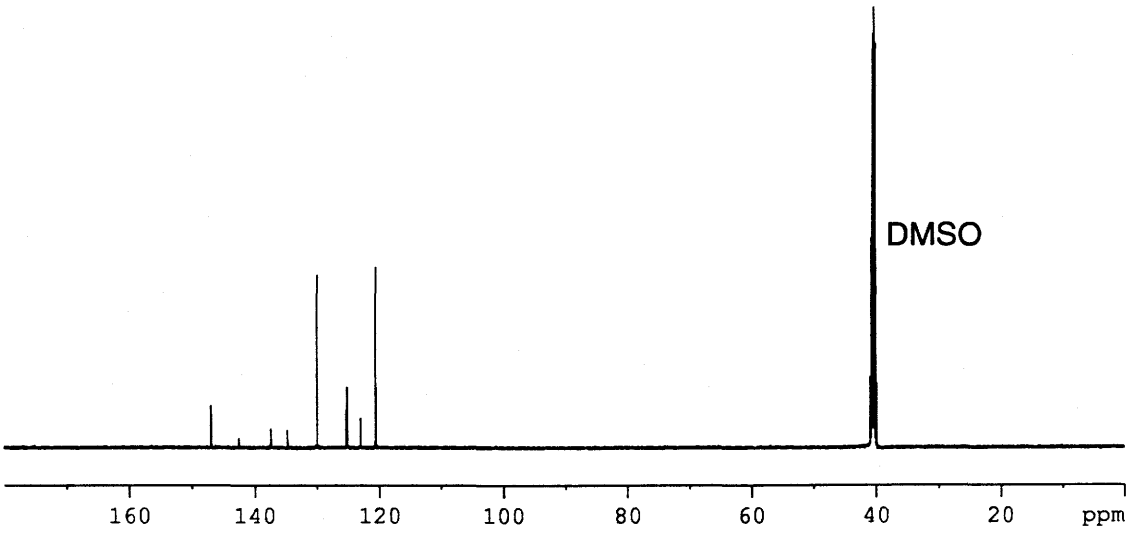

a) The full spectrum

Figure 35: 500 MHz ^{13}C NMR spectrum of K-DP6SH in DMSO-d6 (in air, at room temperature, at 125.80 MHz)

save for the apparent "doubling" of the diphenyl carbon peaks in the DPH^+ salt. This is analogous to the "doubling" of the diphenyl proton chemical shifts in its ^1H NMR spectrum. One other difference between the two "*para*" spectra is the additional peak at ≈ 68 ppm in the spectrum of the potassium salt. This absorption is caused by dioxane present in the crystal matrix of the potassium salt (see Section 3.3). Since dioxane does contain carbon atoms, four "equivalent" carbon atoms, it shows up as a single downfield peak. Both spectra have a "DMSO" peak at ≈ 41 ppm. Realization that the most deshielded carbon was C_7 came from the spectrum of DPH-DP4SH, because the peak that correlates to C_7 (around 147 ppm) in that spectrum is "doubled", though it is hard to see in Figure 37.

Assignments for the picryl carbon atoms of both "*para*" salts can be found in Table 5. They are hard to pinpoint because, like the protons in the picryl ring, the carbons in the picryl ring also exchange "places" due to intramolecular reorientation (see Section 1.6.2.1). As such, the chemical shifts for the picryl carbons are also "time-averaged". The picryl ipso carbons absorb just downfield from C_7. The set of peaks (in the same approximate range as for the *ortho* salt) downfield of the ipso picryl carbons correlate to diphenyl and picryl carbons with attached hydrogen atoms. The absorption for the picryl carbon in this area shows up as only a weak rounded peak again due to averaging of the chemical shifts.

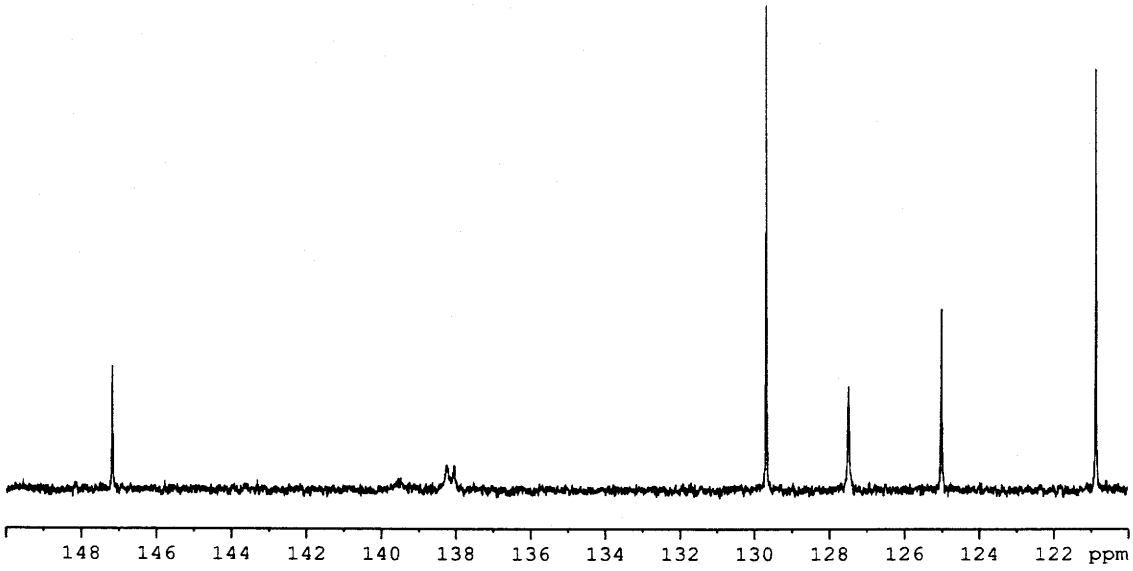

b) Close-up of the "*para* sulfonated diphenylpicryl hydrazine" region

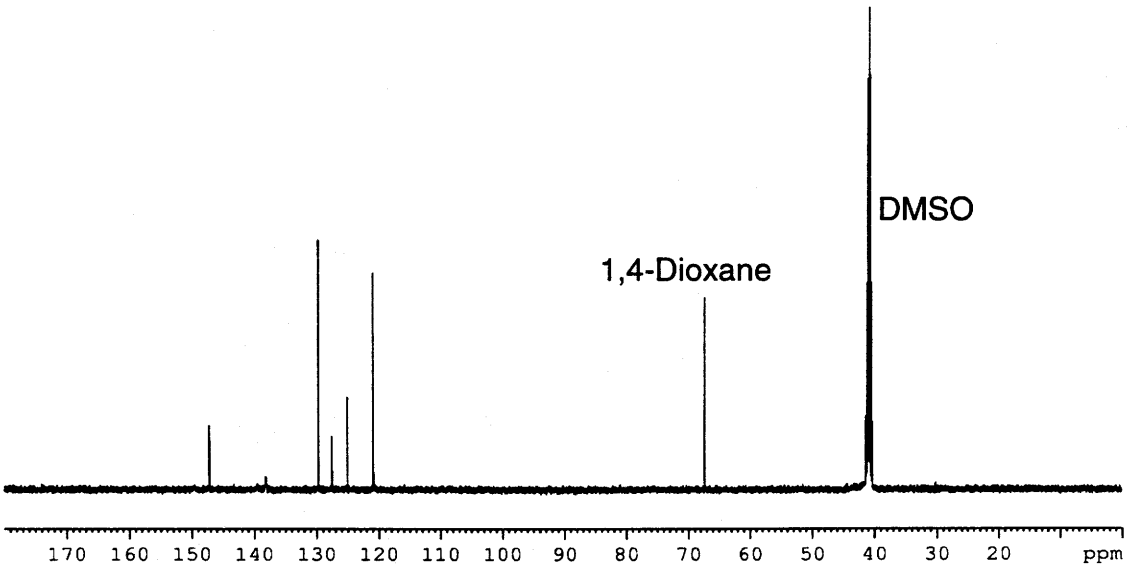

a) The full spectrum

Figure 36: 500 MHz ^{13}C NMR spectrum of K-DP4SH in DMSO-d6 (in air, at room temperature, at 125.80 MHz)

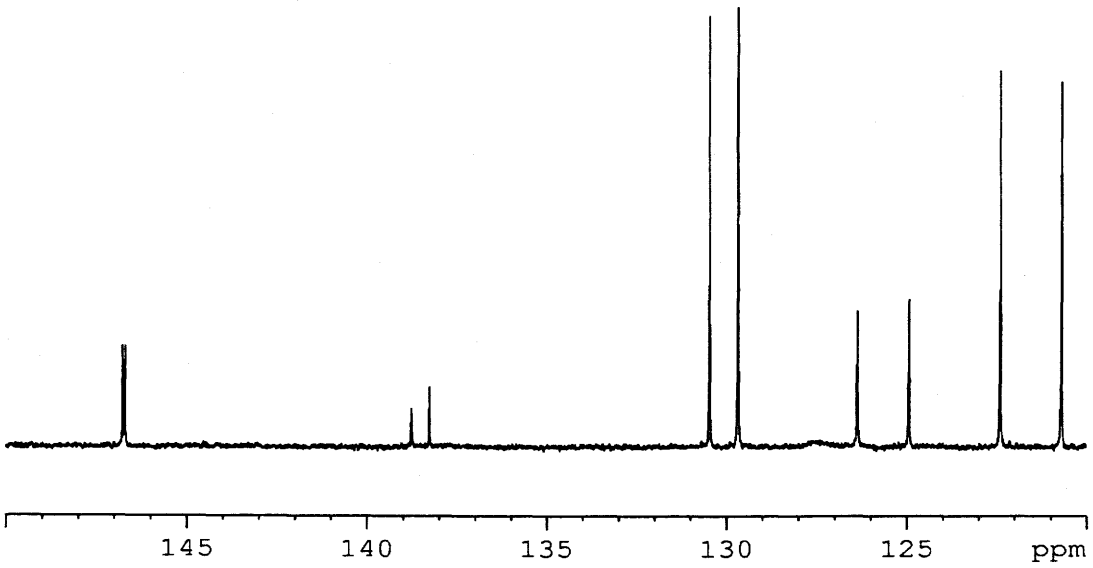

b) Close-up of the "*para* sulfonated diphenylpicryl hydrazine" region

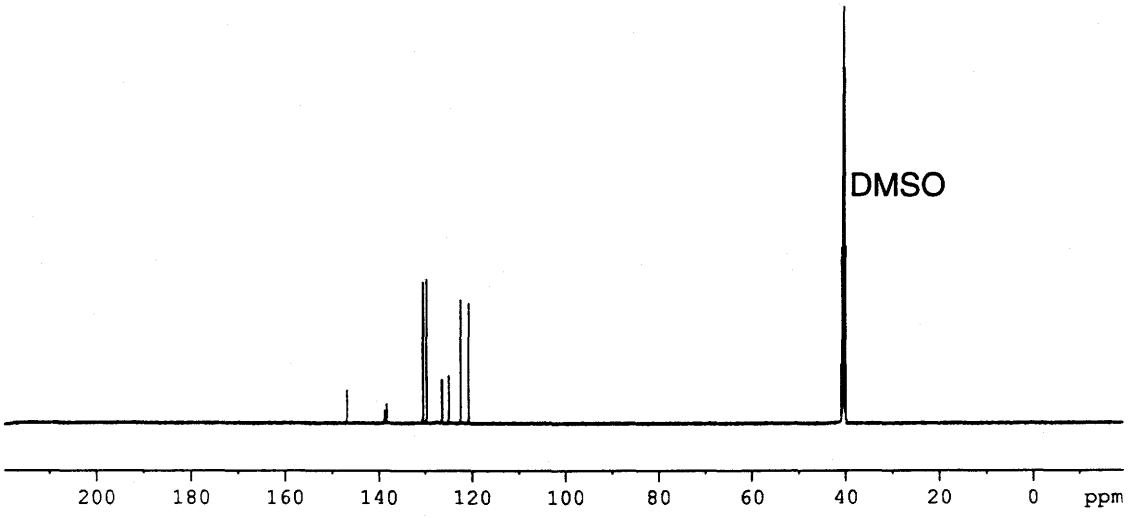

a) The full spectrum

Figure 37: 500 MHz ^{13}C NMR spectrum of DPH-DP4SH in DMSO-d6 (in air, at room temperature, at 125.80 MHz)

Kamlet-Taft solvatochromic parameters

Kamlet-Taft solvatochromic parameters [KAAT83] are employed to study the relationship between solute and solvent in liquid solutions. These parameters are: π^*, a scale which measures the solvent's ability to stabilize a charge or a dipole (dipolarity/ dipolarizability of the solvent); β, a scale which assesses the solvent's ability to donate a pair of electrons (accept a proton) to a solute-solvent hydrogen bond; and α, a scale which gauges the solvent's ability to donate a proton to a solute-solvent bond [KAAT83].

Previous studies by our group employed proton NMR techniques to investigate liquid-solutions of DH_2-H [TW90]. That work demonstrated a quite good correlation between the Kamlet-Taft parameter β of the solvent and certain experimental NMR parameters of the unsulfonated hydrazine. In that study it was observed that the chemical shift of the hydrazinic proton increases with the H-bond (i.e., proton-accepting) strength of the solvent, as measured by the β parameter. As well, the difference between the chemical shifts of the two picryl protons, at low temperature, increase with increasing β. The authors postulated that an increase in intermolecular H-bonding between the solvent and the amino proton results in a corresponding decrease of intramolecular H-bonding between that proton and an oxygen atom of a nitro group in the *ortho* position of the picryl ring (see Section 3.3). To see if these relationships extended to the sulfonated hydrazines, similar NMR experiments were conducted on K-DP4SH.

^{1}H NMR spectra of K-DP4SH in several perdeuterated solvents were acquired at low temperatures. From each spectrum, we determined the chemical shift of the hydrazinic proton (H_0 in Figure 24) and the difference between the chemical shifts of the picryl protons (H_6 and H_7), which at low temperatures resolve into two separate peaks (see the discussion of dynamic NMR in Section 1.6.2.1). A summary of our findings is presented in Table 6. The Kamlet-Taft β parameters listed were obtained from KAAT83 except that for acetic acid, which was obtained from TW90. The list is sorted by increasing β. As can be seen, we found no linear correlation between the Kamlet-Taft β scale and the NMR parameters experimentally measured for K-DP4SH.

Table 9: Summary of ^{1}H NMR parameters determined for K-DP4SH in various perdeuterated solvents, at low temperature (T), in air, and the β parameters that correspond to each solvent

Perdeuterated solvent	T (K)	β (solvent)	δ (H_0) (ppm)	δ (H_6) (ppm)	δ (H_7) (ppm)	Δ δ (H_6)-δ (H_7) (Hz)
D_2O	278.0	0.18	Not seen	8.34	7.82	262.72
Acetic acid	292.0	0.21	Not seen	Did not resolve into two peaks		N/A
Acetonitrile	230.0	0.31	10.02	8.53	8.03	253.66
Acetone	223.0	0.48	10.51	8.60	8.08	261.93
THF	210.0	0.55	10.50	8.65	8.23	99.70
Methanol	212.0	0.62	Not seen	8.66	8.11	274.86
DMSO	293.0	0.76	10.24	Did not resolve into two peaks		N/A

We extended the experiment and acquired room temperature ^{1}H NMR parameters for K-DP6SH in a variety of perdeuterated solvents. Again, no correlation between β and experimental NMR parameters were seen. However, an interesting correlation between the *ortho* and *para* sulfonated salts did emerge. As can be seen from Table 7, the chemical shift of the hydrazinic proton (H_0) in K-DP6SH is consistently downfield from the chemical shift experienced by the same proton in K-DP4SH. As you may recall (Section 3.3), in K-DP6SH the hydrazinic proton forms a hydrogen bond with an oxygen in the *ortho* sulfo group. The corresponding proton in K-DP4SH forms a hydrogen bond with an oxygen of one of the *ortho* nitro groups. The consistent upfield position of H_0 in K-DP4SH indicates that the nitro group exerts a more deshielding effect on the hydrazinic proton than does the sulfo group in K-DP6SH. For completeness, β for each solvent is listed as well.

Table 10: Comparison of the ^{1}H NMR chemical shifts for H_0 in K-DP4SH and K-DP6SH. Spectra were obtained at room temperature (298.0 K) and in air

Perdeuterated Solvent	K-DP4SH δ (H_0) in ppm	K-DP6SH δ (H_0) in ppm	Δ *para-ortho* δ (H_0) in ppm	β
Acetonitrile	9.69	9.10	0.59	0.31
Acetone	10.51	10.04	0.47	0.48
THF	9.91	9.59	0.32	0.55
Pyridine	10.76	10.57	0.18	0.64
DMSO	10.19	9.66	0.53	0.76

Dynamic NMR (^{1}H)

In the same study that showed the relationship between select proton NMR parameters and the Kamlet-Taft β scale of the solvents used [TW90], the authors reported pseudothermodynamic properties for DH_2-H as well. In a like manner, we too investigated the pseudothermodynamic properties of K-DP4SH in order to determine the energy required to break the hydrogen bond between the hydrazinic proton and an oxygen attached to an *ortho* nitro group as the molecule undergoes an intramolecular rearrangement (see Section 1.6.2.1).

As explained previously (Section 1.6.2.1), the Arrhenius model is used to determine kinetic parameters by linear regression analysis of a plot of $\ln k_T$ against T^{-1}, based on the Arrhenius equation

$$\ln k_T = \ln[k_\infty] - E_a/RT$$

where k_T is the rate parameter (obtained by the method described in Section 1.6.2.1), k_∞ is the frequency factor, E_a is the molar activation energy, R is the ideal gas constant, and T is the temperature, in Kelvin, at which k_T is determined. The slope (m) of the Arrhenius plot is equivalent to $-E_a/RT$ and the y-intercept (b) to the natural logarithm of k_∞ ($\ln k_\infty$) in the equation of the line ($y = mx + b$). As such, E_a and k_∞ are taken straight from the graph. The following equations are then used to determine the change (Δ) in standard molar activation enthalpy $\Delta H^\ddagger$, entropy $\Delta S^\ddagger$, and Gibbs free energy $\Delta G^\ddagger$,

$$\Delta H^\ddagger = E_a - RT$$

$$\Delta S^\ddagger = R\{\ln[k_\infty \hbar N_A/(eRT)]\}$$

$$\Delta G^{\ddagger} = \Delta H^{\ddagger} - T\Delta S^{\ddagger}$$

$$\text{or } \Delta G^{\ddagger} = RT\{\ln[RT/(N_A \hbar k)]\}$$

where $\hbar$ is Planck's constant, N_A is Avogadro's number, and e is the base of the natural logarithm (ln).

The 300 MHz ^{1}H NMR spectra of K-DP4SH in perdeuterated methanol, and also in D_2O, were obtained at temperatures that ranged from low (close to the freezing point of the solvent) to high (close to the boiling point of the solvent). Using the method described in Section 1.6.2.1, the rate parameters of each system (K-DP4SH in perdeuterated methanol and K-DP4SH in D_2) were determined from the spectra (one rate parameter for each temperature). An Arrhenius plot was constructed (using MS Excel) from the data and the pseudothermodynamic properties of K-DP4SH were calculated. Our findings are shown in Table 8. For comparison, three sets of kinetic properties that were presented in the previous study by our group [TW90] are also listed. These too were obtained from 300 MHz ^{1}H NMR spectra. The only difference in sample preparation is that DH_2-H samples in the earlier study were degassed; samples of K-DP4SH in this study were not degassed.

The change ($\Delta G^{\ddagger}$) in Gibbs free energy is a measure of the energy barrier that must be overcome in order for intramolecular reorientation to take place. As shown in Table 8, the energy barrier in K-DP4SH (55.44 kJ mol^{-1} in MeOH, 57.31 kJ mol^{-1} in water), is significantly lower than that found in DH_2-H. For DH_2-H, the lowest $\Delta G^{\ddagger}$ reported was that found for MeOH (62.19 kJ mol^{-1}),

and the highest was that found for bromoform (66.49 kJ mol^{-1}) [TW90]). Even so, the magnitude of $\Delta G^{\ddagger}$ for K-DP4SH in either MeOH or water is far greater than the strength of an intramolecular hydrogen bond ($\approx$ 10 kJ mol^{-1} [TW90]. As such, the intramolecular hydrogen bond cannot be the only obstacle to the conformational interchange within the molecule. This is the same situation found in DH_2-H.

Table 11: Pseudothermodynamic properties of K-DP4SH (this study) and DH_2-H [TW90] determined by 300 MHz ^{1}H NMR spectroscopy

	K-DP4SH in perdeuterated		DH_2-H (from TW90) in perdeuterated		
	Methanol	D_2O	Methanol	Benzene	Bromoform
E_a (kJ mol^{-1})	60.9	60.8	60.0	67.0	69.0
ln A (s^{-1})	31.6	30.9	28.6	30.6	30.5
$\Delta H^{\ddagger}$ (kJ mol^{-1})	58.4	58.3	57.6	64.5	66.5
$\Delta S^{\ddagger}$ (J $mol^{-1}K^{-1}$)	9.8	3.4	- 15.5	1.6	0.2
$\Delta G^{\ddagger}$ (kJ mol^{-1})	55.44	57.31	62.19	64.06	66.49

3.6 Electron Paramagnetic Resonance Spectroscopy

Relative Solubility

The sulfonated hydrazyl salts synthesized to date are all water soluble. In fact, they may be described as water-loving. They also display relatively good solubility in solvents with high Kamlet-Taft β values (>0.5). In most cases they are also reasonably soluble in solvents with β between 0.2 to 0.5. Solvents recognized as being poor in H-bond formation capability (β < 0.2) display an inconsistent ability to dissolve these salts. For example, benzene (β = 0.10) is unable to dissolve any of the three salts, whereas toluene ($\beta = 0.11$) minimally dissolves *para*-(DPH^+). Dichloromethane (β = 0) readily dissolves the *para*-(K^+) and *p*-(DPH^+) salts but the *ortho*-(K^+) salt is only slightly soluble.

Relative stability

A qualitative comparison of the EPR spectral intensity of the hydrazyls in several solvents as a function of time, temperature, presence of air and ambient light indicates that both of the *para* substituted hydrazyl salts are more stable than the *ortho*-(K+) salt. In air, at room temperature, with ambient fluorescent light, the latter completely degrades within 1 or 2 days in both acetone and water. Under such conditions the *para* salts generally retain half of their signal intensity after 3 to 4 days, sometimes for at least a week. Photochemical processes appear to be the major source of the degradation. When stored in the dark, the *ortho*-(K+) solutions maintain at least half their

original EPR intensity for several days. The *para* salts are correspondingly more stable with the exclusion of light. The presence or absence of molecular oxygen does not dramatically change the stability of any of the solute/solvent systems examined to date.

Characteristic EPR spectra of the sulfo-picrylhydrazyls

Representative liquid-solution EPR spectra of the three salts of current interest, in distilled H_2O and an organic solvent, are presented in Figures 38 to 40. For brevity, the complete set of spectra obtained in all solvents examined is not included, but the results of the spectral analysis for each solute/solvent system are presented in Tables 12 to 14. The ^{14}N hyperfine structure in the spectra show the interaction (coupling) between the lone electron and the hydrazinic nitrogen atoms. At lower modulation (0.1 G), one can even see coupling of the unpaired electron to other atoms in the molecule (super-hyperfine structure). For ease of comparison, the previously published EPR parameters for the *ortho*- and *para*- (K^+) sulfonated hydrazyl salts are included in Table 15, along with the values we determined for these salts. In each case, there is excellent agreement between our results and the literature values.

The relatively high concentration of molecular oxygen (•O–O•) in un-degassed solutions contributes to line broadening through electron-spin dipole interaction and exchange [WBW94] and is detrimental for the observation of the EPR hyperfine structure [D60]. Lowering the dissolved O_2 concentration in

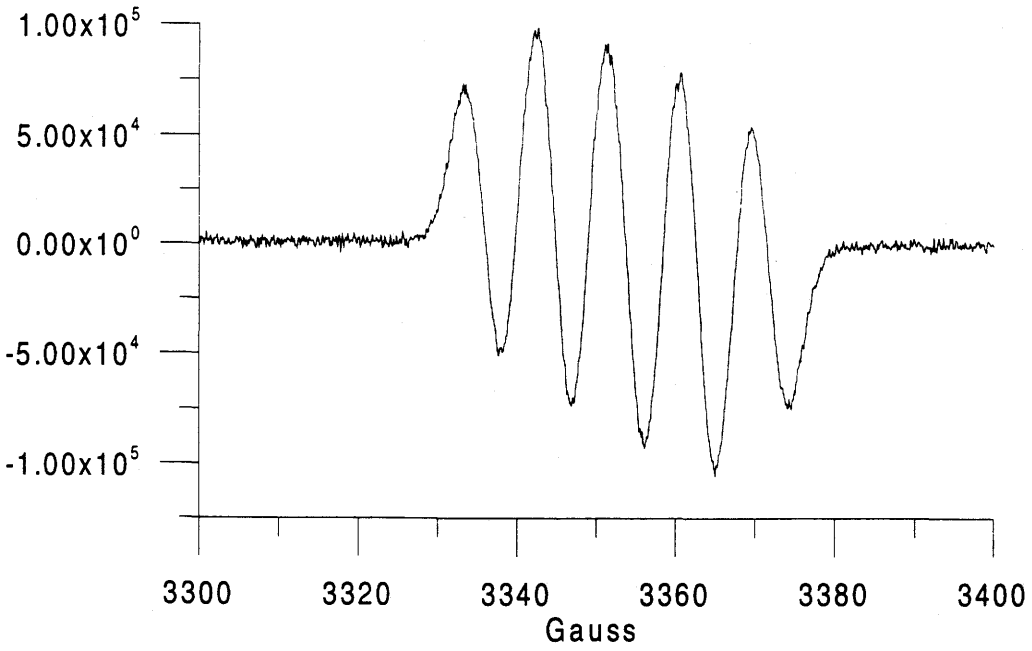

(a) degassed aqueous solution of DPH-DP4SH• ($\approx 10^{-3}$ M)

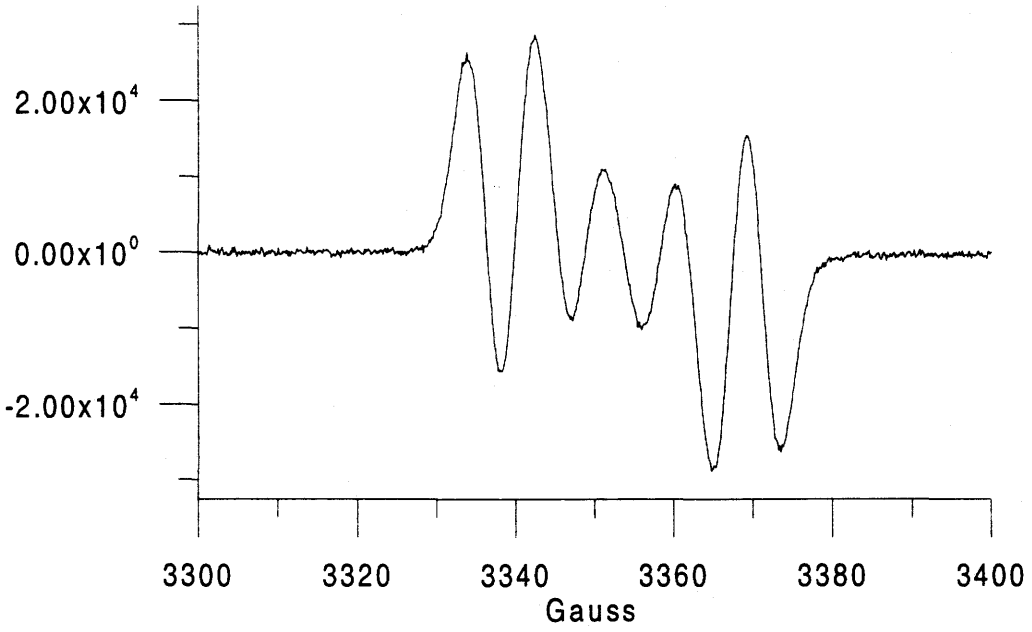

(b) degassed solution of DPH-DP4SH• in DMF ($\approx 10^{-3}$ M)

Figure 38: Characteristic liquid-solution EPR spectra of DPH-DP4SH• at room temperature

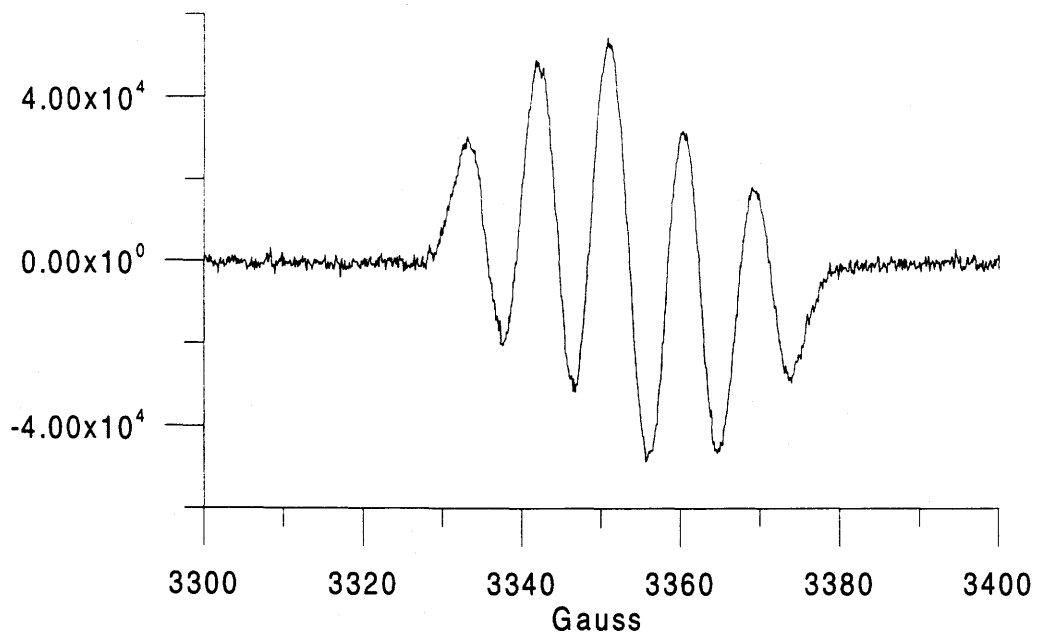

(a) aqueous solution (not degassed) of K-DP4SH• (≈ 10^{-3} M)

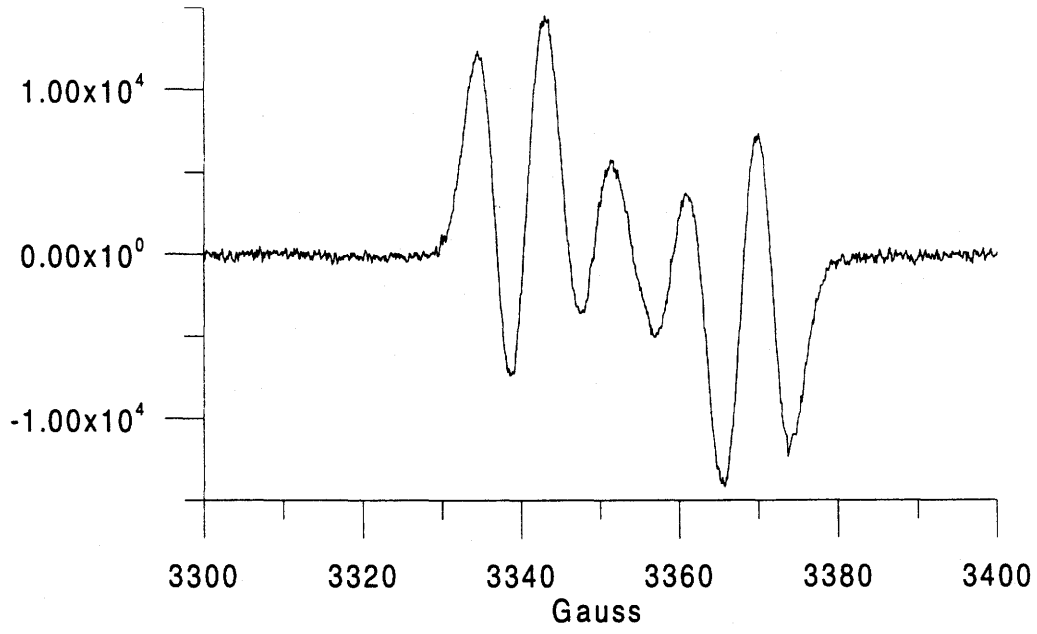

(b) degassed solution of K-DP4SH• in DMF (≈ 10^{-3} M)

Figure 39: Representative liquid-solution EPR spectra of K-DP4SH• at room temperature

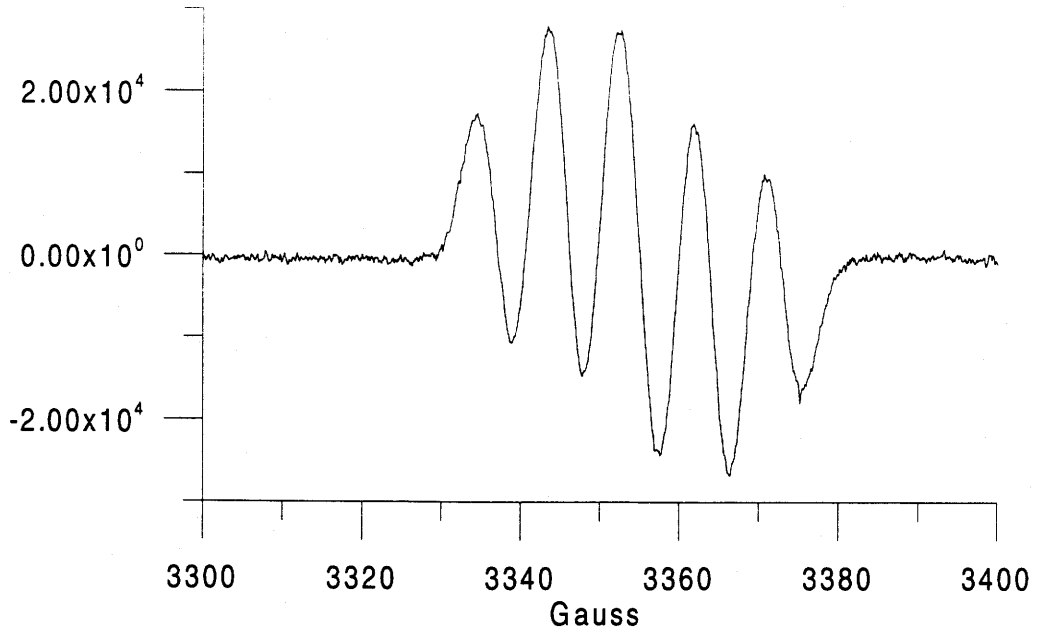

(a) degassed aqueous solution of K-DP6SH• (≈ 10^{-3} M)

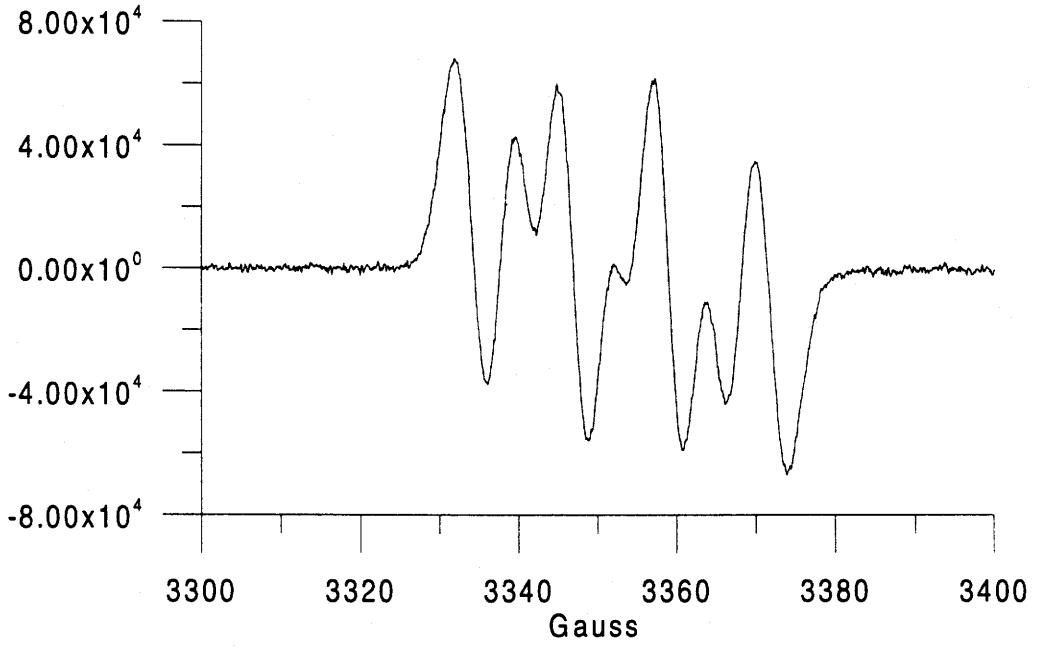

(b) degassed solution of K-DP6SH• in DMF (≈ 10^{-3} M)

Figure 40: Representative liquid-solution EPR spectra of K-DP6SH• at room temperature

dilute solutions (~ 10^{-3} M) using the degassing technique described in Section 2.5 is time-consuming. To date, not all spectra/parameters have been obtained from degassed solutions. Which solutions have been degassed is indicated in the Tables and Figures. This work is ongoing.

Table 12: EPR parameters for degassed liquid solutions of DPH-DP4SH•

Solvent	Linewidth (ΔB, Gauss)	A_i (^{14}N) (Gauss)	$A_1 + A_2$ (Gauss)	A_2 / A_1	$R \equiv A_1/(A_1+A_2)$ ca. $\propto \rho_1/\rho_0$	Frequency ν (GHz)
Distilled deionized H_2O	4.89(2)	A_2 = 7.91(1) A_1 = 9.83(1)	17.74(2)	0.805	0.554	9.40225(2)
Ethanol (100 %)	6.49	A_2 = 7.36(1) A_1 = 10.14(1)	17.50(2)	0.726	0.579	9.40136(1)
DMF	4.78(1)	A_2 = 7.16(1) A_1 = 10.16(1)	17.32(2)	0.705	0.587	9.403294(1)
1,4-Dioxane	5.60(2)	A_2 = 7.21(1) A_1 = 10.24(1)	17.45(2)	0.704	0.587	9.39982(1)
Acetonitrile	5.02(1)	A_2 = 7.18(1) A_1 = 10.21(1)	17.37(2)	0.703	0.588	9.40218(1)
Pyridine	4.91(1)	A_2 = 7.16(1) A_1 = 10.18(1)	17.34(2)	0.703	0.587	9.40227(1)
Acetone	5.23	A_2 = 7.08(1) A_1 = 10.21(1)	17.29(2)	0.693	0.591	9.39758(1)

Effect of pH

The stability of the sulfohydrazyl salts in room-temperature water as a function of pH was monitored by measuring the relative intensities of the EPR spectra upon addition of either dilute acid (0.1 M $HClO_4$ and HNO_3 were used, in

separate acidification experiments) or dilute base (0.1 M NaOH). With no evident need for accurate pH measurement, graduated-colour indicator strips (ColorpHast by EM Science) were used.

Table 13: Liquid solution EPR parameters for K-DP4SH•

Solvent	Linewidth (ΔB, Gauss)	A_i (^{14}N) (Gauss)	$A_1 + A_2$ (Gauss)	A_2 / A_1	$R \equiv A_1/(A_1+A_2)$ ca. $\propto \rho_1/\rho_0$	Frequency (ν, GHz)
Ethanol (100 %, degassed)	4.79	$A_2 = 7.32$ $A_1 = 10.21$	17.53	0.717	0.582	9.402495
DMF (degassed)	4.78(1)	$A_2 = 7.18$ $A_1 = 10.17$	17.35	0.706	0.586	9.404394(1)
Acetone (degassed)	5.16(1)	$A_2 = 7.08$ $A_1 = 10.17$	17.25	0.696	0.590	9.40289(1)
Distilled H_2O	5.19	$A_2 = 8.06$ $A_1 = 9.67$	17.73	0.834	0.545	9.399058
Acetonitrile	6.49	$A_2 = 7.23$ $A_1 = 10.12$	17.35	0.714	0.583	9.399307
Benzaldehyde	5.45	$A_2 = 7.22$ $A_1 = 10.20$	17.42	0.708	0.586	9.401609
Dioxane	5.6(1)	$A_2 = 7.31$ $A_1 = 9.94$	17.25	0.735	0.576	9.40085(1)

Increasing acidity: The *para* DPH^+ salt displays significant acidity in water (pH ~ 5.5). As the pH is lowered, a reduction in the intensity of the EPR signal is readily apparent until it is completely quenched at pH ~ 4.5.

Decreasing acidity: As the pH of the *para*-(DPH^+) solution was increased by addition of dilute NaOH, the intensity of the EPR signal was again observed to decrease, finally disappearing at pH ~ 12. Similar investigations of the potassium salts are planned.

Table 14: Liquid solution EPR parameters for K-DP6SH•

Solvent	Linewidth (ΔB, Gauss)	A_i (^{14}N) (Gauss)	$A_1 + A_2$ (Gauss)	A_2 / A_1	$R \equiv A_1/(A_1+A_2)$ ca. $\propto \rho_1/\rho_0$	Frequency ν (GHz)
Distilled deionized H_2O (degassed)	4.8(1)	A_2 = 8.14(3) A_1 = 10.15(3)	18.29(6)	0.802(5)	0.555	9.395455(9)
Dioxane (degassed)	6.7(1)	A_2 = 7.47 A_1 = 10.86	18.33	0.688	0.592	9.40285
Acetone (degassed)	5.03(1)	A_2 = 6.93(1) A_1 = 11.57(1)	18.50(2)	0.600	0.625	9.40208(1)
DMF (degassed)	4.71(1)	A_2 = 6.87(1) A_1 = 11.85(1)	18.72(2)	0.580	0.633	9.40183(1)
Ethanol (100 %)	6.2(1)	A_2 = 7.38(3) A_1 = 10.96(3)	18.34(6)	0.673(5)	0.598	9.139270(5)
Acetonitrile	6.2(1)	A_2 = 7.06(5) A_1 = 11.31(5)	18.37(10)	0.624(7)	0.616	9.397557(1)

Reversibility: Addition of either 0.1 M $HClO_4$ or HNO_3 to the water solution of the *para*-(DPH^+) salt quenched the EPR absorption, indicating disappearance of the radical anion. A concurrent colour change from purple to orange was also observed. Following neutralization of the acidic solution with 0.1M NaOH the characteristic EPR spectra of the hydrazyl reappeared. In addition, the colour of the solution reverted to the characteristic purple of the hydrazyl in solution. In contrast, while addition of 0.1M NaOH to aqueous DPH^+ quenched the EPR absorption, neutralization of the alkaline solution by dilute (0.1 M) NaOH did not result in the re-emergence of the absorption. However, the neutralized solution was oxidized by addition of MnO_2 and dioxane, and an absorption was recorded similar to, but not the same as, that for the DPH^+ salt. In the case of acidification, it may be that a dimer is created (see Figure 41).

This dimer, if in a triplet state system, would have stong interactions between the two unpaired electrons resulting in "spin pairing" and quenching of the free radical signal [WBW94, page 8]. Further studies are being developed to elucidate the evident equilibrium reactions occurring. The addition of large excess of acid or base irreversibly quenched the EPR signal. Similar experiments with the other hydrazyl salts are ongoing.

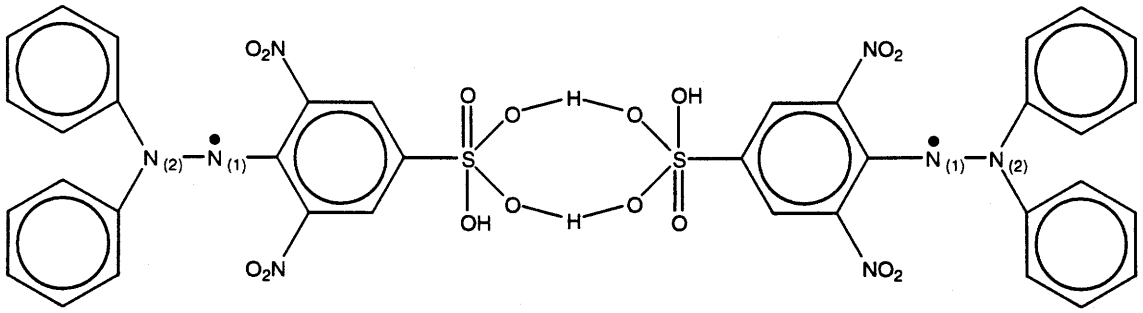

Figure 41: Possible dimerization of the *para* sulfonated hydrazyl salts upon acidification with dilute acids

Kamlet-Taft Solvatochromic Parameters and the Effect of Solvent on the EPR parameters

For reasons discussed in Section 3.5 and clarified below, the Kamlet-Taft solvatochromic parameters α, β and π^* associated with each solvent [KAT81] were used to investigate possible correlations with specific EPR parameters determined from the spectra acquired in this study. The Kamlet-Taft parameters of the solvents used in this study are listed separately at the end of this section in Table 16. These were obtained from literature sources [KAAT83].

EPR A[^{14}N] parameters determined for the hydrazyls in solution, akin to the NMR chemical shifts determined for the hydrazines, would be expected to reflect possible H-bonding between the *ortho* functional group (nitro or sulfo) and the unpaired-electron density at N_1. Such considerations led to our investigating possible correlations between the A [^{14}N] values for the three hydrazyl salts and the Taft parameters α, β and π^*.

Table 15: Comparison of literature values to current values for $A_2(^{14}N)/A_1(^{14}N)$

Salt	Solvent	Current values		Literature values [KY*etal* 63, ILSV66]	
		$A_i(^{14}N)$ (Gauss)	A_2/A_1	$A_i(^{14}N)$ (Gauss)	A_2/A_1
K-DP6SH•	EtOH (95%)	$A_2 = 7.38$ $A_1 = 10.85$	0.68	A_2 = n/a A_1 = n/a	0.68
	EtOH (70%)	$A_2 = 8.81$ $A_1 = 10.10$	0.81	A_2 = n/a A_1 = n/a	0.80
	Dioxane	$A_2 = 7.12$ $A_1 = 10.88$	0.65	$A_2 = 6.76$ $A_1 = 10.91$	0.62
K-DP4SH•	Dioxane	$A_2 = 7.31$ $A_1 = 9.94$	0.74	$A_2 = 7.19$ $A_1 = 9.98$	0.72

However, present data indicate that the sulfonated hydrazyls, like their progenitor molecules, are relatively insensitive to the H-bonding characteristics of most organic solvents (Tables 12 to 14). The relative unpaired-electron probability density ρ_1/ρ_2 for individual hydrazyls is nearly constant over a wide range of Kamlet-Taft β values (between ~ 0.3 to 0.8). Exceptions to this general observation occur when the organic solvent has poor proton-accepting

characteristics (*i.e.*, $\beta < 0.3$). In such solvents, the hydrazyls are either insoluble (or nearly so) or the EPR spectrum exhibits unresolved ^{14}N hyperfine splitting; in some cases, such splitting is not even evident.

Significance of the summed and ratio of nitrogen hyperfine parameters

Three additional parameters are included in the tables, namely, the sum of the two ^{14}N hyperfine parameters, their ratio, and a relative percentage $R[^{14}N] \equiv 100A_1/(A_1+A_2)$ of the unpaired-electron density ρ_1 at N_1 (the assumption has been made that N_1 carries the greater amount of unpaired-electron density). Previous EPR studies of diphenylpicrylhydrazyls in solution have shown that the sum is a measure of the total unpaired-electron probability density ($\rho_1 + \rho_2$) on the two hydrazinic nitrogens (N_1 and N_2) and that the ratio is close to proportional to ρ_1/ρ_2 [CDW61]. Here, the subscripts 1 and 2 follow the conventional labeling of the hydrazinic nitrogens, N_1 being attached to the picryl ring. Although the N_1 of several unsulfonated diphenylhydrazyls have been shown to carry a greater proportion of the unpaired-electron density [CDW61], no such assignment has yet been made for the sulfonated hydrazyls. We make the tentative assumption that the N_1 of the latter also has the greater unpaired-electron probability density.

Unpaired-electron distribution in aqueous solution

The detailed results (Tables 12 to 14) show that, in aqueous solutions, the sum of both $A[^{14}N]$ values (an approximate measure of the total unpaired-

electron density on the hydrazinic N atoms) is measurably different for the two varieties of the radical anion (the *ortho* version exhibiting ~ 3% greater density than the *para*). The pairs of EPR parameters A[^{14}N] determined for aqueous solutions of both the *ortho* and *para* versions indicate that approximately 55% (*i.e.*, the value of R) of the unpaired-electron density at the hydrazinic nitrogen atoms resides at N_1.

Unpaired-electron distribution in non-aqueous solutions

In organic solvents, the sums for the *ortho*- and *para*- anions are relatively insensitive to the solvent. In the case of the *ortho* anion, preliminary results indicate a slightly higher total density at the hydrazinic nitrogen atoms as compared to its aqueous solution. The *para* version has a somewhat smaller total unpaired-electron density at N_1 and N_2 in most organic solvents as compared to its aqueous solution.

The values of R determined for the sulfohydrazyls in various organic solvents show that for the *ortho* anion, the unpaired-electron density at N_1 contributes~ 62 % of the total, and for the *para* version ~ 59%. Although significantly higher than in water, the R values are generally insensitive to the H-bonding characteristics of the organic solvents, as measured by the solvatochromic Taft parameter β [KAAT83].

The evident shift of the unpaired-electron density from N_1 to N_2 in aqueous solutions, as compared to organic solutions, once again demonstrates that water is a special solvent [S97b, S2001]. For example, it could be that the

relatively small size of the H_2O solvent molecules allows a "tighter" cage, and likely more intimacy with the hydrazinic nitrogen atoms.

Table 16: Kamlet-Taft Solvatochromic Parameters

Solvent	β	α	π^*	Reference
Dichloromethane	0.00	0.30	0.82	KAAT83
Water	0.18	1.17	1.09	KAAT83
Anisole	0.22	0.00	0.73	KAAT83
Acetonitrile	0.31	0.19	0.75	KAAT83
Dioxane	0.37	0.00	0.55	KAAT83
Nitrobenzene	0.39	0.00	1.01	KAAT83
Benzaldehyde	0.44	0.00	0.92	KAAT83
Acetone	0.48	0.08	0.71	KAAT83
Tetrahydrofuran	0.55	0.00	0.58	KAAT83
Pyridine	0.64	0.00	0.87	KAAT83
Dimethylformamide	0.69	0.00	0.88	KAAT83
Ethanol	0.77	0.83	0.54	KAAT83

3.7 Bio-medical Testing

The three sulfohydrazines as well as the three sulfohydrazyls have been sent "out-of-house" for examination. As of yet, final results have not bee received. However, preliminary results from NINDS indicate that the six compounds are well tolerated in mice (up to doses of 300 mg/kg). There is evidence that K-DP6SH and K-DP4SH• are able to penetrate the central nervous system. Since many of the compounds proved to be more active in rats, further testing, in the form of rat screening, is being carried out.

3.8 Summary and Conclusions

Numerous diseases that afflict living organisms have been linked to cellular/biomolecular damage caused by reactive nitrogenic and oxygenic species, many of which are free radicals. In response, we have synthesized stable water-soluble free radicals that could, in theory, act as free-radical scavengers *in vivo* and detect, decrease or eliminate harmful free-radical activity. These water-soluble free radicals are analogs of the well-known free radical DH_2•. As well, the diamagnetic precursors of the water-soluble free radicals were also synthesized.

In summary, the following was accomplished:

- Preparation of picryl-substituted sulfohydrazine salts
    - Substitution at the *ortho* position on the picryl ring

        - Synthesis of the K^+ salt
        - Ample supply and detailed description of synthesis
    - Substitution at the *para* position on the picryl ring
        - Synthesis of the K^+ salt and a DPH^+ salt
        - Ample supply and detailed description of synthesis
- Preparation of picryl-substituted sulfohydrazyl salts
    - Substitution at the *ortho* position on the picryl ring
        - Synthesis of the K^+ salt
        - Ample supply and detailed description of synthesis
    - Substitution at the *para* position on the picryl ring
        - Synthesis of the K^+ salt and a DPH^+ salt
        - Ample supply and detailed description of synthesis
- Characterization of the compounds synthesized
    - Melting points were obtained for all compounds synthesized
    - Elemental analyses were performed for all compounds synthesized
    - Uv-visible light spectra were obtained for all the compounds synthesized
    - Confirmation of structure and purity by crystallography was achieved for the diamagnetic sulfohydrazine salts only
    - NMR parameters for the diamagnetic sulfohydrazine salts (spectra and interpretation) were obtained
    - EPR parameters for the paramagnetic sulfohydrazyl salts (spectra and interpretation) in liquid solution were obtained

While solids of the synthesized sulfohydrazyl salts were obtained, to date we have been unable to obtain appropriate crystals for x-ray diffraction studies. We are still working at purifying the sulfohydrazyls in order to acquire crystals for confirmation of their structure. Although culturing of cell lines was accomplished, toxicology of the synthesized diamagnetic and paramagnetic sulfo salts has not, as yet, been done. However, the molecules were sent "out-of-house" for biomedical testing in April 2002. Final results have not yet been received. As well, experiments to determine the reactions of the sulfohydrazines and sulfohydrazyls are only in preliminary stages.

4. IDEAS FOR FUTURE RESEARCH

The scope of this research project was very extensive and could easily have been extended to a Ph.D. program. However, as much as could be, was accomplished as an M.Sc. program. As a result, ideas for future research are mostly self-evident.

Some suggestions for future research, in order of priority are:

- Purification of the synthesized sulfohydrazyl salts and acquisition of crystals suitable for x-ray diffraction studies.
    - The purity of these free radicals is required for biomedical testing. The acquisition of crystals is an indication of the purity of molecules and will confirm their molecular structure.
    - This could be accomplished by experimenting with other oxidizing agents (i.e., $Pb(OAc)_4$, or by the electrochemical generation of the free radicals thus eliminating the need to remove excess oxidant from the molecules.
- Reactions of the synthesized molecules (both paramagnetic and diamagnetic species).
    - We need to determine the reactivity of both the diamagnetic and the paramagnetic salts (Fenton Reaction, $NO_2\bullet$).
- Titration/reduction of the sulfohydrazyls by TSA and other reducing agents such as H_2O_2 and V_2O_5 gel.

- Determination of the potential of the synthesized sulfohydrazyls as free-radical scavengers (antioxidants).
- Measurement of actual solubilities in H_2O of both the sulfo- hydrazines and hydrazyls.
- Biomedical testing of the diamagnetic and paramagnetic salts
    - Evaluate toxicity in cell lines (PC-12 and SH-SY5Y cell lines) by use of the MTT assay and, later, in primary cells.
    - Evaluate anticonvulsant activity in chicken models of epilepsy in collaboration with Dr. J. Tucheck, Department of Pharmacology, University of Saskatchewan.
    - Evaluate anticancer activity in appropriate cell lines in collaboration with Dr. R. A. Hickie, Department of Pharmacology, University of Saskatchewan.
- Synthesis of the protonated (H^+) forms of these molecules as well as synthesis of other salts (i.e., Na^+, Li^+, ...)
- Determination of the effect on the stability of these molecules by substitution (i.e., OH, SO_3, $NO_2\bullet$, halogens) at the *para* diphenyl position.
- Elucidation of the unpaired-electron density by isotopic ^{15}N at one of the hydrazinic nitrogen positions.
- Determination of the extent of delocalization experienced by the unpaired electron in DPH-DP4SH• by ENDOR
    - Does the unpaired electron spend any time on the DPH cation?

- Further pH and kinetic studies of the sulfohydrazyls to clarify what happens during acidification/basification.
    - Does dimerization occur with acidification?
    - What is produced when the hydrazyl is basified, neutralized, then oxidized?
- Further investigation into correlating sulfohydrazine NMR parameters and sulfohydrazyl EPR data with Kamlet-Taft solvatochromic parameters
    - Respective parameters of the sulfo- hydrazines and hydrazyls really don't seem to correlate too well at this time. Is this a consequence of the "water-loving" nature of these molecules?

5. REFERENCES

ADKB2000 Arefiev D.V., Domnina N.S., Komarova E.A., Bilibin A.Y., Sterically hindered phenol-dextran conjugates: radical scavenging activity in water and water-organic media. *Eur. Polym. J.*, 2000, **36**, 857-860.

AV57 Arbuzov A.E., Valitova F.G., Some details of the preparation of the free radical 2,2-diphenyl-1-trinitrophenylhydrazyl. *Zhur. Obshchei Khim.* 1957, **27**, 2354-2356.

B58 Blois M., Antioxidant determination by the use of a stable free radical. *Nature* (London), 1958, **181**, 1199-1200.

B65 Buchachenko A.L., Stable Radicals, 1965, Consultants Bureau, New York, NY, U.S.A.

B78 Baranyovits F.L.C., Cochineal carmine: an ancient dye with a modern role. *Endeavour*, 1978, **2**(2), 85-92.

BCB95 Brand-Williams W., Cuvelier M.E., Berset C., Use of a free radical method to evaluate antioxidant activity. *Food Sci. Technol.: Lebensm.-Wiss. u. Technol.*, 1995, **28**(1), 25-30.

BFMB61 Balaban A.T., Frangopol P.T., Marculescu M., Bally J., Factors affecting stability and equilibria of free radicals: steric factors in hydrazyls. *Tetrahedron*, 1961, **13**, 258-267.

BHS73 Biedler J.L., Helson L., Spengler B.A., Morphology and growth, tumorigenicity, and cytogenetics of human neuroblastoma cells in continuous culture. *Cancer Res.*, 1973, **33**, 2643-2652.

BNQRWZ99 Brown K.C., Nelson B.R., Quail J.W., Robertson B.E., Weil J.A., Zimpel Z., The structure and some molecular properties of acetone-picrylhydrazone. *Can. J. Chem.*, 1999, **77**, 1295-1304.

BR-TSF78 Biedler J.L., Roffler-Tarlov S., Schachner M., Freedman L.S., Multiple neurotransmitter synthesis by human neuroblastoma cell line and clones. *Cancer Res.*, 1978, **38**, 3751-3757.

BS86 Bax A., Summers M.F., ^{1}H and ^{13}C assignments from sensitivity-enhanced detection of heteronuclear multiple-bond connectivity by 2D multiple quantum NMR. *J. Am. Chem. Soc.*, 1986, **108**, 2093-2094.

BTW98 Brown K.C., Tyson R.L., Weil J.A., Conformation Interchange in nuclear magnetic resonance spectroscopy. *J. Chem. Ed.*, 1998, **75**, 1632-1635.

BW86 Brown K.C., Weil J.A., Preparation of 2,2-diphenyl-1-picrylhydrazyls using potassium permanganate. *Can. J. Chem.*, 1986, **64**, 1836-1838.

C64 Carrington, A., Orbital degeneracy and spin resonance in free-radical ions. *Roy. Inst. Chem. (London), Lecture Ser.*, 1964, (3), 1-22.

CDW61 Chen M.M., D'Adamo Jr. A.F., Walter R.I., The preparation of substituted 1-picryl-2,2-diphenylhydrazyl free radicals. *J. Org. Chem.* 1961, **26**, 2721-2727.

CQRW83 Currie P.F., Quail J.W., Rusk A.C.M., Weil J.A., A study of Br/NO_2 substitution reactions and nuclear magnetic resonance of 2,2-diaryl-1-picrylhydrazines. *Can. J. Chem.*, 1983, **61**(8), 1760-1765.

CS99 Chen S.X., Schopfer P., Hydroxyl-radical production in physiological reactions: a novel function of peroxidase. *Eur. J. Biochem.*, 1999, **260**(3), 726-735.

Cweb2002 Chapdelaine J.M., "MTT reduction – a tetrazolium-based colorimetric assay for cell survival and proliferation". From http://www.moleculardevices.com/pdfs/maxline_05.pdf on 31-JAN-02, Pharmakon Research International, Inc.

D60 Deguchi Y., Proton hyperfine spectra of diphenylpicrylhydrazyl (DPPH). *J. Chem. Phys.*, 1960, **32**, 1584-1585.

DAKB99 Domnina N., Aref'ev D., Komarova E., Bilibin, A., Dextran as antioxidant's activity carrier. *Macromol. Symp.*, 1999, **144**, 339-350.

DO71 Dearden J.C., Odusina A.O., A stable free radical for the investigation of hydrogen abstraction reactions in aqueous solutions. *J. Pharm. Pharmac.*, 1971, **23**, *Suppl.*, 217S.

EN92 Enraf-Nonius (1992). CAD-4 EXPRESS. Version 1.1. Enraf-Nonius, Delft, The Netherlands.

ENGM80 Eisner T., Nowicki S., Goetz M., Meinwald J., Red cochineal dye (carminic acid): its role in nature. *Science*, 1980, **208**(4447), 1039-1042.

F1891 Fischer P., About *p*-chloro-*m*-nitrobenzenesulfonic acid and a-*o*-chloro-*m*-nitrobenzenesulfonic acid. *Berichte*, 1891, **24**(2), 3185-3197.

F76 Fatiadi A.J., Active manganese dioxide oxidation in organic chemistry – Parts I and II. *Synthesis*, 1976, (2), 65-104, (3), 133-167.

FHT68 Forrester A.R., Hay J.M., Thomson R.H., Organic Chemistry of Stable Free Radicals. 1968, Academic Press Inc. Ltd., London, England.

G63 Glavind J., Antioxidants in animal tissue. *Acta Chem. Scand.*, 1963, **17**, 1635-1640.

G90 Griscom, D.L., Electron spin resonance. *Glass: Sci. Technol.*, 1990, **4**(B), 151-251.

GFCP98 Greene L.A., Farinelli S.E., Cunningham M.E., Park D.S., "Culture and experimental use of the PC12 rat pheochromocytoma cell line", in Baker E., Goslin K., Eds., Culturing Nerve Cells. 2nd ed., 1998, Cambridge, Massachusetts, U.S.A.: The MIT Press, 161-188.

GR22 Goldschmidt S., Renn K., Amine oxidation. IV. 2,2-Diphenyl-1-trinitrophenylhydrazyl. *Berichte*, 1922, **55**B, 638-643.

GS64I Glavind J. and Sondergaard E., Studies on the effects of the nutrition on antioxidant levels of the body. I. Tissue antioxidants in chicks on an encephalomalacia-producing diet. *Acta Chem. Scand.*, 1964, **18**, 2173-2178.

GS64II Glavind J. and Sondergaard E., Studies on the effects of the nutrition on antioxidant levels of the body. II. Antioxidant levels in livers of rats on a necrogenic diet. *Acta Chem. Scand.*, 1964, **18**, 2179-2181.

Harms2001 From a memorandum to Dr. J.S. Richardson from Diane Harms, UST Inc., October 4, 2001.

HB98 Higgins D., Banker G., "Primary dissociated cell cultures", in Baker E., Goslin K., Eds., Culturing Nerve Cells. 2nd ed., 1998, Cambridge, Massachusetts, U.S.A.: The MIT Press, 37-78.

HBO2000 Hall S.R., du Boulay D.J., Olthof-Hazekamp R. (2000) Eds. The Xtal 3.7 System, University of Western Australia, Australia.

HG99 Halliwell B., Gutteridge J.M.C., Free Radicals in Biology and Medicine. 3rd ed., 1999, Oxford University Press, New York, NY, U.S.A.

HJ91 Hurd R.E., John B.K., Gradient-enhanced proton-detected heteronuclear multiple-quantum coherence spectroscopy. *J. Mag. Res.*, 1991, **91**, 648-653.

I58 Ingram D.J.E., Free Radicals as Studied by Electron Spin Resonance. 1958, Butterworths Scientific Publications, London, England.

ICB2000 Ionita P., Caproiu M.T, Balaban A.T., New sulfonyl derivatives of 2,2-diphenyl-1-picrylhydrazyl and their supramolecular complexes with crown ethers and kryptands. *Rev. Roum. Chim.*, 2000, **45**(10), 935-941.

IISL2001 Ionita G., Ionita P., Sahini V.Em., Luca C., Influence of cyclodextrins on the kinetics of oxidation of amino acids and BSA by hydrazyl radicals. *J. Incl. Phenom. Macrocyc. Chem.*, 2001, **39**, 269-271.

ILSV66 Il'yasov A.V., Levin Y.A., Sotnikova N.N., Valitova F.G., The electrochemical generation of hydrazyl radicals. *Theor. And Exptl. Chem.*, 1966, **2**(1), 142-143.

IM62 Ikrina M.A., Matevosyan R.O., Investigation in the field of the chemistry of free radicals of the hydrazine series. VIII. Synthesis of 2,2-diphenyl-1-(2,6-dinitro-4-sulfophenyl)hydrazyl and 2,2-diphenyl-1-(2,6-dinitro-4-sulfophenyl)hydrazyl. *J. Gen. Chem.* USSR (Engl. Transl.) 1962, **32**(12), 3878-3881.

J53 Jarrett H.S., Paramagnetic resonance absorption: hyperfine structure in dilute solutions of hydrazyl compounds. *J. Phys. Chem.*, 1953, **21**, 761-762.

J76 Johnson C.K. (1976). ORTEPII. Report ORNL-5138. Oak Ridge National Laboratory, Tennessee, U.S.A.

JHAPA90 Jalava A.M., Heikkila J, Akerlind G., Pettit G.R., Akerman K.E.O., Effects of bryostatins 1 and 2 on morphological and functional differentiation of SH-SY5Y human neuroblastoma cells. *Cancer Res.*, 1990, **50**, 3422-3428.

K98 Katzung B.G., Basic and Clinical Pharmacology. 7th ed., 1998, Appleton and Lange, Stamford.

KAAT83 Kamlet M.J., Abboud J-L.M., Abraham M.H., Taft R.W., Linear solvation energy relationships. 23. A comprehensive collection of the solvatochromic parameters π^*, α, β, and some methods for simplifying the generalized solvatochromic equation. *J. Org. Chem.*, 1983, **48**, 2877-2887.

KAT81 Kamlet M.J., Abboud J.L.M., Taft R.W., An examination of linear solvation energy relationships. *Prog. Phys. Org. Chem.*, 1981, **13**, 485-630.

KJGS93 Krabill K., Jamison J.M., Gilloteaux J., Summers J.L., Subcellular localization and antiviral activity of carminic acid/poly r(A-U) combinations. *Cell Biol. Int.*, 1993, **17**(10), 919-934.

KMOW98 Kellner R., Mermet J.-M., Otto M., Widmer, H.M., Eds., Analytical Chemistry: The Approved Text to the FECS Curriculum Analytical Chemistry. 1998, Wiley-VCH Verlag GmbH, D-69469 Weinheim, Germany.

KS95 Kocherginsky N., Swartz H.M., Nitroxide Spin Labels: Reactions in Biology and Chemistry. 1995, CRC Press, Boca Raton, FL, U.S.A.

KvLdE2002 Koleva I.I., van Beek T.A., Linssen J.P.H., de Groot A., Evstatieva L.N., Screening of plant extracts for antioxidant activity: a comparative study on three testing methods. *Phytochem. Anal.*, 2002, **13**(1), 8-17.

KY*etal*63 Kozyrev B.M., Yablokov Y.V., Matevosyan R.O., Ikrina M.A., Il'yasov A.V., Ryzhmanov Y.M., Stashkov L.I., Shatrukov L.F., Electron paramagnetic resonance of substituted diphenylpicryl-hydrazyls. *Optics and Spectrosc.*, 1963, **15**, 340-345.

L2001 Letourneau P.C., "Preparation of substrata for *in vitro* culture of neurons", in Fedoroff S., Richardson A., Eds., Protocols for Neural Cell Cultures. 3rd ed., 2001, Humana Press, Totowa, NJ, U.S.A., 245-254.

L77 Lillie R.D., Ed., Natural Dyes. In: H.J. Conn's Biological Stains. 9th ed., 1977, Williams and Wilkins, Baltimore, MD, U.S.A., 458-488.

L-BH69 Lynden-Bell R.M., Harris R.K., Nuclear Magnetic Resonance Spectroscopy. 1969, Thomson Nelson and Sons Ltd., London, England.

LC77 Leyden D.E., Cox R.H., Analytical Applications of NMR. 1977, John Wiley & Sons, Inc., New York, NY, U.S.A.

LLP99 Leonard J., Lygo B., Procter G., Advanced Practial Organic Chemistry. 2nd ed., 1999, Blackie Academic & Professional.

LO69 Leibler K., Okon K., Possible new standards for electron paramagnetic resonance. *J. Chim. Phys. Physiochim. Biol.*, 1969, **66**(7-8), 1316-1317.

LRF99 Lawson J.A., Rokach J., FitzGerald G.A., Isoprostanes: formation, analysis and use as indices of lipid peroxidation *in vivo*. *J. Biol. Chem.*, 1999, **274** (35), 24441-24444.

M71 McKenzie R.M., The synthesis of birnessite, cryptomelane, and some other oxides and hydroxides of manganese. *Min. Mag.* 1971, **38**, 493-502.

M83 Mosmann, T., Rapid colorimetric assay for cellular growth and survival: applications to proliferation and cytotoxicity assays. *J. Immunol. Methods*, 1983, **65**, 55-63.

MIC61 Matevosyan R.O., Ikrina M.A., Chirkov, A.K., Investigation in the field of the chemistry of free radicals of the hydrazine series. V. Synthesis of 2,2-diphenyl-1-(2,6-dinitrophenyl)hydrazyl and 2,2-diphenyl-1-(2,4-dinitrophenyl)hydrazyl and the study of their chemical and physical properties. *J. Gen. Chem. U.S.S.R.*, 1961, **31**(11), 3301-3305.

MSHB2001 Murayama K., Singh N.N., Helmrich A., Barnes D.W., "Neural cell lines", in Fedoroff S., Richardson A., Eds., Protocols for Neural Cell Cultures. 3rd ed., 2001, Humana Press, Totowa, NJ, U.S.A., 219-228.

MVP71 Meloan S.N., Valentine L.S., Puchtler H., On the structure of carminic acid and carmine. *Histochemie*, 1971, **27**, 87-95.

MW2001 Mombourquette M.J., Weil J.A. (2001). Fortran Computer Program EPR-NMR, Version 6.50. Department of Chemistry, University of Saskatchewan, Saskatoon, SK, Canada.

PLTRF98 Pratico D., Lee V.M.-Y., Trojanowski J.Q., Rokach J., FitzGerald G.A., Increased F_2-isoprostanes in Alzheimer's disease: evidence for enhanced lipid peroxidation *in vivo*. *FASEB*, 1998, **12**, 1777-1783.

PM74 Putirskaya G.V., Matus Mrs. L., Reactions of stable SDPPH [2-phenyl-2-(*p*-sulfophenyl)-2-picrylhydrazyl sodium salt] radicals with hydroxide ions. I. Determination of the alkali consumption and evidence of hydrogen peroxide formation. *Magy. Kem. Foly.*, 1974, **80**(6), 241-246.

PMLSJ91 Pahlman S., Meyerson G., Lindgren E., Schalling M., Johansson I., Insulin-like growth factor I shifts from promoting cell division to potentiating maturation during neuronal differentiation. *Proceedings of the National Academy of Sciences of the United States of America*, 1991, **88**, 9994-9998.

PS71 Putirskaya G.V., Szilagyi J., Synthesis of *p*-sulfo-2,2'-diphenyl-1-picrylhydrazyl and *p,p'*-disulfo-2,2'-diphenyl-1-picrylhydrazyl. *Magy. Kem. Foly.*, 1971, **77**(12), 659-663.

PV74 Putirskaya G.V., Vinkler P., Reactions of stable SDPPH [2-phenyl-2-(*p*-sulfophenyl)-1-picrylhydrazyl sodium salt] radicals with hydroxide ions. IV. Synthesis of the hydroxy derivative of SDPPH. *Magy. Kem. Foly.*, 1974, **80**(6), 246-249.

QWS2000 Quail J.W., Weil J.A., Singh M.P., 2,2-Dimethyl-1-(2,4,6-trinitrophenyl)hydrazine. *Acta Cryst.*, 2000, **C56**, 235-236.

R86 Rahman A.U., Nuclear Magnetic Resonance: Basic Principles. 1986, Springer-Verlag, New York, NY, U.S.A.

RMEAJP85 Ruusala A.I., Mattsson M., Esscher T., Abrahamsson L., Jergil B., Pahlman S., 12-O-tetradecanoyl-phorbol-13-acetate-induced differentiation of human neuroblastoma cells is not accompanied by an increase in the intracellular concentration of cyclic AMP. *Brain Res.*, 1985, **350**(1-2), 27-35.

RVMGCZ92 Ruiz-Cabello J., Vuister G.W., Moonen C.T.W., van Gelderen P., Cohen J.S., van Zijl P.C.M., Gradient-enhanced heteronuclear correlation spectroscopy: theory and experimental aspects. *J. Mag. Res.*, 1992, **100**, 282-302.

RW51 Rabinowitz J.L., Wagner E.C., Restriction of tautomerism in the amidine system by hydrogen bonding: the case of 4 (7)-nitrobenzimidazole. *J. Am. Chem. Soc.* 1951, **73**, 3030-3037.

RWin97 Reich H.J., WinDNMR: NMR Spectrum Calculations, Version 1.50, *J. Chem. Educ. Software*, 1997.

S2001 Schmid R., Recent advances in the description of the structure of water, the hydrophobic effect, and the like-dissolves-like rule. *Monatsh. für Chem.*, 2001, **132**, 1295-1326.

S79 Svehla G., Ed., Vogel's Textbook of Macro and Semimicro Qualitative Inorganic Analysis. 5th ed., 1979, Longman Group Limited, London, England and New York, NY,U.S.A.

S82 Sandström J., Dynamic NMR Spectroscopy. 1982, Academic Press, Toronto, Ont., Canada.

S97a Sheldrick G.M. (1997) SHELXLS97 and SHELXL97. University of Göttingen, Germany.

S97b Symons, M.C.R. 1997, The Whelen Lecture Series, University of Saskatchewan

SciFS2000 SciFinder Scholar, Version 2000, 0, 0, 0; copyright © 1995-1997 American Chemical Society, Chemical Abstracts Service.

SHBB2002 Schlesier K., Harwat M., Bohm V., Bitsch R., Assessment of antioxidant activity by using different *in vitro* methods. *Free Rad. Res.*, 2002, **36**(2), 177-187.

T57 Thomson, R.H., Naturally Occurring Quinones. 1957, Butterworth's Scientific Publications, London, England.

TJWE95 Taylor D.D., Jortner B.S., Walton A. Ehrich M., An immunohistochemical study of the cytoskeleton of SH-SY5Y human neuroblastoma cells, and the effects of acrylamide. *In Vitro Toxicol.*, 1995, **8**, 323-333.

TW90 Tyson R.L., Weil J.A., Effect of solvent on intramolecular reorientation in 2,2-diphenyl-1-(2,4,6-trinitrophenyl)hydrazine. *J. Phys. Chem.*, 1990, **94**, 3951-3958.

TZY99 Tieu K., Zuo D.M., Yu P.H., Differential effects of staurosporine and retinoic acid on the vulnerability of the SH-SY5Y neuroblastoma cells: the involvement of Bcl-2 and p53 proteins. *J. Neurosci. Res.*, 1999, **58**, 426-435.

UEWKH09 Ullman F., Engi G., Wosnessensky E., Kuhn E., Herre E., Aromatic compounds with labile hydrogen. *Liebig's Annalen* 1909, **366**, 79-118. Translated from the German by J.A. Weil, March 1995.

UJ09 Ullman F., Juengel K., About amino-oxy-diphenylamine. *Berichte*, 1909, **42**(1), 1077-1083. Revised by T. Bergfeldt, August 1995.

W91 Wade L.G. Jr., Organic Chemistry. 2nd ed., 1991, Prentice-Hall, Inc., Englewood Cliffs, NJ, U.S.A.

WA65 Weil J.A., Anderson J.K., The determination and reaction of 2,2-diphenyl-1-picrylhydrazyl with thiosalicylic acid. *J. Chem. Soc.*, 1965, Oct., 5567-5570.

WBRW91 Wang H., Barton R.J., Robertson B.E., Weil J.A., Structural studies of 2,2-diphenyl-1-picrylhydrazine: a clathrate-forming compound. *J. Incl. Phenom. Mol. Recog. Chem.*, 1991, **10**, 203-217.

WBW94 Weil J.A., Bolton J.R., and Wertz J.E., Electron Paramagnetic Resonance: Elementary Theory and Practical Applications. 1994, John Wiley & Sons, Inc., New York, NY, U.S.A.

WJ62 Weil J.A., Janusonis G. A., The alkali salts of 2,2-diphenyl-1-picrylhydrazine. *J. Org. Chem.*, 1962, **27**, 1248-1250.

WLKB93 Willker W., Leibfritz D., Kerssebaum R., Bermel W., Gradient selection in inverse heteronuclear correlation spectroscopy. *Mag. Res. Chem.*, 1993, **31**, 287-292.

WSK61 Weil J.A., Sane K.V., Kinkade J.M. Jr., The reaction between 2,2-diphenyl-1-picrylhydrazyl and nitrogen dioxide. *J. Phys. Chem.*, 1961, **65**, 710-712.

Y96 Yordanov, N.D., Is our knowledge about the chemical and physical properties of DPPH enough to consider it as a primary standard for quantitative EPR spectrometry? *Appl. Magn. Reson.*, 1996, **10**, 339-350.

ZRMW95 Zhou Y., Richardson J.S., Mombourquette M.J., Weil J.A., Free radical formation in autopsy samples of Alzheimer and control cortex. *Neurosci. Lett.*, 1995, **195**, 89-92.

APPENDICES

A1 Toxicology of the Sulfo- Hydrazines and Hydrazyls

A1.1 The PC-12 Cell Line

PC12 cells are routinely used as models in the study of neuronal cell function and differentiation. Differentiation is the developmental process by which a cell takes on its specialized function. PC12 cells are an immortal (cancerous) cell line derived from a rat pheochromocytoma, a catecholamine-secreting tumour of the chromaffin tissue of the adrenal gland. There is good reason for the widespread use of PC12 cells as, prior to differentiation, they exhibit many of the neuron-like properties of chromaffin cells, their non-cancerous counterparts. They are able to synthesize, store, release and uptake the neurotransmitters dopamine and noradrenaline (but not adrenaline), to express choline acetyltransferase and tyrosine hydroxylase, and to develop additional neuron-like traits in response to the presence of mitogens like nerve-growth factor or cAMP (cyclic adenosine-3',5'-monophosphate). After differentiation is induced, they also share many common characteristics with sympathetic neurons [GFCP98, MSHB2001].

The cell line itself is reasonably stable and homogeneous. The PC12 cell model is used in a wide range of studies that include neurotoxicology, hypoxia and oxidative stress reactions, neuronal-substratum and neuronal-receptor

interactions, neurotransmitter synthesis and storage, and apoptosis (programmed cell-death) [GFCP98, MSHB2001].

PC12 cells are anchorage-dependent and must adhere to the culture substratum in order to flourish. The sterile *in-vitro* tissue-culture vessels used are made of bacteriological-grade plastic that have been treated to be hydrophilic. The resultant overall negative surface charge repels the anionic groups of a myriad of glycolipids and glycoproteins contained on the neuronal surface. As such, PC12 cells do not stick well to polystyrene, and the culture flasks must be coated with an appropriate macromolecule (e.g. collagen) to which the cells can adhere. The culture flask must also be transparent (which polystyrene is) to facilitate observation by conventional light microscopy [L2001].

Collagen, a macromolecule and the most plentiful protein in the human body, is an extracellular matrix molecule (ECM) composed of large complicated proteins and protein complexes. Other ECMs include fibronectins, laminins, tenascins, thrombospondins, and proteoglycans. Although the understanding of ECMs is incomplete, it is known that *in vivo* they are active contributors to cellular adhesions and contacts, and that they are an essential component in the regulation of cell metabolism and signalling. Collagen, as well as other extracellular matrix molecules, has a considerable variety of suitable binding domains that form a connecting link for interactions with other ECM components and molecules on the surface of the cell, including receptors [L2001].

A1.1.1 **Preparation of PC-12 Cell Cultures**

The PC12 cells have been donated by Dr. X.-M. Li from the Neuropsychiatric Research Unit, University of Saskatchewan, Saskatoon, SK, Canada. The cells had been ordered from the American Type Culture Collection (ATCC # CRL-1721). PC12 cells from ATCC are from a male rat. The cells are seeded on collagen-coated tissue-culture flasks containing RPMI-1640 with 10 % horse serum (HS), 5 % fetal bovine serum (FBS), penicillin 25 U/mL, and streptomycin 25 µg/mL. They are then incubated at 37 °C in 95 % air and 5 % CO_2, and the medium changed every other day. When the cells are confluent, they are flushed from the flask with a stream of medium from a pipette. The suspension is transferred to new flasks. All cells used for the experiments should be within 8 passages of each other.

Each of the synthesized sulfo- hydrazines and hydrazyls need to be tested for their concentration-dependent cytotoxicity. When enough cells are cultured (2×10^4 cells), they are plated in collagen-coated tissue-culture 96-well plates with 100 µL RPMI-1640/10 % FBS. Twenty-four hours later, the medium is replaced with solutions of the synthesized salts dissolved in medium to give a range of concentrations. After another twenty-four hours, cell viability is determined by the MTT assay (see Section A1.3).

A1.2 <u>The SH-SY5Y Cell Line</u>

The SH-SY5Y cell line is a neuroblast-like third-generation clonally derived subline (SK-N-SH → SH-SY → SH-SY5 → SH-SY5Y) of the

neuroepithelioma cell line SK-N-SH [BR-TSF78]. Established in 1970, the parent cell line (SK-N-SH) is of neuronal origin and was derived from the bone-marrow biopsy of a four-year-old girl (Caucasian) with a metastatic neuroblastoma [BHS73]. A neuroblastoma is a malignant tumour, usually of childhood, derived from immature ganglion cells, and commonly found in the adrenal medulla and retroperitoneal tissue. Both the parent line and the SH-SY5Y line are immortal cell lines.

Human SH-SY5Y neuroblastoma cells resemble mature adrenergic neurons and exhibit moderate levels of dopamine-β-hydroxylase activity [BR-TSF78], an enzyme that is used in the biosynthesis of adrenergic transmitters (e.g., dopamine, noradrenaline, and adrenaline) and found only in sympathetic nervous tissue [BHS73]. SH-SY5Y cells are able to convert tyrosine to dopamine but do not form noradrenaline even though dopamine-β-hydroxylase activity is present. It is believed that something, which is found in normal adrenergic cells, is missing. One possibility offered is that noradrenaline is produced but not properly stored in vesicles therefore subject to rapid destruction by monoamine oxidase [BR-TSF78]. Although predominantly adrenergic, SH-SY5Y cells have multiple neurochemical traits and can convert choline to acetylcholine, a cholinergic characteristic [BR-TSF78].

SH-SY5Y cells can be compelled to differentiate into mature ganglion cells by treatment with various agents. These include the phorbol esters 12-O-tetradecanoylphorbo-13-acetate [RMEAJP85] and phorbol-12-myristate-13-acetate [PMLSJ91], staurosporine [TZY99], all *trans*-retinoic acid [TJWE95,

TZY99], and dibutyryl cAMP in conjunction with 3-isobutyl-1-methylxanthine [TJWE95]. Differentiation of SH-SY5Y cells is related to a greatly increased noradrenaline concentration, the expansion of long neurite-like processes, the emergence of voltage-dependent Ca^{2+} channels, a reduction in the sensitivity of muscarinic-receptors relating to agonist-induced activation of intracellular free Ca^{2+}, and a down-regulation of c-*myc* mRNA expression [JHAPA90].

SH-SY5Y cells are anchorage-independent and are uncomplicated in their substrate requirements. This is thought to be in part due to their ability to produce molecules that create a surface to which they may adhere. They grow well in tissue-culture flasks with plastic substrates. As such, the tissue-culture flasks do not need to be coated with an appropriate ECM molecule (e.g., collagen) in the manner of PC12 cells [HB98].

A1.2.1 **Preparation of SH-SY5Y Cell Cultures**

The SH-SY5Y cells have been donated by Dr. P. Yu from the Neuropsychiatric Research Unit, University of Saskatoon, Saskatoon, SK, Canada. The cells had been ordered from the American Type Culture Collection (ATCC # CRL-2266). The cells are seeded in tissue-culture flasks containing DMEM with 10 % FBS, penicillin 25 U/mL, and streptomycin 25 µg/mL. They are then incubated at 37 °C in 95 % air and 5 % CO_2, and the medium is changed every other day. When the cells are confluent, they are flushed from the flask with a stream of medium from a pipette. The suspension is transferred to new flasks. All cells that are used for the experiments should be within 8 passages of each other.

Each of the synthesized sulfo- hydrazines and hydrazyls need to be tested for their concentration-dependent cytotoxicity. When enough cells are cultured (1 x 10^4 cells), they are plated in tissue-culture 96-well plates with 100 µL DMEM/10 % FBS. Twenty-four hours later, the medium is replaced with solutions of the synthesized salts dissolved in medium to give a range of concentrations. After another twenty-four hours, cell viability is determined by the MTT assay (see Section A1.3).

A1.3 The MTT Assay

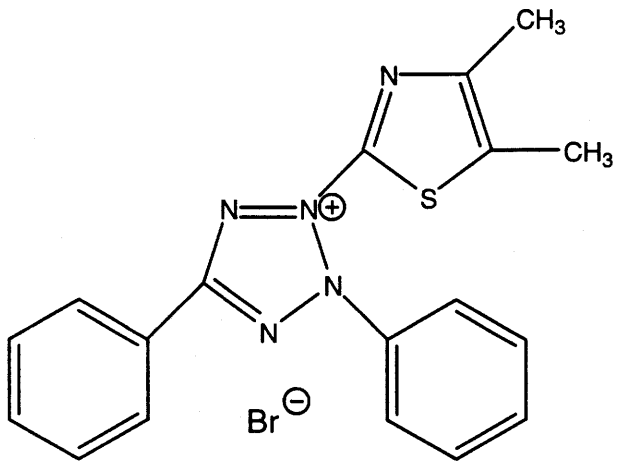

Figure A1: 3-(4,5-dimethylthiazol-2-yl)-2,5-diphenyl tetrazolium bromide

Once the cells (either PC-12 or SH-SY5Y) have been grown and treated with the molecule under study (*i.e.*, β-amyloid pentapeptide, water-soluble hydrazyl), an MTT assay is employed to evaluate the response of the cell population to the external insult. MTT, shown in Figure A1, is the acronym used for 3-(4,5-dimethylthiazol-2-yl)-2,5-diphenyl tetrazolium bromide. First proposed

by Mossmann [M83] in 1983, the MTT colorimetric end-point assay is determined by the reduction of the tetrazolium salt into insoluble formazan crystals when taken up by metabolically active cells. In the cell, MTT acts as an electron acceptor. Only viable cells with functional mitochondria have the enzyme, mitochondrial dehydrogenase, needed to convert the tetrazolium salt to the reduced blue/purple formazan product. The assay determines cell respiration. The number of viable cells present in culture is directly proportional to the amount of reduction product formed. Since reduction of MTT can only occur in metabolically active cells, the amount of formazon produced is a measure of the viability of the cells. The formazan crystals are solubilized with an acidic alcohol solution. The alcohol component dissolves the formazan without (hopefully) precipitating serum proteins. The acidic component lowers the pH of the medium in order to diminish possible interference by the phenol-red indicator present in the culture medium. Absorbance is measured using a photometric microplate reader. The plates are read at 570 nm. To eliminate error due to the presence of debris, the plates should be read at both a principal (570 nm) and a reference (630 nm) wavelength [Cweb2002].

A1.3.1 **MTT Assay Procedures**

Once experimental manipulation of the cell cultures is complete, the medium in all the 96 wells is replaced with RPMI-1640 (PC12 cells) or DMEM (SH-SY5Y cells) containing 1 % FBS and 0.5 mg/mL MTT. The plates are incubated at 37 °C for four hours. Then, each well is treated with acid-isopropanol (0.04 M HCl in isopropanol) and the plates are shaken at room

temperature to dissolve the blue formazan crystals. Subsequently, the optical density in each well is measured at a wavelength of 570 nm using a microELISA UV max, kinetic microplate reader equipped with Softmax version 881 for the Macintosh (Molecular Devices Corporation, Menlo Park, CA, U.S.A.).

A2 A Patent Application for Anticancer and Antiviral Agents

During one of the literature searches that accompany research, a Patent Co-operation Treaty (PCT) application was discovered through SciFinder Scholar [SciFS2000] and obtained from the esp@cenet database. The PCT, in particular PCT/GB91/00517 which is the same as WO91/15200 (the international publication number), is entitled Use of trinitrobenzenes or carminic acid in the treatment of cancer or viral diseases. The inventor and applicant is a Mr. Washington O. Ayuko [UG/GB]; 25 Sundridge Road, Kingstanding, Birmingham B44 9NY (GB). In 1991 Mr. Ayuko filed the application in several countries. The corresponding Canadian application, CA#2,079,803, while filed in the same year (1991), was only examined in 1999. To date, the patent has been neither granted nor issued [Harms 2001].

The patent application is rather broad in scope while at the same time rather vague in its intentions. It was published "without [an] international search report and [is] to be republished upon receipt of that report." Mr. Ayuko wishes to patent a number of molecular structures that are not of his invention. These include 1,1-diphenyl-2-picrylhydrazine, 1,1-diphenyl-2-picrylhydrazyl as well as analogs based on sulfo-substitution at the *para* position of the picryl ring, picric acid, and carminic acid. Most of these structures are well known and there has been literature published on the water-soluble sulfo-analogs of $DH_2\bullet$. They do not appear to be patentable because, as already stated, Mr. Ayuko did not invent them.

Mr. Ayuko wishes to use the aforementioned molecules as anticancer and antiviral agents. He has found that these compounds are efficacious "in the therapy or prophylaxis of neoplasm or viral infection." At low concentrations of the order 10^{-3} to 10^{-15} moles per litre (M), Mr. Ayuko presents a few cases where administration was successful and seemed to show no toxic side effects. The compounds employed in the presented pilot studies include "diphenyl dinitrosulphonate phenylhydrazyl" and carminic acid specifically. The low to zero toxicity of these compounds bodes well for upcoming toxicology studies of our sulfo-hydrazyls. In the application Mr Ayuko does refer to the Ikrina and Matesvoyan [IM62] paper in which the synthesis of the sulfo-analogs of DH_2-H and DH_2• were published and states that the trinitrobenzene compounds and carminic acid are readily available. However, none of the compounds have been properly characterized nor has any modifications to synthetic procedures been alluded to.

Mr. Ayuko proposes "that the compounds referred to ... function by initiating and propagating a free-radical mechanism, thereby producing active chemical species that selectively attack abnormal cell structures." He postulates, "these drugs may generate oxygen-dependent free radicals such as superoxide or hydroxyl radical" which "selectively attack cancer cells or viruses." As such, Mr. Ayuko is patenting the molecules for their pro-oxidant activity. The use of the sulfo-analogs of DH_2• as pro-oxidants is contrary to our proposed use for them as anti-oxidants. We are interested in their potential to act as free-radical scavengers and to stop the radical chain reaction. As well, since the sulfo-

hydrazyls have distinctive and vivid colouring that is lost upon reduction, we also wish to utilize their visible colour change (loss of purple) and loss of EPR signal to follow their reduction if and when they scavenge other free radicals.

A2.1 Cochineal Carmine

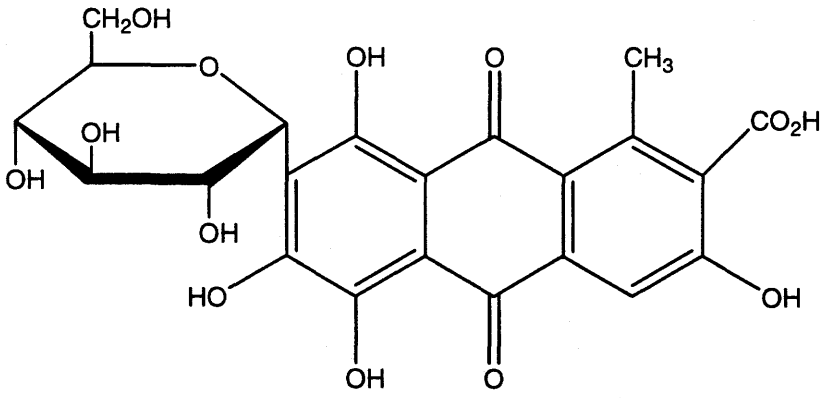

Figure A2: Carminic Acid (C.I. 75470, Natural Red 4)

In the aforementioned patent, carminic acid is co-listed as one of the agents of interest. Carminic acid is the active colouring component of cochineal carmine, a traditional red dye of pre-Hispanic Mexico harvested from the insect *Dactylopius coccus* Costa. After the Spanish conquest of Mexico in the early 16th century, cochineal carmine was introduced into Europe and soon became the pre-eminent red dye used by the luxury textile trade. In the mid-18th century, the increasing mechanization of the European textile industry led to a growth in production that drove up the demand for dyestuffs. This growth in the textile trade consequently advanced the development of a chemical industry that could provide necessary bleaches and detergents. During the latter half of the 19th

century, carmine was also used extensively as a histological stain. However, by the end of the century, the advent of cheaper and more available synthetic dyes (mainly aniline derivatives) from a flourishing chemical industry caused a dramatic decline in the use of all natural dyestuffs. Today, due to its lack of carcinogenicity, mutagenicity, and genotoxicity, it is utilized as a colourant in cosmetics, drink, food, and in pharmaceuticals. It is also still used in histology to stain glycogen (Best's carmine), acid mucopolysaccharides (Mucicarmine), and nuclei (Carmalum) [L77, KJGS93, MVP71, T57, B78, ENGM80].

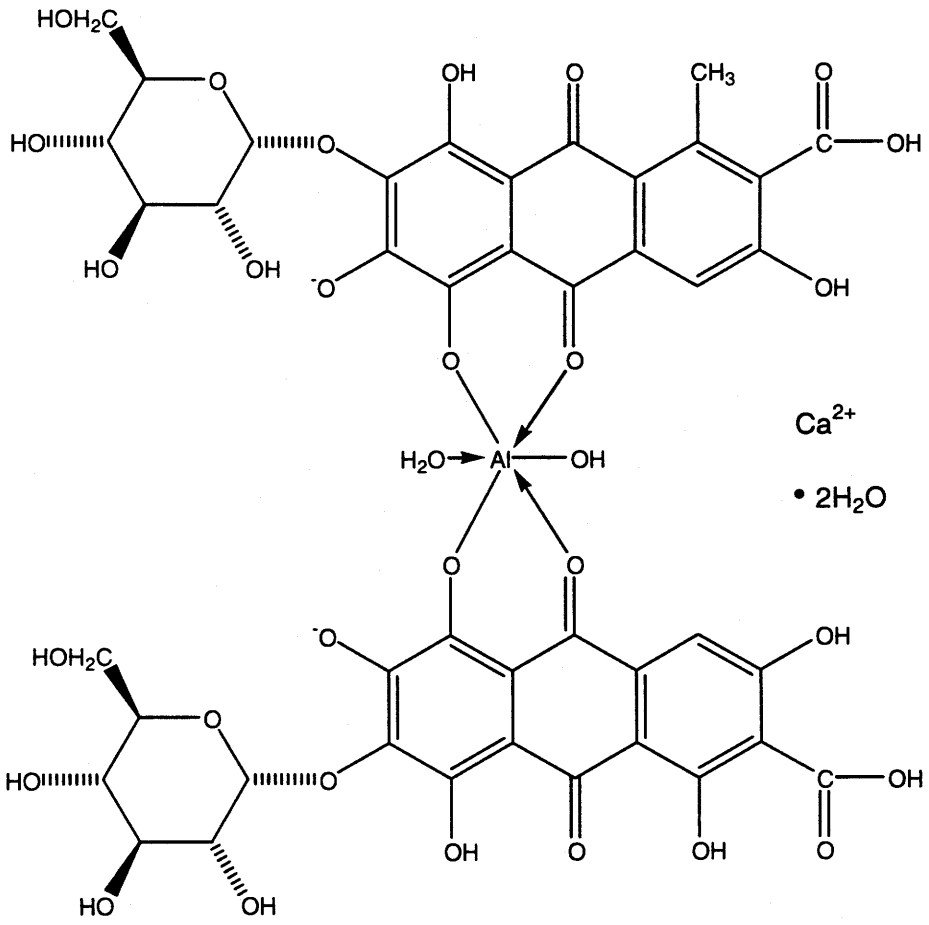

Figure A3: Cochineal Carmine (Alum Lake of Carminic Acid)

Carminic acid is an anthraquinone used by the cochineal insects as an effective deterrent to feeding ants [ENGM80]. As a dye, it is invariably applied in combination with a mordant (usually aluminum). As a food additive used in foodstuffs, cosmetics and drugs, its identification code is E-120. The interest in carminic acid seems to be linked to its close structural similarities to doxorubicin

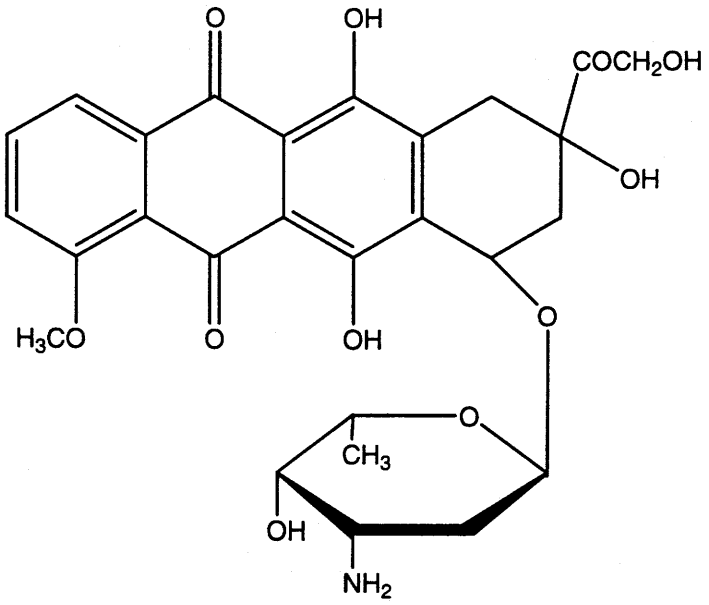

Figure A4: Doxorubicin (Adriamycin)

[HG99]. Doxorubicin (Adriamycin) is an anthracycline antibiotic. It is one of the major anticancer drugs, with primary clinical application in carcinomas (malignant neoplasia of epithelial cells; a very common type of tumour) and sarcomas (malignant tumours derived from connective tissue). It has proven useful in hematological cancers as well. Other anthracyline analogs in use as chemotherapy are daunorubicin and idarubicin [K98]. Seeing the importance of doxorubicin and analogs, the interest in carminic acid is easily understood.

A3 NMR Spectrum Simulation of the Chemical Shifts Associated with the Diphenyl Protons in 2,2-Diphenyl-1-picryl Hydrazine

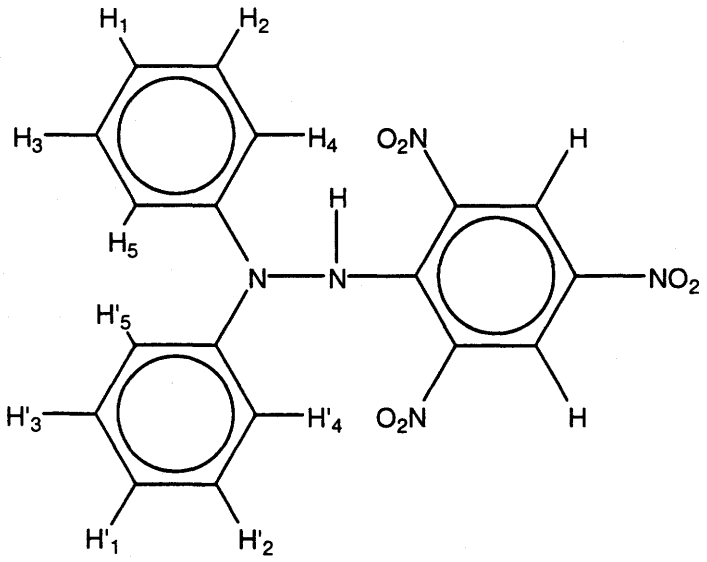

Figure A5: Assignment of the protons in 2,2-diphenyl-1-picryl hydrazine

To determine the NMR time-averaged coupling constants (J_{xy}) associated with the "diphenyl" protons of 2,2-diphenyl-1-picrylhydrazine (DH_2-H), its proton (^{1}H) NMR spectrum was simulated. Figure A5 shows the labelling of the diphenyl protons. The phenyl protons of interest have been labelled as H_1 to H_5 and H'_1 to H'_5. The prime (') designation differentiates the protons of the two phenyl rings. The simulation assumes that H_i has the same coupling constants and chemical shift as H'_i because magnetic differences due to neighbouring constituents are averaged in room- temperature NMR. That is to say, each phenyl group will "time-share" equally in their allowable molecular orientations.

Currie *et al.* [CQRW83] reported the chemical shifts (δ) exhibited by the *ortho*, *meta* and *para* protons of the unsubstituted phenyl rings of DH_2-H; the chemical shifts were measured relative to the internal standard: tetramethyl-silane (TMS), whose peak is assumed to be at δ = 0. The solvent they used was perdeuterated dichloromethane (CD_2Cl_2). It was not stated if the solvent had been dried or used as is. The instrument employed was a Bruker WH-400 spectrometer running at 300 MHz at ambient temperature. The chemical shifts associated with the diphenyl protons were given as δ(*m*) = 7.357 ppm; δ(*o*) = 7.130 ppm; δ(*p*) = 7.207 ppm. No coupling constants were listed and the proton (^1H) NMR spectrum was not included.

It is interesting to note that the *para* protons are not the most shielded of the "diphenyl" protons. The *para* protons, being directly opposite the number one position of the aromatic ring (the carbon bonded to the hydrazinic nitrogen), are farther removed than either the *ortho* or *meta* protons from the rest of the molecule. As such, the *para* protons would likely be influenced less by the other molecular constituents than would the *ortho* or *meta* protons thereby being more shielded and appearing further upfield. However, in dichloromethane the *ortho* protons are the most shielded. This shielding must be imparted by the hydrazine linkage.

CD_2Cl_2 was purchased from Sigma Aldrich to repeat the results reported by CQRW83. A sample of DH_2-H, previously synthesized by our lab and used as is, was dissolved in the perdeuterated solvent (used as is, immediately upon cracking the vial). Spectra were recorded on a Bruker AMX-300 spectrometer

running at 300.14 MHz, at room temperature (298.0 K). The experimental spectrum was analyzed and apparent coupling constants (because of the complexity of the multiplets, the experimental coupling constants are not true) were calculated (see Figure A6). The chemical shifts reported in the CQRW83 were converted to hertz (multiplied the ppm by the operating frequency) to give $\delta(m)$ = 2208.10 Hz; $\delta(o)$ = 2139.97 Hz; $\delta(p)$ = 2163.08 Hz. These were used in the simulation. All simulations were performed using WINDNMR: NMR Spectrum Calculations, Version 1.50, 1997, H. J. Reich, ***Journal of Chemical Education*: *Software***.

The experimental spectrum of DH_2-H shows complex splitting. The Currie *et al.* paper lists three separate δ associated with the *meta*, *ortho*, and *para* protons, therefore they assumed they had a 3-spin system. Some time was spent trying to fit a 3-spin system to the experimental spectra by using the chemical shifts garnered from CQRW83. Apparent coupling constants calculated from the experimental spectrum were used initially and then manipulated to fit the simulation. The diphenyl-proton splitting could not be simulated in that manner. A bit of time was spent manipulating a 4-spin system, but a decision had to be made as to which pair of protons (the meta protons or the ortho protons) had differing chemical shifts. Since there was no logic that could aid in choosing one pair over the other, it was decided to go to a 5-spin system simulation instead.

Using the same δ values used in the 3-spin system, the *meta* and *ortho* protons were each assigned unique chemical shifts that differed by

approximately 1 Hz. So the five spins were initially assigned values as follows: $\delta(m_1)$ = 2207.5 Hz; $\delta(m_2)$ = 2208.5 Hz; $\delta(o_1)$ = 2139.5 Hz; $\delta(o_2)$ = 2140.5 Hz; $\delta(p)$ =2163 Hz. Assignment of coupling constants were based on experimental calculations and included 8.13 Hz, 7.61 Hz, 7.57 Hz, 7.37 Hz, 7.34 Hz, 1.94 Hz, and 1.13 Hz. Initially it was assumed that no intramolecular coupling existed between the *meta* protons and that none existed between the *ortho* protons. After much manipulation, the introduction of m_1 - m_2 coupling and o_1 - o_2 coupling, and adjustment of the variation between $\delta(m_1)$ and $\delta(m_2)$ and $\delta(o_1)$ and $\delta(o_2)$, a reasonable facsimile of the experimental spectrum was obtained (see Figure A7). However, the simulated "apparent" chemical shifts needed fine-tuning to fit better with the experimental spectrum (see Table A1). This was done by slightly adjusting the chemical shifts of the *meta*, *ortho*, and *para* protons until the "apparent" chemical shifts matched, and the experimental and simulated spectra closely resembled each other (see Figure A8). The results are summarized in Table A2.

The simulated spectrum closely resembles the experimental spectrum. The greatest difference between "apparent" chemical shifts is between the experimental peak at 2156.03 Hz and its corresponding simulated peak at 2155.4 Hz. The difference was 0.63 Hz or 0.029% error. The simulated chemical shifts for the *ortho*, *meta*, and *para* protons of 7.13 ppm and 7.13 ppm, 7.36 ppm and 7.36 ppm, and 7.21 ppm respectively, compare favourably with those reported by Currie *et al.* of 7.13 ppm, 7.36 ppm, and 7.21 ppm [CQRW83]. The experimental spectrum shows "bumps" along the leading edge of each well-

defined upsweep. These were impossible to simulate. They could be due to inhomogeneity of the magnetic field. A perfectly shimmed spectrum might not exhibit these bumps. It would be interesting to see what effect concentration would have on the spectrum.

The simulation was then used to predict what the proton (^{1}H) NMR spectrum would look like at an operating frequency of 500 MHz (see Figure A9). This was verified by obtaining an experimental spectrum at 500 MHz, at room temperature, and using perdeuterated dichloromethane. This simulation is only applicable to a sample of DH_2-H in CD_2Cl_2. Changing the solvent results in an altered splitting pattern. Minimal changes in the simulation parameters should result in a fit to any solvent used.

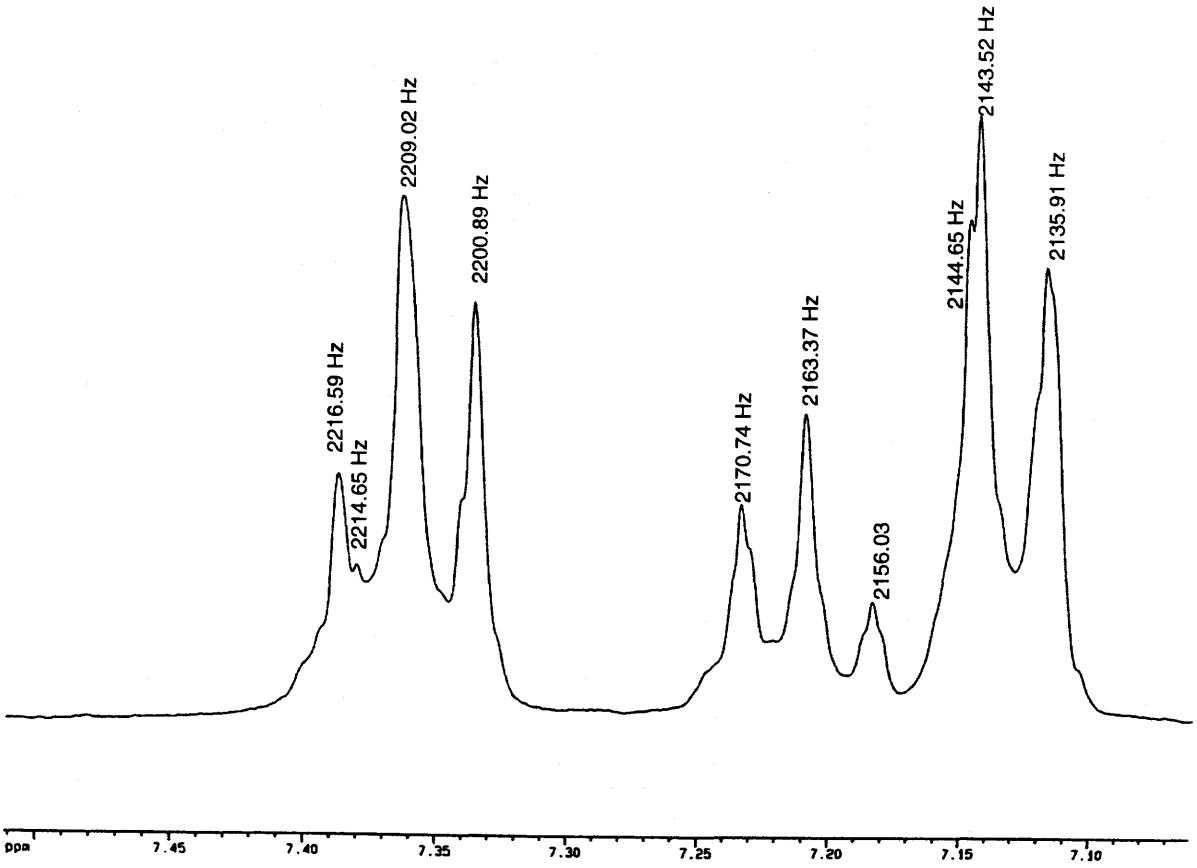

Figure A6: Experimental ^{1}H NMR spectrum of the chemical shifts of the diphenyl protons of DH_2-H in CD_2Cl_2 at 294.0 K, $\upsilon_{spectrometer}$ = 300.14 MHz

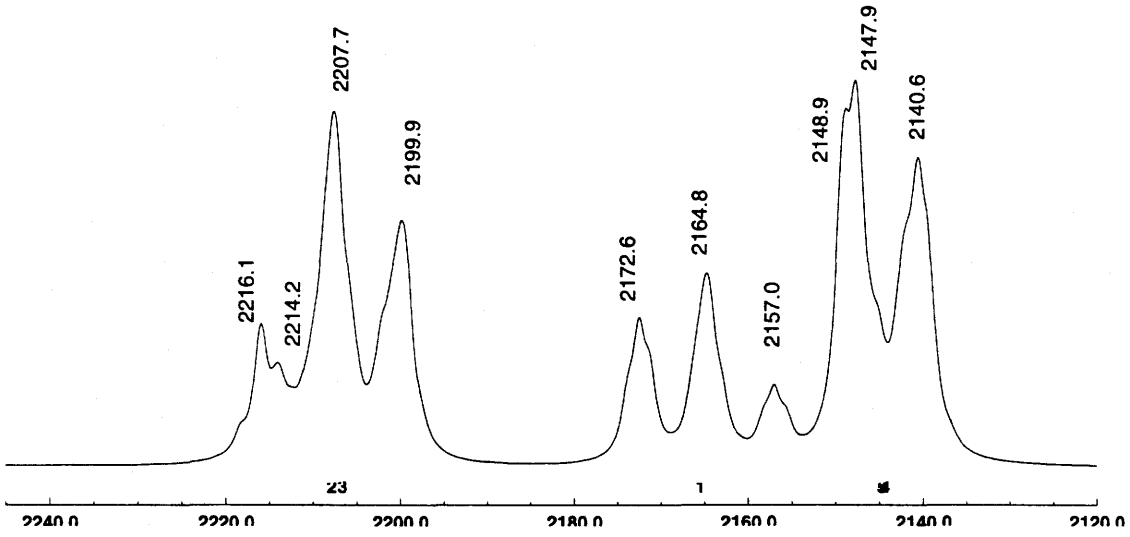

Figure A7: Initial 300 MHz spectral simulation Figure A6

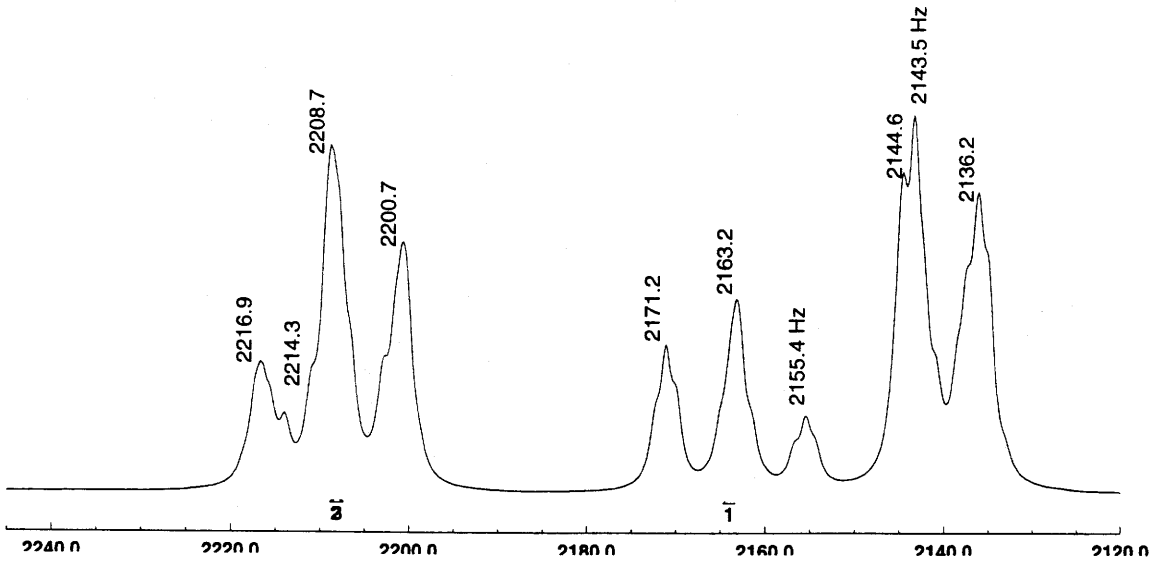

Figure A8: Simulated 300 MHz ^{1}H NMR spectrum of Figure A6 (Simulation adjusted to experimental peaks)

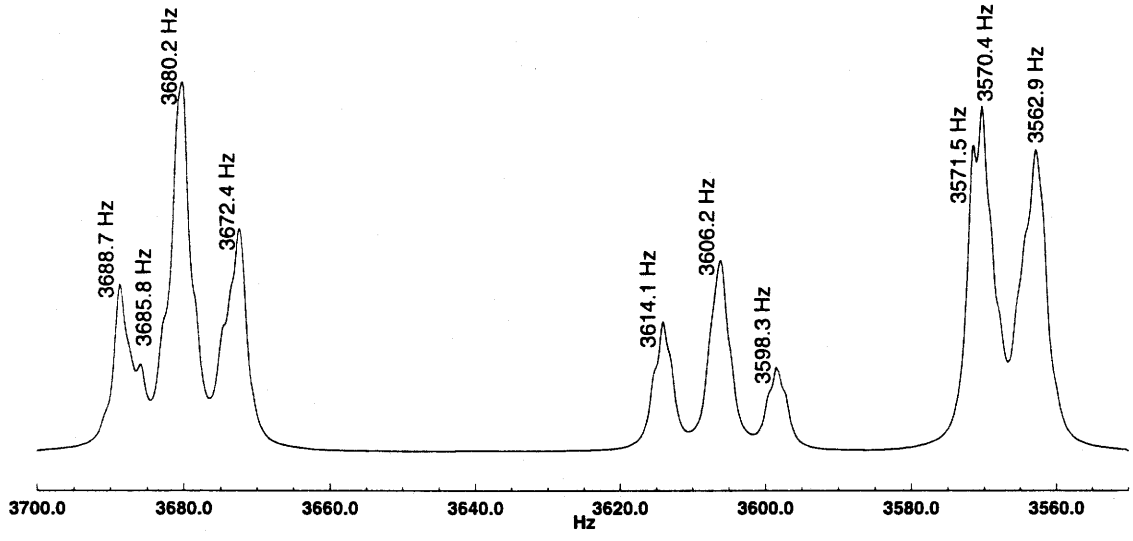

Figure A9: 300 MHz ^{1}H NMR spectral simulation extrapolated to 500 MHz

Table A1: "Apparent" chemical shifts (δ) of the 300 MHz ^1H spectrum of DH_2-H in CD_2Cl_2

Experimental ($\upsilon_{spectrometer}$ **= 300 MHz)**		**Simulation #1 (300 MHz)**		**Simulation #2 (300 MHz)**	
Hz	**ppm**	**Hz**	**ppm**	**Hz**	**ppm**
2216.59	7.39	2216.1	7.38	2216.9	7.39
2214.65	7.38	2214.2	7.38	2214.3	7.38
2209.02	7.36	2207.7	7.36	2208.7	7.36
2200.89	7.33	2199.9	7.33	2200.7	7.33
2170.74	7.23	2172.6	7.24	2171.2	7.23
2163.37	7.21	2164.8	7.21	2163.2	7.21
2156.03	7.18	2157.0	7.19	2155.4	7.18
2144.65	7.15	2148.9	7.16	2144.6	7.15
2143.52	7.14	2147.9	7.16	2143.5	7.14
2135.91	7.12	2140.6	7.13	2136.2	7.12

Table A2: Summary of ^1H NMR parameters, experiemental and simulated, for the diphenyl protons in DH_2-H

Parameter	Figure A6 (at 300 MHz)	Figure A7 (at 300 MHz)	Figure A8 (at 500 MHz)
υ_1 in Hz	2165.51	2164.00	3606.67
υ_2 in Hz	2207.90	2208.20	3680.33
υ_3 in Hz	2206.70	2208.00	3680.00
υ_4 in Hz	2144.40	2139.90	3566.50
υ_5 in Hz	2144.70	2140.30	3567.17
J_{12} in Hz	8.17	8.17	8.17
J_{13} in Hz	7.57	7.57	7.57
J_{14} in Hz	1.14	1.04	1.04
J_{15} in Hz	1.14	1.24	1.24
J_{23} in Hz	2.20	2.10	2.10
J_{24} in Hz	7.67	7.77	7.77
J_{25} in Hz	1.13	0.93	0.93
J_{34} in Hz	1.13	1.33	1.33
J_{35} in Hz	7.37	7.27	7.27
J_{45} in Hz	1.94	1.84	1.84

A4 Crystallography Data Tables for the Sulfonated Diphenylpicryl Hydrazine Salts.

Table A3: Crystal data and structure refinement for DPH-DP4SH

Empirical formula	$C_{30}H_{26}N_6O_7S$	
Molar mass	614.63 g/mol	
Temperature	150(2) K	
Wavelength	0.71073 Å	
Crystal system	Triclinic	
Space group	p_-1	
Unit-cell dimensions	a = 5.7938(8) Å	α= 69.54(2)°.
	b = 15.805(4) Å	β= 83.940(16)°.
	c = 16.849(4) Å	γ = 87.348(17)°.
Volume	1437.4(5) $Å^3$	
Z	2	
Density (calculated)	1.420 Mg/m^3	
Absorption coefficient	0.172 mm^{-1}	
F(000)	640	
Crystal size	0.40 x 0.13 x 0.08 mm^3	
Theta range for data collection	2.48 to 26.30°.	
Index ranges	-7<=h<=0, -19<=k<=19, -20<=l<=20	
Reflections collected	6874	
Independent reflections	5814 [R(int) = 0.0462]	
Completeness to theta = 26.30°	99.6 %	
Absorption correction	None	
Refinement method	Full-matrix least-squares on F^2	
Data / restraints / parameters	5814 / 0 / 397	
Goodness-of-fit on F^2	1.053	
Final R indices [I > 2sigma(I)]	R1 = 0.0646, wR2 = 0.1418	
R indices (all data)	R1 = 0.1295, wR2 = 0.1716	
Largest diff. peak and hole	0.370 and -0.477 $e.Å^{-3}$	

Table A4: Atomic coordinates (x 10^4) and equivalent isotropic displacement parameters (Å^2 x 10^3) for DPH-DP4SH. U(eq) is defined as one third of the trace of the orthogonalized U^{ij} tensor (describes physical/vibrational motion)

	x	y	z	U(eq)
S(4)	5846(2)	6149(1)	516(1)	26(1)
N(2)	3739(5)	7406(2)	2914(2)	22(1)
N(6)	10656(5)	8646(2)	821(2)	25(1)
N(7)	7559(5)	8709(2)	2284(2)	18(1)
N(8)	5815(5)	8935(2)	2823(2)	18(1)
N(9)	8933(7)	5493(2)	8724(2)	53(1)
N(10)	9166(6)	6065(2)	7841(2)	31(1)
O(21)	1712(4)	7635(2)	2813(2)	38(1)
O(22)	4488(5)	7028(2)	3606(2)	27(1)
O(41)	7202(5)	6479(2)	-293(2)	36(1)
O(42)	3359(5)	6183(2)	459(2)	58(1)
O(43)	6555(8)	5270(2)	1045(2)	73(1)
O(61)	11958(5)	8511(2)	256(2)	43(1)
O(62)	10949(5)	9270(2)	1073(2)	44(1)
C(1)	7199(6)	8124(2)	1891(2)	17(1)
C(2)	5317(6)	7506(2)	2146(2)	17(1)
C(3)	4886(6)	6938(2)	1728(2)	21(1)
C(4)	6385(6)	6897(2)	1041(2)	20(1)
C(5)	8301(6)	7452(2)	787(2)	21(1)
C(6)	8679(6)	8053(2)	1189(2)	17(1)
C(11)	4401(6)	9700(2)	2389(2)	16(1)
C(12)	5061(6)	10279(2)	1572(2)	22(1)
C(13)	3615(6)	10993(2)	1173(2)	26(1)
C(14)	1538(6)	11135(3)	1594(2)	27(1)
C(15)	882(6)	10559(2)	2406(2)	25(1)
C(16)	2279(6)	9833(2)	2807(2)	21(1)
C(21)	6681(6)	8872(2)	3613(2)	18(1)
C(22)	6413(6)	9565(2)	3942(2)	22(1)
C(23)	7412(6)	9489(3)	4678(2)	26(1)
C(24)	8679(6)	8728(3)	5091(2)	29(1)
C(25)	8914(7)	8035(3)	4766(2)	29(1)
C(26)	7941(6)	8100(2)	4036(2)	23(1)
C(31)	9025(6)	5545(2)	7289(3)	27(1)
C(32)	10755(7)	4944(3)	7205(3)	32(1)
C(33)	10592(8)	4485(3)	6647(3)	37(1)
C(34)	8736(8)	4641(3)	6163(3)	38(1)
C(35)	7006(8)	5239(4)	6259(3)	53(1)
C(36)	7143(7)	5690(3)	6822(3)	45(1)
C(41)	11071(6)	6672(2)	7641(2)	22(1)
C(42)	11737(7)	7144(3)	6783(2)	30(1)
C(43)	13523(7)	7761(3)	6552(3)	34(1)
C(44)	14665(7)	7908(3)	7170(3)	34(1)
C(45)	13997(7)	7449(3)	8014(3)	34(1)
C(46)	12196(7)	6835(2)	8256(2)	29(1)

Table A5: Bond lengths [Å] and angles [°] for DPH-DP4SH

S(4)-O(43)	1.434(3)	C(13)-H(13)	0.9500
S(4)-O(41)	1.436(3)	C(14)-C(15)	1.378(5)
S(4)-O(42)	1.451(3)	C(14)-H(14)	0.9500
S(4)-C(4)	1.761(4)	C(15)-C(16)	1.384(5)
N(2)-O(21)	1.224(4)	C(15)-H(15)	0.9500
N(2)-O(22)	1.225(4)	C(16)-H(16)	0.9500
N(2)-C(2)	1.468(4)	C(21)-C(22)	1.387(5)
N(6)-O(61)	1.223(4)	C(21)-C(26)	1.396(5)
N(6)-O(62)	1.226(4)	C(22)-C(23)	1.388(5)
N(6)-C(6)	1.456(4)	C(22)-H(22)	0.9500
N(7)-C(1)	1.346(4)	C(23)-C(24)	1.383(5)
N(7)-N(8)	1.405(4)	C(23)-H(23)	0.9500
N(7)-H(7)	0.8800	C(24)-C(25)	1.381(5)
N(8)-C(21)	1.442(4)	C(24)-H(24)	0.9500
N(8)-C(11)	1.444(4)	C(25)-C(26)	1.377(5)
N(9)-N(10)	1.441(5)	C(25)-H(25)	0.9500
N(9)-H(9A)	0.9100	C(26)-H(26)	0.9500
N(9)-H(9B)	0.9100	C(31)-C(36)	1.376(6)
N(9)-H(9C)	0.9100	C(31)-C(32)	1.379(5)
N(10)-C(41)	1.430(5)	C(32)-C(33)	1.387(5)
N(10)-C(31)	1.452(5)	C(32)-H(32)	0.9500
C(1)-C(6)	1.421(4)	C(33)-C(34)	1.378(6)
C(1)-C(2)	1.426(5)	C(33)-H(33)	0.9500
C(2)-C(3)	1.366(5)	C(34)-C(35)	1.381(7)
C(3)-C(4)	1.390(5)	C(34)-H(34)	0.9500
C(3)-H(3)	0.9500	C(35)-C(36)	1.382(7)
C(4)-C(5)	1.383(5)	C(35)-H(35)	0.9500
C(5)-C(6)	1.381(5)	C(36)-H(36)	0.9500
C(5)-H(5)	0.9500	C(41)-C(46)	1.381(5)
C(11)-C(12)	1.385(5)	C(41)-C(42)	1.396(5)
C(11)-C(16)	1.397(5)	C(42)-C(43)	1.384(5)
C(12)-C(13)	1.389(5)	C(42)-H(42)	0.9500
C(12)-H(12)	0.9500	C(43)-C(44)	1.379(6)
C(13)-C(14)	1.381(5)	C(43)-H(43)	0.9500

C(44)-C(45)	1.374(6)	C(45)-H(45)	0.9500
C(44)-H(44)	0.9500	C(46)-H(46)	0.9500
C(45)-C(46)	1.388(5)		

O(43)-S(4)-O(41)	113.4(2)	C(1)-C(2)-N(2)	121.7(3)
O(43)-S(4)-O(42)	110.7(3)	C(2)-C(3)-C(4)	120.6(3)
O(41)-S(4)-O(42)	114.1(2)	C(2)-C(3)-H(3)	119.7
O(43)-S(4)-C(4)	106.47(18)	C(4)-C(3)-H(3)	119.7
O(41)-S(4)-C(4)	105.34(16)	C(5)-C(4)-C(3)	118.4(3)
O(42)-S(4)-C(4)	106.10(17)	C(5)-C(4)-S(4)	121.2(3)
O(21)-N(2)-O(22)	124.7(3)	C(3)-C(4)-S(4)	120.4(3)
O(21)-N(2)-C(2)	117.1(3)	C(6)-C(5)-C(4)	120.9(3)
O(22)-N(2)-C(2)	117.9(3)	C(6)-C(5)-H(5)	119.6
O(61)-N(6)-O(62)	122.1(3)	C(4)-C(5)-H(5)	119.6
O(61)-N(6)-C(6)	118.3(3)	C(5)-C(6)-C(1)	123.0(3)
O(62)-N(6)-C(6)	119.6(3)	C(5)-C(6)-N(6)	115.6(3)
C(1)-N(7)-N(8)	122.1(3)	C(1)-C(6)-N(6)	121.4(3)
C(1)-N(7)-H(7)	118.9	C(12)-C(11)-C(16)	120.0(3)
N(8)-N(7)-H(7)	118.9	C(12)-C(11)-N(8)	122.0(3)
N(7)-N(8)-C(21)	110.8(3)	C(16)-C(11)-N(8)	118.0(3)
N(7)-N(8)-C(11)	113.8(3)	C(11)-C(12)-C(13)	119.9(3)
C(21)-N(8)-C(11)	119.9(3)	C(11)-C(12)-H(12)	120.1
N(10)-N(9)-H(9A)	109.5	C(13)-C(12)-H(12)	120.1
N(10)-N(9)-H(9B)	109.5	C(14)-C(13)-C(12)	120.1(3)
H(9A)-N(9)-H(9B)	109.5	C(14)-C(13)-H(13)	119.9
N(10)-N(9)-H(9C)	109.5	C(12)-C(13)-H(13)	119.9
H(9A)-N(9)-H(9C)	109.5	C(15)-C(14)-C(13)	120.0(4)
H(9B)-N(9)-H(9C)	109.5	C(15)-C(14)-H(14)	120.0
C(41)-N(10)-N(9)	112.4(3)	C(13)-C(14)-H(14)	120.0
C(41)-N(10)-C(31)	116.7(3)	C(14)-C(15)-C(16)	120.7(3)
N(9)-N(10)-C(31)	111.1(3)	C(14)-C(15)-H(15)	119.6
N(7)-C(1)-C(6)	123.2(3)	C(16)-C(15)-H(15)	119.6
N(7)-C(1)-C(2)	123.4(3)	C(15)-C(16)-C(11)	119.3(3)
C(6)-C(1)-C(2)	113.4(3)	C(15)-C(16)-H(16)	120.3
C(3)-C(2)-C(1)	123.6(3)	C(11)-C(16)-H(16)	120.3
C(3)-C(2)-N(2)	114.6(3)	C(22)-C(21)-C(26)	119.1(3)

C(22)-C(21)-N(8)	122.6(3)	C(33)-C(34)-H(34)	120.3
C(26)-C(21)-N(8)	118.2(3)	C(35)-C(34)-H(34)	120.3
C(21)-C(22)-C(23)	120.0(3)	C(34)-C(35)-C(36)	120.7(4)
C(21)-C(22)-H(22)	120.0	C(34)-C(35)-H(35)	119.7
C(23)-C(22)-H(22)	120.0	C(36)-C(35)-H(35)	119.7
C(24)-C(23)-C(22)	120.9(3)	C(31)-C(36)-C(35)	119.6(4)
C(24)-C(23)-H(23)	119.5	C(31)-C(36)-H(36)	120.2
C(22)-C(23)-H(23)	119.5	C(35)-C(36)-H(36)	120.2
C(25)-C(24)-C(23)	118.8(3)	C(46)-C(41)-C(42)	119.3(3)
C(25)-C(24)-H(24)	120.6	C(46)-C(41)-N(10)	122.9(3)
C(23)-C(24)-H(24)	120.6	C(42)-C(41)-N(10)	117.7(3)
C(26)-C(25)-C(24)	121.1(4)	C(43)-C(42)-C(41)	120.3(4)
C(26)-C(25)-H(25)	119.5	C(43)-C(42)-H(42)	119.9
C(24)-C(25)-H(25)	119.5	C(41)-C(42)-H(42)	119.9
C(25)-C(26)-C(21)	120.1(3)	C(44)-C(43)-C(42)	120.1(4)
C(25)-C(26)-H(26)	119.9	C(44)-C(43)-H(43)	120.0
C(21)-C(26)-H(26)	119.9	C(42)-C(43)-H(43)	120.0
C(36)-C(31)-C(32)	120.4(4)	C(45)-C(44)-C(43)	119.7(4)
C(36)-C(31)-N(10)	118.0(4)	C(45)-C(44)-H(44)	120.2
C(32)-C(31)-N(10)	121.6(4)	C(43)-C(44)-H(44)	120.2
C(31)-C(32)-C(33)	119.7(4)	C(44)-C(45)-C(46)	120.9(4)
C(31)-C(32)-H(32)	120.2	C(44)-C(45)-H(45)	119.5
C(33)-C(32)-H(32)	120.2	C(46)-C(45)-H(45)	119.5
C(34)-C(33)-C(32)	120.3(4)	C(41)-C(46)-C(45)	119.7(4)
C(34)-C(33)-H(33)	119.8	C(41)-C(46)-H(46)	120.1
C(32)-C(33)-H(33)	119.8	C(45)-C(46)-H(46)	120.1
C(33)-C(34)-C(35)	119.3(4)		

Table A6: Anisotropic displacement parameters ($Å^2 \times 10^3$)for DPH-DP4SH.
The anisotropic displacement factor exponent takes the form:

$$-2\pi^2[\, h^2 a^{*2} U^{11} + \ldots + 2\, h\, k\, a^*\, b^*\, U^{12} \,]$$

	U^{11}	U^{22}	U^{33}	U^{23}	U^{13}	U^{12}
S(4)	35(1)	23(1)	22(1)	-11(1)	2(1)	-6(1)
N(2)	19(2)	27(2)	24(2)	-14(1)	4(1)	-1(1)
N(6)	22(2)	31(2)	24(2)	-13(1)	3(1)	-7(1)
N(7)	11(1)	27(2)	23(2)	-16(1)	4(1)	-2(1)
N(8)	15(2)	24(2)	18(1)	-12(1)	-1(1)	3(1)
N(9)	77(3)	36(2)	48(2)	-25(2)	37(2)	-31(2)
N(10)	29(2)	26(2)	39(2)	-17(2)	11(2)	-10(1)
O(21)	11(1)	57(2)	52(2)	-30(2)	2(1)	7(1)
O(22)	32(2)	31(1)	19(1)	-8(1)	1(1)	-6(1)
O(41)	43(2)	47(2)	24(1)	-22(1)	14(1)	-20(1)
O(42)	25(2)	87(3)	93(3)	-72(2)	11(2)	-21(2)
O(43)	162(4)	17(2)	45(2)	-10(1)	-46(2)	11(2)
O(61)	31(2)	56(2)	48(2)	-32(2)	25(1)	-18(1)
O(62)	38(2)	53(2)	55(2)	-40(2)	22(2)	-29(2)
C(1)	16(2)	17(2)	20(2)	-8(1)	-4(1)	4(1)
C(2)	12(2)	21(2)	19(2)	-8(1)	2(1)	0(1)
C(3)	17(2)	21(2)	23(2)	-7(2)	-3(1)	1(1)
C(4)	19(2)	22(2)	20(2)	-8(1)	-1(1)	0(2)
C(5)	22(2)	22(2)	20(2)	-9(2)	0(2)	2(2)
C(6)	12(2)	21(2)	18(2)	-6(1)	1(1)	-2(1)
C(11)	13(2)	17(2)	22(2)	-9(1)	-5(1)	2(1)
C(12)	16(2)	27(2)	24(2)	-8(2)	0(2)	-3(2)
C(13)	24(2)	26(2)	24(2)	-3(2)	-3(2)	-5(2)
C(14)	22(2)	25(2)	33(2)	-7(2)	-6(2)	4(2)
C(15)	17(2)	23(2)	34(2)	-9(2)	-1(2)	2(2)
C(16)	16(2)	22(2)	23(2)	-9(2)	1(1)	-2(1)
C(21)	14(2)	26(2)	17(2)	-9(1)	1(1)	-4(1)
C(22)	17(2)	25(2)	26(2)	-12(2)	-1(2)	-1(2)
C(23)	19(2)	37(2)	30(2)	-21(2)	2(2)	-1(2)
C(24)	22(2)	44(2)	22(2)	-15(2)	-5(2)	-2(2)
C(25)	27(2)	33(2)	24(2)	-7(2)	-7(2)	6(2)
C(26)	16(2)	28(2)	28(2)	-11(2)	-3(2)	1(2)
C(31)	18(2)	26(2)	39(2)	-17(2)	7(2)	-6(2)
C(32)	31(2)	32(2)	38(2)	-18(2)	-9(2)	5(2)

C(33)	43(3)	35(2)	37(2)	-18(2)	-1(2)	3(2)
C(34)	43(3)	41(2)	34(2)	-17(2)	2(2)	-17(2)
C(35)	34(3)	69(3)	69(3)	-35(3)	-19(2)	-7(2)
C(36)	18(2)	49(3)	77(4)	-32(3)	-6(2)	3(2)
C(41)	21(2)	16(2)	30(2)	-7(2)	-2(2)	1(1)
C(42)	28(2)	30(2)	29(2)	-6(2)	-8(2)	-2(2)
C(43)	31(2)	28(2)	35(2)	-1(2)	1(2)	-6(2)
C(44)	27(2)	21(2)	51(3)	-7(2)	-4(2)	-7(2)
C(45)	34(2)	26(2)	48(3)	-16(2)	-16(2)	-1(2)
C(46)	37(2)	21(2)	28(2)	-7(2)	-2(2)	1(2)

Table A7: Hydrogen coordinates (x 10^4) and isotropic displacement parameters ($Å^2$ x 10^3) for DPH-DP4SH

	x	y	z	U(eq)
H(7)	8933	8957	2201	22
H(9A)	7703	5120	8823	80
H(9B)	8698	5841	9057	80
H(9C)	10251	5157	8850	80
H(3)	3550	6567	1908	25
H(5)	9371	7419	331	25
H(12)	6500	10187	1285	27
H(13)	4055	11385	609	31
H(14)	563	11630	1324	33
H(15)	-545	10661	2694	30
H(16)	1799	9430	3362	25
H(22)	5547	10092	3664	26
H(23)	7221	9966	4900	32
H(24)	9377	8683	5591	34
H(25)	9760	7506	5051	34
H(26)	8127	7618	3819	28
H(32)	12052	4845	7529	38
H(33)	11765	4061	6597	45
H(34)	8647	4339	5769	46
H(35)	5710	5340	5935	64
H(36)	5944	6099	6886	55
H(42)	10962	7041	6357	35
H(43)	13963	8084	5968	41
H(44)	15906	8324	7012	41
H(45)	14781	7554	8438	41
H(46)	11738	6527	8842	35

Table A8: Torsion angles [°] for DPH-DP4SH

C(1)-N(7)-N(8)-C(21)	131.6(3)
C(1)-N(7)-N(8)-C(11)	-89.7(4)
N(8)-N(7)-C(1)-C(6)	163.5(3)
N(8)-N(7)-C(1)-C(2)	-17.5(5)
N(7)-C(1)-C(2)-C(3)	177.1(3)
C(6)-C(1)-C(2)-C(3)	-3.7(5)
N(7)-C(1)-C(2)-N(2)	-5.8(5)
C(6)-C(1)-C(2)-N(2)	173.4(3)
O(21)-N(2)-C(2)-C(3)	-68.1(4)
O(22)-N(2)-C(2)-C(3)	105.6(4)
O(21)-N(2)-C(2)-C(1)	114.6(4)
O(22)-N(2)-C(2)-C(1)	-71.8(4)
C(1)-C(2)-C(3)-C(4)	3.8(5)
N(2)-C(2)-C(3)-C(4)	-173.5(3)
C(2)-C(3)-C(4)-C(5)	-0.7(5)
C(2)-C(3)-C(4)-S(4)	179.0(3)
O(43)-S(4)-C(4)-C(5)	102.1(4)
O(41)-S(4)-C(4)-C(5)	-18.6(3)
O(42)-S(4)-C(4)-C(5)	-140.0(3)
O(43)-S(4)-C(4)-C(3)	-77.6(4)
O(41)-S(4)-C(4)-C(3)	161.7(3)
O(42)-S(4)-C(4)-C(3)	40.3(3)
C(3)-C(4)-C(5)-C(6)	-2.0(5)
S(4)-C(4)-C(5)-C(6)	178.3(3)
C(4)-C(5)-C(6)-C(1)	1.9(5)
C(4)-C(5)-C(6)-N(6)	-175.5(3)
N(7)-C(1)-C(6)-C(5)	-179.9(3)
C(2)-C(1)-C(6)-C(5)	0.9(5)
N(7)-C(1)-C(6)-N(6)	-2.7(5)
C(2)-C(1)-C(6)-N(6)	178.1(3)
O(61)-N(6)-C(6)-C(5)	-7.6(5)
O(62)-N(6)-C(6)-C(5)	171.3(3)
O(61)-N(6)-C(6)-C(1)	175.0(3)
O(62)-N(6)-C(6)-C(1)	-6.2(5)
N(7)-N(8)-C(11)-C(12)	-14.7(4)
C(21)-N(8)-C(11)-C(12)	119.8(3)
N(7)-N(8)-C(11)-C(16)	163.3(3)
C(21)-N(8)-C(11)-C(16)	-62.1(4)
C(16)-C(11)-C(12)-C(13)	0.4(5)
N(8)-C(11)-C(12)-C(13)	178.4(3)
C(11)-C(12)-C(13)-C(14)	0.9(5)
C(12)-C(13)-C(14)-C(15)	-1.0(6)
C(13)-C(14)-C(15)-C(16)	-0.3(6)
C(14)-C(15)-C(16)-C(11)	1.6(5)
C(12)-C(11)-C(16)-C(15)	-1.6(5)
N(8)-C(11)-C(16)-C(15)	-179.7(3)
N(7)-N(8)-C(21)-C(22)	129.1(3)
C(11)-N(8)-C(21)-C(22)	-6.7(5)
N(7)-N(8)-C(21)-C(26)	-47.4(4)
C(11)-N(8)-C(21)-C(26)	176.8(3)
C(26)-C(21)-C(22)-C(23)	0.7(5)
N(8)-C(21)-C(22)-C(23)	-175.9(3)
C(21)-C(22)-C(23)-C(24)	0.0(5)
C(22)-C(23)-C(24)-C(25)	-0.8(6)
C(23)-C(24)-C(25)-C(26)	1.0(6)
C(24)-C(25)-C(26)-C(21)	-0.4(6)
C(22)-C(21)-C(26)-C(25)	-0.5(5)
N(8)-C(21)-C(26)-C(25)	176.2(3)
C(41)-N(10)-C(31)-C(36)	-116.1(4)
N(9)-N(10)-C(31)-C(36)	113.2(4)
C(41)-N(10)-C(31)-C(32)	61.6(5)
N(9)-N(10)-C(31)-C(32)	-69.1(5)
C(36)-C(31)-C(32)-C(33)	0.0(6)
N(10)-C(31)-C(32)-C(33)	-177.6(4)
C(31)-C(32)-C(33)-C(34)	1.3(6)
C(32)-C(33)-C(34)-C(35)	-1.9(7)
C(33)-C(34)-C(35)-C(36)	1.1(7)
C(32)-C(31)-C(36)-C(35)	-0.8(7)
N(10)-C(31)-C(36)-C(35)	176.9(4)
C(34)-C(35)-C(36)-C(31)	0.2(7)
N(9)-N(10)-C(41)-C(46)	-14.1(5)
C(31)-N(10)-C(41)-C(46)	-144.2(4)
N(9)-N(10)-C(41)-C(42)	168.6(3)
C(31)-N(10)-C(41)-C(42)	38.5(5)
C(46)-C(41)-C(42)-C(43)	0.6(6)
N(10)-C(41)-C(42)-C(43)	178.0(3)
C(41)-C(42)-C(43)-C(44)	0.5(6)
C(42)-C(43)-C(44)-C(45)	-1.0(6)
C(43)-C(44)-C(45)-C(46)	0.3(6)
C(42)-C(41)-C(46)-C(45)	-1.3(6)
N(10)-C(41)-C(46)-C(45)	-178.5(3)
C(44)-C(45)-C(46)-C(41)	0.8(6)

Table A9: Hydrogen bonds for DPH-DP4SH [Å and °]

D-H...A	d(D-H)	d(H...A)	d(D...A)	<(DHA)
N(7)-H(7)...O(21)#1	0.88	2.56	2.912(4)	104.8
N(7)-H(7)...O(62)	0.88	2.04	2.618(4)	122.7
N(7)-H(7)...N(6)	0.88	2.63	2.919(4)	100.5
N(9)-H(9A)...O(42)#2	0.91	2.07	2.841(5)	141.1
N(9)-H(9A)...O(43)#2	0.91	2.54	3.388(6)	155.6
N(9)-H(9B)...O(41)#3	0.91	1.86	2.735(4)	160.9
N(9)-H(9C)...O(43)#4	0.91	1.94	2.834(6)	165.4
C(5)-H(5)...O(41)	0.95	2.54	2.894(4)	102.4
C(5)-H(5)...O(61)	0.95	2.30	2.641(4)	100.3
C(13)-H(13)...O(61)#5	0.95	2.58	3.249(5)	127.8
C(26)-H(26)...O(21)#1	0.95	2.53	3.085(4)	117.1
C(26)-H(26)...O(22)	0.95	2.45	2.979(4)	114.7
C(32)-H(32)...O(43)#4	0.95	2.56	3.385(5)	145.5

Symmetry transformations used to generate equivalent atoms:

#1 x+1, y, z #2 -x+1, -y+1, -z+1 #3 x, y, z+1 #4 -x+2, -y+1, -z+1 #5 -x+2 ,-y+2, -z

Table A10: Crystal data and structure refinement for K-DP4SH

Empirical formula	$C_{24}H_{25}KN_4O_{10}S$	
Molar mass	600.65 g/mol	
Temperature	193(2) K	
Wavelength	0.71073 Å	
Crystal system	Monoclinic	
Space group	$P2_1/c$	
Unit-cell dimensions	a = 24.911(2) Å	α= 90°.
	b = 5.8875(5) Å	β= 99.64(1)°.
	c = 18.0156(15) Å	γ = 90°.
Volume	2604.9(4) $Å^3$	
Z	4	
Density (calculated)	1.532 Mg/m^3	
Absorption coefficient	0.350 mm^{-1}	
F(000)	1248	
Crystal size	0.58 x 0.18 x 0.06 mm^3	
Theta range for data collection	1.66 to 26.45°.	
Index ranges	-30<=h<=31, -6<=k<=7, -21<=l<=22	
Reflections collected	12178	
Independent reflections	5298 [R(int) = 0.0400]	
Completeness to theta = 26.45°	98.5 %	
Absorption correction	Semi-empirical from equivalents	
Max. and min. transmission	0.9793 and 0.8229	
Refinement method	Full-matrix least-squares on F^2	
Data / restraints / parameters	5298 / 1 / 365	
Goodness-of-fit on F^2	1.010	
Final R indices [I > 2sigma(I)]	R1 = 0.0402, wR2 = 0.0906	
R indices (all data)	R1 = 0.0596, wR2 = 0.0987	
Largest diff. peak and hole	0.394 and -0.336 $e.Å^{-3}$	

Table A11: Atomic coordinates (x 10^4) and equivalent isotropic displacement parameters ($Å^2$ x 10^3) for K-DP4SH. U(eq) is defined as one third of the trace of the orthogonalized U^{ij} tensor (describes physical/vibrational motion)

	x	y	z	U(eq)
K(1)	505(1)	1822(1)	6874(1)	30(1)
S(1)	845(1)	6685(1)	7846(1)	24(1)
O(1)	505(1)	4995(3)	8122(1)	35(1)
O(2)	829(1)	6538(3)	7037(1)	34(1)
O(3)	760(1)	8960(3)	8096(1)	38(1)
O(4)	2709(1)	638(2)	9629(1)	26(1)
O(5)	1839(1)	376(3)	9533(1)	31(1)
O(6)	2923(1)	9823(3)	8068(1)	38(1)
O(7)	3100(1)	6762(3)	7495(1)	33(1)
N(1)	3153(1)	4030(3)	9009(1)	20(1)
N(2)	3578(1)	5582(3)	8998(1)	19(1)
N(3)	2246(1)	1337(3)	9393(1)	20(1)
N(4)	2877(1)	7786(3)	7947(1)	22(1)
C(1)	2628(1)	4614(3)	8759(1)	17(1)
C(2)	2174(1)	3370(3)	8926(1)	17(1)
C(3)	1639(1)	3995(3)	8665(1)	20(1)
C(4)	1524(1)	5928(3)	8240(1)	19(1)
C(5)	1950(1)	7222(3)	8062(1)	19(1)
C(6)	2475(1)	6530(3)	8297(1)	18(1)
C(11)	4025(1)	4610(3)	8697(1)	20(1)
C(12)	3916(1)	3177(3)	8075(1)	23(1)
C(13)	4338(1)	2152(4)	7790(1)	29(1)
C(14)	4875(1)	2560(4)	8107(1)	33(1)
C(15)	4981(1)	4003(4)	8714(1)	35(1)
C(16)	4565(1)	5033(4)	9014(1)	27(1)
C(21)	3687(1)	7041(3)	9646(1)	19(1)
C(22)	3512(1)	6519(4)	10317(1)	26(1)
C(23)	3616(1)	8018(4)	10916(1)	34(1)
C(24)	3898(1)	10003(4)	10857(1)	38(1)
C(25)	4075(1)	10510(4)	10191(1)	34(1)
C(26)	3965(1)	9060(4)	9578(1)	25(1)
O(30)	1605(1)	1124(3)	6606(1)	37(1)
O(31)	2430(1)	938(3)	5710(1)	33(1)
C(31)	1911(1)	3094(4)	6469(2)	37(1)
C(32)	2468(1)	2455(4)	6328(1)	33(1)
C(33)	2135(1)	-1032(4)	5851(2)	35(1)
C(34)	1575(1)	-402(4)	5984(1)	35(1)
O(32)	257(1)	3072(3)	5357(1)	48(1)
C(35)	-302(1)	3115(6)	5085(2)	61(1)
C(36)	-520(1)	5455(6)	5097(2)	64(1)

Table A12: Bond lengths [Å] and angles [°] for K-DP4SH

K(1)-O(1)#1	2.7373(15)	C(13)-C(14)	1.384(3)
K(1)-O(3)#2	2.7608(17)	C(13)-H(13)	0.9500
K(1)-O(32)	2.7980(19)	C(14)-C(15)	1.376(3)
K(1)-O(30)	2.8910(16)	C(14)-H(14)	0.9500
K(1)-O(2)	2.8923(18)	C(15)-C(16)	1.386(3)
K(1)-O(1)	2.9235(19)	C(15)-H(15)	0.9500
K(1)-O(2)#2	3.2146(18)	C(16)-H(16)	0.9500
K(1)-O(3)#1	3.4024(17)	C(21)-C(22)	1.387(3)
K(1)-K(1)#3	4.6893(7)	C(21)-C(26)	1.392(3)
S(1)-O(3)	1.4401(17)	C(22)-C(23)	1.385(3)
S(1)-O(1)	1.4483(16)	C(22)-H(22)	0.9500
S(1)-O(2)	1.4539(16)	C(23)-C(24)	1.377(4)
S(1)-C(4)	1.7769(19)	C(23)-H(23)	0.9500
O(1)-K(1)#3	2.7373(14)	C(24)-C(25)	1.379(4)
O(2)-K(1)#4	3.2146(18)	C(24)-H(24)	0.9500
O(3)-K(1)#4	2.7608(17)	C(25)-C(26)	1.385(3)
O(3)-K(1)#3	3.4024(17)	C(25)-H(25)	0.9500
O(4)-N(3)	1.231(2)	C(26)-H(26)	0.9500
O(5)-N(3)	1.225(2)	O(30)-C(34)	1.429(3)
O(6)-N(4)	1.221(2)	O(30)-C(31)	1.431(3)
O(7)-N(4)	1.219(2)	O(31)-C(32)	1.418(3)
N(1)-C(1)	1.353(2)	O(31)-C(33)	1.419(3)
N(1)-N(2)	1.401(2)	C(31)-C(32)	1.498(3)
N(1)-H(1)	0.866(16)	C(31)-H(31A)	0.9900
N(2)-C(11)	1.437(2)	C(31)-H(31B)	0.9900
N(2)-C(21)	1.438(3)	C(32)-H(32A)	0.9900
N(3)-C(2)	1.456(2)	C(32)-H(32B)	0.9900
N(4)-C(6)	1.469(2)	C(33)-C(34)	1.499(3)
C(1)-C(6)	1.416(3)	C(33)-H(33A)	0.9900
C(1)-C(2)	1.423(3)	C(33)-H(33B)	0.9900
C(2)-C(3)	1.387(3)	C(34)-H(34A)	0.9900
C(3)-C(4)	1.375(3)	C(34)-H(34B)	0.9900
C(3)-H(3)	0.9500	O(32)-C(35)	1.398(3)
C(4)-C(5)	1.389(3)	O(32)-C(36)#5	1.423(3)
C(5)-C(6)	1.368(3)	C(35)-C(36)	1.482(5)
C(5)-H(5)	0.9500	C(35)-H(35A)	0.9900
C(11)-C(12)	1.392(3)	C(35)-H(35B)	0.9900
C(11)-C(16)	1.394(3)	C(36)-O(32)#5	1.423(3)
C(12)-C(13)	1.384(3)	C(36)-H(36A)	0.9900
C(12)-H(12)	0.9500	C(36)-H(36B)	0.9900
O(1)#1-K(1)-O(3)#2	81.18(5)	O(3)#2-K(1)-O(32)	157.41(6)
O(1)#1-K(1)-O(32)	93.05(5)	O(1)#1-K(1)-O(30)	147.37(5)

O(3)#2-K(1)-O(30)	87.09(5)	O(5)-N(3)-O(4)	122.37(16)
O(32)-K(1)-O(30)	86.22(5)	O(5)-N(3)-C(2)	118.12(16)
O(1)#1-K(1)-O(2)	128.13(5)	O(4)-N(3)-C(2)	119.51(15)
O(3)#2-K(1)-O(2)	118.83(5)	O(7)-N(4)-O(6)	124.44(18)
O(32)-K(1)-O(2)	81.87(5)	O(7)-N(4)-C(6)	117.19(17)
O(30)-K(1)-O(2)	84.12(4)	O(6)-N(4)-C(6)	117.91(17)
O(1)#1-K(1)-O(1)	97.49(3)	N(1)-C(1)-C(6)	123.28(17)
O(3)#2-K(1)-O(1)	78.84(5)	N(1)-C(1)-C(2)	123.79(18)
O(32)-K(1)-O(1)	123.69(5)	C(6)-C(1)-C(2)	112.93(16)
O(30)-K(1)-O(1)	110.00(4)	C(3)-C(2)-C(1)	123.01(18)
O(2)-K(1)-O(1)	49.04(4)	C(3)-C(2)-N(3)	115.70(16)
O(1)#1-K(1)-O(2)#2	80.56(4)	C(1)-C(2)-N(3)	121.29(16)
O(3)#2-K(1)-O(2)#2	46.84(4)	C(4)-C(3)-C(2)	120.52(17)
O(32)-K(1)-O(2)#2	110.77(5)	C(4)-C(3)-H(3)	119.7
O(30)-K(1)-O(2)#2	69.37(4)	C(2)-C(3)-H(3)	119.7
O(2)-K(1)-O(2)#2	149.15(5)	C(3)-C(4)-C(5)	119.14(17)
O(1)-K(1)-O(2)#2	125.50(4)	C(3)-C(4)-S(1)	121.72(14)
O(1)#1-K(1)-O(3)#1	44.85(4)	C(5)-C(4)-S(1)	118.92(15)
O(3)#2-K(1)-O(3)#1	107.64(3)	C(6)-C(5)-C(4)	119.62(18)
O(32)-K(1)-O(3)#1	82.22(5)	C(6)-C(5)-H(5)	120.2
O(30)-K(1)-O(3)#1	164.10(5)	C(4)-C(5)-H(5)	120.2
O(2)-K(1)-O(3)#1	83.47(4)	C(5)-C(6)-C(1)	124.66(17)
O(1)-K(1)-O(3)#1	68.40(4)	C(5)-C(6)-N(4)	113.73(17)
O(2)#2-K(1)-O(3)#1	125.11(4)	C(1)-C(6)-N(4)	121.17(16)
S(1)-K(1)-O(3)#1	80.29(3)	C(12)-C(11)-C(16)	118.90(18)
O(3)-S(1)-O(1)	113.94(10)	C(12)-C(11)-N(2)	119.07(17)
O(3)-S(1)-O(2)	112.86(10)	C(16)-C(11)-N(2)	122.02(18)
O(1)-S(1)-O(2)	112.55(10)	C(13)-C(12)-C(11)	120.28(19)
O(3)-S(1)-C(4)	106.77(10)	C(13)-C(12)-H(12)	119.9
O(1)-S(1)-C(4)	105.25(9)	C(11)-C(12)-H(12)	119.9
O(2)-S(1)-C(4)	104.53(9)	C(14)-C(13)-C(12)	120.9(2)
S(1)-O(1)-K(1)#3	108.80(8)	C(14)-C(13)-H(13)	119.5
S(1)-O(1)-K(1)	95.69(8)	C(12)-C(13)-H(13)	119.5
K(1)#3-O(1)-K(1)	111.83(5)	C(15)-C(14)-C(13)	118.61(19)
S(1)-O(2)-K(1)	96.86(8)	C(15)-C(14)-H(14)	120.7
S(1)-O(2)-K(1)#4	89.91(8)	C(13)-C(14)-H(14)	120.7
K(1)-O(2)-K(1)#4	149.15(5)	C(14)-C(15)-C(16)	121.6(2)
S(1)-O(3)-K(1)#4	110.13(9)	C(14)-C(15)-H(15)	119.2
S(1)-O(3)-K(1)#3	81.17(7)	C(16)-C(15)-H(15)	119.2
K(1)#4-O(3)-K(1)#3	98.55(5)	C(15)-C(16)-C(11)	119.7(2)
C(1)-N(1)-N(2)	121.27(16)	C(15)-C(16)-H(16)	120.1
C(1)-N(1)-H(1)	116.6(15)	C(11)-C(16)-H(16)	120.1
N(2)-N(1)-H(1)	120.9(15)	C(22)-C(21)-C(26)	120.0(2)
N(1)-N(2)-C(11)	112.44(15)	C(22)-C(21)-N(2)	122.06(18)
N(1)-N(2)-C(21)	114.73(15)	C(26)-C(21)-N(2)	117.95(18)
C(11)-N(2)-C(21)	119.42(15)	C(23)-C(22)-C(21)	119.5(2)

C(23)-C(22)-H(22)	120.2	H(32A)-C(32)-H(32B)	108.1
C(21)-C(22)-H(22)	120.2	O(31)-C(33)-C(34)	110.50(18)
C(24)-C(23)-C(22)	120.8(2)	O(31)-C(33)-H(33A)	109.5
C(24)-C(23)-H(23)	119.6	C(34)-C(33)-H(33A)	109.5
C(22)-C(23)-H(23)	119.6	O(31)-C(33)-H(33B)	109.5
C(23)-C(24)-C(25)	119.5(2)	C(34)-C(33)-H(33B)	109.5
C(23)-C(24)-H(24)	120.2	H(33A)-C(33)-H(33B)	108.1
C(25)-C(24)-H(24)	120.2	O(30)-C(34)-C(33)	110.62(19)
C(24)-C(25)-C(26)	120.7(2)	O(30)-C(34)-H(34A)	109.5
C(24)-C(25)-H(25)	119.7	C(33)-C(34)-H(34A)	109.5
C(26)-C(25)-H(25)	119.7	O(30)-C(34)-H(34B)	109.5
C(25)-C(26)-C(21)	119.5(2)	C(33)-C(34)-H(34B)	109.5
C(25)-C(26)-H(26)	120.3	H(34A)-C(34)-H(34B)	108.1
C(21)-C(26)-H(26)	120.3	C(35)-O(32)-C(36)#5	108.4(2)
C(34)-O(30)-C(31)	109.51(17)	C(35)-O(32)-K(1)	112.99(17)
C(34)-O(30)-K(1)	107.10(12)	C(36)#5-O(32)-K(1)	132.34(18)
C(31)-O(30)-K(1)	117.44(13)	O(32)-C(35)-C(36)	111.0(3)
C(32)-O(31)-C(33)	110.03(17)	O(32)-C(35)-H(35A)	109.4
O(30)-C(31)-C(32)	111.11(19)	C(36)-C(35)-H(35A)	109.4
O(30)-C(31)-H(31A)	109.4	O(32)-C(35)-H(35B)	109.4
C(32)-C(31)-H(31A)	109.4	C(36)-C(35)-H(35B)	109.4
O(30)-C(31)-H(31B)	109.4	H(35A)-C(35)-H(35B)	108.0
C(32)-C(31)-H(31B)	109.4	O(32)#5-C(36)-C(35)	110.8(2)
H(31A)-C(31)-H(31B)	108.0	O(32)#5-C(36)-H(36A)	109.5
O(31)-C(32)-C(31)	110.47(19)	C(35)-C(36)-H(36A)	109.5
O(31)-C(32)-H(32A)	109.6	O(32)#5-C(36)-H(36B)	109.5
C(31)-C(32)-H(32A)	109.6	C(35)-C(36)-H(36B)	109.5
O(31)-C(32)-H(32B)	109.6	H(36A)-C(36)-H(36B)	108.1
C(31)-C(32)-H(32B)	109.6		

Symmetry transformations used to generate equivalent atoms:

#1 -x, y-1/2, -z+3/2 #2 x, y-1, z #3 -x, y+1/2, -z+3/2 #4 x, y+1, z #5 -x, -y+1, -z+1

Table A13: Anisotropic displacement parameters ($Å^2 \times 10^3$)for K-DP4SH. The anisotropic displacement factor exponent takes the form:

$$-2\pi^2[\, h^2 a^{*2} U^{11} + \ldots + 2\, h\, k\, a^*\, b^*\, U^{12} \,]$$

	U^{11}	U^{22}	U^{33}	U^{23}	U^{13}	U^{12}
K(1)	21(1)	37(1)	33(1)	5(1)	3(1)	-3(1)
S(1)	13(1)	29(1)	30(1)	6(1)	1(1)	3(1)
O(1)	13(1)	43(1)	48(1)	15(1)	3(1)	1(1)
O(2)	22(1)	50(1)	28(1)	5(1)	-3(1)	0(1)
O(3)	31(1)	33(1)	48(1)	3(1)	2(1)	15(1)
O(4)	19(1)	27(1)	32(1)	9(1)	2(1)	7(1)
O(5)	21(1)	31(1)	41(1)	13(1)	4(1)	-5(1)
O(6)	43(1)	27(1)	43(1)	0(1)	9(1)	-17(1)
O(7)	30(1)	46(1)	24(1)	6(1)	12(1)	5(1)
N(1)	15(1)	20(1)	25(1)	5(1)	2(1)	-1(1)
N(2)	12(1)	24(1)	21(1)	-2(1)	3(1)	-2(1)
N(3)	19(1)	20(1)	21(1)	2(1)	4(1)	1(1)
N(4)	18(1)	29(1)	19(1)	4(1)	1(1)	-5(1)
C(1)	15(1)	21(1)	14(1)	-3(1)	2(1)	1(1)
C(2)	17(1)	18(1)	18(1)	1(1)	3(1)	1(1)
C(3)	15(1)	23(1)	21(1)	0(1)	4(1)	-2(1)
C(4)	14(1)	24(1)	19(1)	0(1)	1(1)	3(1)
C(5)	21(1)	18(1)	17(1)	1(1)	1(1)	1(1)
C(6)	17(1)	20(1)	16(1)	-2(1)	4(1)	-3(1)
C(11)	15(1)	23(1)	21(1)	3(1)	3(1)	3(1)
C(12)	19(1)	25(1)	25(1)	0(1)	2(1)	-1(1)
C(13)	36(1)	28(1)	23(1)	-2(1)	8(1)	4(1)
C(14)	25(1)	42(1)	34(1)	0(1)	11(1)	11(1)
C(15)	15(1)	50(2)	38(2)	-5(1)	3(1)	5(1)
C(16)	18(1)	35(1)	28(1)	-5(1)	1(1)	1(1)
C(21)	13(1)	24(1)	20(1)	1(1)	0(1)	6(1)
C(22)	18(1)	34(1)	25(1)	3(1)	4(1)	5(1)
C(23)	29(1)	53(2)	21(1)	-2(1)	5(1)	15(1)
C(24)	39(1)	41(1)	29(1)	-13(1)	-5(1)	13(1)
C(25)	30(1)	26(1)	40(2)	-6(1)	-8(1)	3(1)
C(26)	21(1)	26(1)	26(1)	3(1)	-1(1)	1(1)
O(30)	36(1)	35(1)	43(1)	-6(1)	20(1)	-7(1)
O(31)	39(1)	28(1)	36(1)	-3(1)	18(1)	0(1)
C(31)	45(1)	29(1)	40(2)	-10(1)	18(1)	-7(1)
C(32)	33(1)	34(1)	33(1)	-2(1)	5(1)	-11(1)
C(33)	43(1)	24(1)	40(2)	-5(1)	12(1)	-2(1)
C(34)	35(1)	30(1)	38(2)	-2(1)	3(1)	-8(1)
O(32)	45(1)	51(1)	45(1)	14(1)	-1(1)	7(1)
C(35)	49(2)	68(2)	59(2)	21(2)	-11(1)	-20(2)
C(36)	37(2)	97(3)	60(2)	29(2)	15(1)	16(2)

Table A14: Hydrogen coordinates (x 10^4) and isotropic displacement parameters (Å^2 x 10^3) for K-DP4SH

	x	y	z	U(eq)
H(1)	3206(9)	2780(30)	9262(12)	24(6)
H(3)	1349	3080	8780	24
H(5)	1878	8581	7778	23
H(12)	3550	2900	7846	28
H(13)	4259	1156	7372	34
H(14)	5164	1857	7909	40
H(15)	5349	4301	8934	41
H(16)	4648	6023	9434	33
H(22)	3321	5143	10365	31
H(23)	3492	7672	11374	41
H(24)	3970	11016	11272	45
H(25)	4274	11868	10151	41
H(26)	4078	9441	9116	30
H(31A)	1945	4120	6909	44
H(31B)	1715	3920	6026	44
H(32A)	2667	3839	6221	40
H(32B)	2674	1727	6784	40
H(33A)	2331	-1834	6298	42
H(33B)	2106	-2073	5415	42
H(34A)	1372	323	5526	41
H(34B)	1376	-1791	6087	41
H(35A)	-492	2117	5400	73
H(35B)	-372	2524	4564	73
H(36A)	-916	5442	4906	77
H(36B)	-462	6026	5621	77

Table A15: Torsion angles [°] for K-DP4SH

O(3)-S(1)-O(1)-K(1)#3	38.12(12)	O(2)#2-K(1)-O(2)-K(1)#4	180.0
O(2)-S(1)-O(1)-K(1)#3	-92.01(10)	O(3)#1-K(1)-O(2)-K(1)#4	-20.38(11)
C(4)-S(1)-O(1)-K(1)#3	154.75(8)	O(1)-S(1)-O(3)-K(1)#4	-124.33(9)
O(3)-S(1)-O(1)-K(1)	153.50(8)	O(2)-S(1)-O(3)-K(1)#4	5.64(11)
O(2)-S(1)-O(1)-K(1)	23.37(9)	C(4)-S(1)-O(3)-K(1)#4	119.93(9)
C(4)-S(1)-O(1)-K(1)	-89.87(8)	O(1)-S(1)-O(3)-K(1)#3	-28.41(9)
O(1)#1-K(1)-O(1)-S(1)	-149.39(8)	O(2)-S(1)-O(3)-K(1)#3	101.56(7)
O(3)#2-K(1)-O(1)-S(1)	131.19(7)	C(4)-S(1)-O(3)-K(1)#3	-144.15(7)
O(32)-K(1)-O(1)-S(1)	-50.64(9)	C(1)-N(1)-N(2)-C(11)	-133.40(19)
O(30)-K(1)-O(1)-S(1)	48.48(8)	C(1)-N(1)-N(2)-C(21)	85.8(2)
O(2)-K(1)-O(1)-S(1)	-14.12(6)	N(2)-N(1)-C(1)-C(6)	17.1(3)
O(2)#2-K(1)-O(1)-S(1)	126.89(7)	N(2)-N(1)-C(1)-C(2)	-163.25(18)
O(3)#1-K(1)-O(1)-S(1)	-114.59(8)	N(1)-C(1)-C(2)-C(3)	179.94(19)
O(1)#1-K(1)-O(1)-K(1)#3	-36.51(7)	C(6)-C(1)-C(2)-C(3)	-0.4(3)
O(3)#2-K(1)-O(1)-K(1)#3	-115.93(6)	N(1)-C(1)-C(2)-N(3)	0.2(3)
O(32)-K(1)-O(1)-K(1)#3	62.24(8)	C(6)-C(1)-C(2)-N(3)	179.85(17)
O(30)-K(1)-O(1)-K(1)#3	161.36(5)	O(5)-N(3)-C(2)-C(3)	-1.7(3)
O(2)-K(1)-O(1)-K(1)#3	98.76(7)	O(4)-N(3)-C(2)-C(3)	177.99(18)
O(2)#2-K(1)-O(1)-K(1)#3	-120.23(5)	O(5)-N(3)-C(2)-C(1)	178.12(18)
O(3)#1-K(1)-O(1)-K(1)#3	-1.71(5)	O(4)-N(3)-C(2)-C(1)	-2.2(3)
O(3)-S(1)-O(2)-K(1)	-154.37(8)	C(1)-C(2)-C(3)-C(4)	-1.9(3)
O(1)-S(1)-O(2)-K(1)	-23.70(9)	N(3)-C(2)-C(3)-C(4)	177.87(17)
C(4)-S(1)-O(2)-K(1)	89.99(8)	C(2)-C(3)-C(4)-C(5)	1.4(3)
O(3)-S(1)-O(2)-K(1)#4	-4.54(9)	C(2)-C(3)-C(4)-S(1)	175.97(16)
O(1)-S(1)-O(2)-K(1)#4	126.13(7)	O(3)-S(1)-C(4)-C(3)	125.41(18)
C(4)-S(1)-O(2)-K(1)#4	-120.18(7)	O(1)-S(1)-C(4)-C(3)	4.0(2)
O(1)#1-K(1)-O(2)-S(1)	76.59(9)	O(2)-S(1)-C(4)-C(3)	-114.78(18)
O(3)#2-K(1)-O(2)-S(1)	-25.51(9)	O(3)-S(1)-C(4)-C(5)	-60.03(18)
O(32)-K(1)-O(2)-S(1)	164.08(8)	O(1)-S(1)-C(4)-C(5)	178.55(16)
O(30)-K(1)-O(2)-S(1)	-108.91(7)	O(2)-S(1)-C(4)-C(5)	59.79(18)
O(1)-K(1)-O(2)-S(1)	14.09(5)	C(3)-C(4)-C(5)-C(6)	1.4(3)
O(2)#2-K(1)-O(2)-S(1)	-78.56(14)	S(1)-C(4)-C(5)-C(6)	-173.32(16)
O(3)#1-K(1)-O(2)-S(1)	81.05(7)	C(4)-C(5)-C(6)-C(1)	-4.0(3)
O(1)#1-K(1)-O(2)-K(1)#4	-24.85(14)	C(4)-C(5)-C(6)-N(4)	168.48(17)
O(3)#2-K(1)-O(2)-K(1)#4	-126.95(11)	N(1)-C(1)-C(6)-C(5)	-176.96(19)
O(32)-K(1)-O(2)-K(1)#4	62.64(12)	C(2)-C(1)-C(6)-C(5)	3.3(3)
O(30)-K(1)-O(2)-K(1)#4	149.65(12)	N(1)-C(1)-C(6)-N(4)	11.1(3)
O(1)-K(1)-O(2)-K(1)#4	-87.35(12)	C(2)-C(1)-C(6)-N(4)	-168.58(17)

O(7)-N(4)-C(6)-C(5)	-109.8(2)
O(6)-N(4)-C(6)-C(5)	62.8(2)
O(7)-N(4)-C(6)-C(1)	63.0(2)
O(6)-N(4)-C(6)-C(1)	-124.5(2)
N(1)-N(2)-C(11)-C(12)	40.4(2)
C(21)-N(2)-C(11)-C(12)	179.20(18)
N(1)-N(2)-C(11)-C(16)	-138.7(2)
C(21)-N(2)-C(11)-C(16)	0.1(3)
C(16)-C(11)-C(12)-C(13)	1.4(3)
N(2)-C(11)-C(12)-C(13)	-177.65(18)
C(11)-C(12)-C(13)-C(14)	-1.1(3)
C(12)-C(13)-C(14)-C(15)	0.2(4)
C(13)-C(14)-C(15)-C(16)	0.4(4)
C(14)-C(15)-C(16)-C(11)	0.0(4)
C(12)-C(11)-C(16)-C(15)	-0.9(3)
N(2)-C(11)-C(16)-C(15)	178.2(2)
N(1)-N(2)-C(21)-C(22)	18.9(2)
C(11)-N(2)-C(21)-C(22)	-119.0(2)
N(1)-N(2)-C(21)-C(26)	-159.31(17)
C(11)-N(2)-C(21)-C(26)	62.8(2)
C(26)-C(21)-C(22)-C(23)	-0.1(3)
N(2)-C(21)-C(22)-C(23)	-178.31(18)
C(21)-C(22)-C(23)-C(24)	-0.9(3)
C(22)-C(23)-C(24)-C(25)	0.5(3)
C(23)-C(24)-C(25)-C(26)	0.9(3)
C(24)-C(25)-C(26)-C(21)	-1.9(3)
C(22)-C(21)-C(26)-C(25)	1.4(3)
N(2)-C(21)-C(26)-C(25)	179.72(18)
O(1)#1-K(1)-O(30)-C(34)	35.36(18)
O(3)#2-K(1)-O(30)-C(34)	104.02(14)
O(32)-K(1)-O(30)-C(34)	-54.40(14)
O(2)-K(1)-O(30)-C(34)	-136.60(14)
O(1)-K(1)-O(30)-C(34)	-178.98(13)
O(2)#2-K(1)-O(30)-C(34)	59.47(14)
O(3)#1-K(1)-O(30)-C(34)	-97.7(2)
O(1)#1-K(1)-O(30)-C(31)	158.97(15)
O(3)#2-K(1)-O(30)-C(31)	-132.38(16)
O(32)-K(1)-O(30)-C(31)	69.21(16)
O(2)-K(1)-O(30)-C(31)	-13.00(16)
O(1)-K(1)-O(30)-C(31)	-55.37(16)
O(2)#2-K(1)-O(30)-C(31)	-176.93(17)
O(3)#1-K(1)-O(30)-C(31)	25.9(3)
C(34)-O(30)-C(31)-C(32)	-56.7(3)
K(1)-O(30)-C(31)-C(32)	-179.11(15)
C(33)-O(31)-C(32)-C(31)	-57.9(2)
O(30)-C(31)-C(32)-O(31)	57.6(3)
C(32)-O(31)-C(33)-C(34)	58.5(3)
C(31)-O(30)-C(34)-C(33)	57.0(3)
K(1)-O(30)-C(34)-C(33)	-174.68(15)
O(31)-C(33)-C(34)-O(30)	-58.5(3)
O(1)#1-K(1)-O(32)-C(35)	17.69(19)
O(3)#2-K(1)-O(32)-C(35)	91.9(2)
O(30)-K(1)-O(32)-C(35)	165.00(19)
O(2)-K(1)-O(32)-C(35)	-110.41(19)
O(1)-K(1)-O(32)-C(35)	-83.41(19)
O(2)#2-K(1)-O(32)-C(35)	98.74(19)
O(3)#1-K(1)-O(32)-C(35)	-25.94(18)
O(1)#1-K(1)-O(32)-C(36)#5	165.9(2)
O(3)#2-K(1)-O(32)-C(36)#5	-119.9(2)
O(30)-K(1)-O(32)-C(36)#5	-46.8(2)
O(2)-K(1)-O(32)-C(36)#5	37.8(2)
O(1)-K(1)-O(32)-C(36)#5	64.8(2)
O(2)#2-K(1)-O(32)-C(36)#5	-113.1(2)
S(1)-K(1)-O(32)-C(36)#5	44.8(2)
O(3)#1-K(1)-O(32)-C(36)#5	122.2(2)
C(36)#5-O(32)-C(35)-C(36)	-58.2(4)
K(1)-O(32)-C(35)-C(36)	97.6(2)
O(32)-C(35)-C(36)-O(32)#5	59.6(4)

Symmetry transformations used to generate equivalent atoms:

#1 -x, y-1/2, -z+3/2

#2 x, y-1, z

#3 -x, y+1/2, -z+3/2

#4 x, y+1, z

#5 -x, -y+1, -z+1

Table A16: Hydrogen bonds for K-DP4SH [Å and °]

D-H...A	d(D-H)	d(H...A)	d(D...A)	<(DHA)
N(1)-H(1)...O(4)	0.866(16)	1.956(19)	2.620(2)	132.5(19)

Symmetry transformations used to generate equivalent atoms:

#1 -x, y-1/2, -z+3/2 #2 x, y-1, z #3 -x, y+1/2, -z+3/2 #4 x, y+1, z #5 -x, -y+1, -z+1

Table A17: Crystal data and structure refinement for K-DP6SH

Empirical formula	$C_{18}H_{15}KN_4O_{8.076}S$	
Molar mass	487.72 g/mol	
Temperature	193(2) K	
Wavelength	0.71073 Å	
Crystal system	Monoclinic	
Space group	$P2_1/c$	
Unit-cell dimensions	a = 14.1374(9) Å	α = 90°.
	b = 8.7410(10) Å	β = 90.600(10)°.
	c = 16.6082(11) Å	γ = 90°.
Volume	2052.2(3) $Å^3$	
Z	4	
Density (calculated)	1.579 Mg/m^3	
Absorption coefficient	0.417 mm^{-1}	
F(000)	1002	
Crystal size	0.50 x 0.19 x 0.08 mm^3	
Theta range for data collection	2.45 to 26.37°.	
Index ranges	-17<=h<=17, -9<=k<=10, -20<=l<=19	
Reflections collected	11653	
Independent reflections	4187 [R(int) = 0.1206]	
Completeness to theta = 26.37°	99.9 %	
Absorption correction	Semi-empirical from equivalents	
Max. and min. transmission	0.9674 and 0.8186	
Refinement method	Full-matrix least-squares on F^2	
Data / restraints / parameters	4187 / 3 / 304	
Goodness-of-fit on F^2	0.996	
Final R indices [I > 2sigma(I)]	R1 = 0.0454, wR2 = 0.1172	
R indices (all data)	R1 = 0.0587, wR2 = 0.1231	
Largest diff. peak and hole	0.765 and -0.409 $e.Å^{-3}$	

Table A18: Atomic coordinates (x 10^4) and equivalent isotropic displacement parameters ($Å^2$ x 10^3) for K-DP6SH. U(eq) is defined as one third of the trace of the orthogonalized U^{ij} tensor (describes physical/vibrational motion)

	x	y	z	U(eq)
K(1)	5980(1)	7940(1)	5341(1)	31(1)
S(1)	4383(1)	8508(1)	3403(1)	24(1)
O(1)	4884(1)	7718(2)	4043(1)	42(1)
O(2)	3801(1)	9727(2)	3704(1)	43(1)
O(3)	4977(1)	8951(3)	2750(1)	51(1)
O(4)	3762(1)	5856(2)	648(1)	36(1)
O(5)	2710(1)	4087(2)	798(1)	40(1)
O(6)	2257(1)	3402(2)	4208(1)	34(1)
O(7)	1019(1)	3893(2)	3473(1)	39(1)
N(1)	2832(1)	6811(2)	4306(1)	22(1)
N(2)	1950(1)	6555(2)	4678(1)	23(1)
N(3)	3184(1)	5153(2)	1062(1)	27(1)
N(4)	1848(1)	4095(2)	3667(1)	25(1)
C(1)	2929(1)	6365(3)	3524(1)	18(1)
C(2)	3584(1)	7113(3)	3011(1)	20(1)
C(3)	3649(1)	6731(3)	2212(1)	20(1)
C(4)	3080(1)	5588(3)	1896(1)	21(1)
C(5)	2462(1)	4767(3)	2373(1)	23(1)
C(6)	2412(1)	5164(3)	3176(1)	20(1)
C(11)	2026(1)	6072(3)	5493(1)	22(1)
C(12)	2812(2)	5245(3)	5757(1)	27(1)
C(13)	2864(2)	4700(3)	6541(1)	32(1)
C(14)	2138(2)	4980(3)	7075(1)	35(1)
C(15)	1367(2)	5816(3)	6820(1)	35(1)
C(16)	1298(2)	6375(3)	6037(1)	28(1)
C(21)	1203(1)	7576(3)	4420(1)	22(1)
C(22)	1371(2)	9101(3)	4245(1)	28(1)
C(23)	628(2)	10018(3)	3984(1)	33(1)
C(24)	-275(2)	9432(3)	3904(1)	34(1)
C(25)	-440(2)	7903(3)	4073(2)	36(1)
C(26)	300(2)	6975(3)	4328(1)	30(1)
O(30)	4781(1)	4396(2)	3919(1)	41(1)
O(31)	3793(18)	2360(30)	3037(15)	44(6)

Table A19: Bond lengths [Å] and angles [°] for K-DP6SH

K(1)-O(2)#1	2.6002(19)	C(1)-C(2)	1.424(3)
K(1)-O(30)#2	2.620(2)	C(2)-C(3)	1.373(3)
K(1)-O(1)	2.6478(18)	C(3)-C(4)	1.382(3)
K(1)-O(31)#2	2.72(3)	C(3)-H(3)	0.9500
K(1)-O(5)#3	2.8420(18)	C(4)-C(5)	1.386(3)
K(1)-O(6)#2	2.8476(18)	C(5)-C(6)	1.381(3)
K(1)-O(4)#3	3.0563(19)	C(5)-H(5)	0.9500
K(1)-N(3)#3	3.2584(19)	C(11)-C(12)	1.393(3)
K(1)-O(4)#4	3.3526(18)	C(11)-C(16)	1.403(3)
K(1)-S(1)#1	3.7798(8)	C(12)-C(13)	1.388(3)
K(1)-K(1)#1	4.6767(12)	C(12)-H(12)	0.9500
S(1)-O(3)	1.4321(17)	C(13)-C(14)	1.385(3)
S(1)-O(2)	1.440(2)	C(13)-H(13)	0.9500
S(1)-O(1)	1.4468(19)	C(14)-C(15)	1.376(4)
S(1)-C(2)	1.781(2)	C(14)-H(14)	0.9500
S(1)-K(1)#1	3.7798(8)	C(15)-C(16)	1.391(3)
O(2)-K(1)#1	2.6002(19)	C(15)-H(15)	0.9500
O(4)-N(3)	1.237(2)	C(16)-H(16)	0.9500
O(4)-K(1)#5	3.0563(19)	C(21)-C(22)	1.385(3)
O(4)-K(1)#6	3.3526(18)	C(21)-C(26)	1.388(3)
O(5)-N(3)	1.227(3)	C(22)-C(23)	1.387(3)
O(5)-K(1)#5	2.8420(18)	C(22)-H(22)	0.9500
O(6)-N(4)	1.223(2)	C(23)-C(24)	1.380(4)
O(6)-K(1)#2	2.8476(18)	C(23)-H(23)	0.9500
O(7)-N(4)	1.226(2)	C(24)-C(25)	1.386(4)
N(1)-C(1)	1.364(3)	C(24)-H(24)	0.9500
N(1)-N(2)	1.415(2)	C(25)-C(26)	1.387(3)
N(1)-H(1)	0.89(3)	C(25)-H(25)	0.9500
N(2)-C(11)	1.420(3)	C(26)-H(26)	0.9500
N(2)-C(21)	1.444(3)	O(30)-K(1)#2	2.620(2)
N(3)-C(4)	1.446(3)	O(30)-H(30A)	0.860(17)
N(3)-K(1)#5	3.2584(19)	O(30)-H(30B)	0.816(17)
N(4)-C(6)	1.479(3)	O(31)-K(1)#2	2.72(3)
C(1)-C(6)	1.400(3)		

O(2)#1-K(1)-O(30)#2	111.80(7)	O(2)#1-K(1)-O(1)	128.21(7)

O(30)#2-K(1)-O(1)	94.88(6)	O(5)#3-K(1)-S(1)#1	99.83(5)
O(2)#1-K(1)-O(31)#2	57.2(6)	O(6)#2-K(1)-S(1)#1	108.45(4)
O(30)#2-K(1)-O(31)#2	60.4(6)	O(4)#3-K(1)-S(1)#1	68.22(3)
O(1)-K(1)-O(31)#2	149.4(6)	N(3)#3-K(1)-S(1)#1	87.68(4)
O(2)#1-K(1)-O(5)#3	93.17(6)	O(4)#4-K(1)-S(1)#1	61.64(4)
O(30)#2-K(1)-O(5)#3	149.37(6)	O(2)#1-K(1)-K(1)#1	67.03(5)
O(1)-K(1)-O(5)#3	82.20(6)	O(30)#2-K(1)-K(1)#1	117.91(5)
O(31)#2-K(1)-O(5)#3	128.4(6)	O(1)-K(1)-K(1)#1	61.26(5)
O(2)#1-K(1)-O(6)#2	93.68(6)	O(31)#2-K(1)-K(1)#1	112.1(6)
O(30)#2-K(1)-O(6)#2	85.31(6)	O(5)#3-K(1)-K(1)#1	87.48(4)
O(1)-K(1)-O(6)#2	133.43(6)	O(6)#2-K(1)-K(1)#1	153.60(4)
O(31)#2-K(1)-O(6)#2	66.8(6)	O(4)#3-K(1)-K(1)#1	45.68(3)
O(5)#3-K(1)-O(6)#2	75.30(5)	N(3)#3-K(1)-K(1)#1	65.69(4)
O(2)#1-K(1)-O(4)#3	70.10(6)	O(4)#4-K(1)-K(1)#1	40.71(3)
O(30)#2-K(1)-O(4)#3	162.53(6)	S(1)#1-K(1)-K(1)#1	54.343(15)
O(1)-K(1)-O(4)#3	72.30(6)	O(3)-S(1)-O(2)	113.85(14)
O(31)#2-K(1)-O(4)#3	126.7(6)	O(3)-S(1)-O(1)	113.56(13)
O(5)#3-K(1)-O(4)#3	42.81(5)	O(2)-S(1)-O(1)	112.01(12)
O(6)#2-K(1)-O(4)#3	112.10(5)	O(3)-S(1)-C(2)	106.46(10)
O(2)#1-K(1)-N(3)#3	85.94(6)	O(2)-S(1)-C(2)	105.73(10)
O(30)#2-K(1)-N(3)#3	162.09(6)	O(1)-S(1)-C(2)	104.25(11)
O(1)-K(1)-N(3)#3	71.04(5)	O(3)-S(1)-K(1)#1	106.27(10)
O(31)#2-K(1)-N(3)#3	136.4(6)	O(2)-S(1)-K(1)#1	28.12(8)
O(5)#3-K(1)-N(3)#3	21.85(5)	O(1)-S(1)-K(1)#1	93.11(8)
O(6)#2-K(1)-N(3)#3	96.33(5)	C(2)-S(1)-K(1)#1	132.42(7)
O(4)#3-K(1)-N(3)#3	22.29(5)	S(1)-O(1)-K(1)	147.26(12)
O(2)#1-K(1)-O(4)#4	76.47(5)	S(1)-O(2)-K(1)#1	136.75(11)
O(30)#2-K(1)-O(4)#4	77.49(5)	N(3)-O(4)-K(1)#5	88.09(13)
O(1)-K(1)-O(4)#4	66.82(5)	N(3)-O(4)-K(1)#6	149.88(14)
O(31)#2-K(1)-O(4)#4	88.8(5)	K(1)#5-O(4)-K(1)#6	93.61(5)
O(5)#3-K(1)-O(4)#4	127.41(5)	N(3)-O(5)-K(1)#5	98.54(12)
O(6)#2-K(1)-O(4)#4	155.04(4)	N(4)-O(6)-K(1)#2	143.43(13)
O(4)#3-K(1)-O(4)#4	86.39(5)	C(1)-N(1)-N(2)	117.89(17)
N(3)#3-K(1)-O(4)#4	105.62(5)	C(1)-N(1)-H(1)	118.4(16)
O(2)#1-K(1)-S(1)#1	15.13(4)	N(2)-N(1)-H(1)	115.6(16)
O(30)#2-K(1)-S(1)#1	108.79(5)	N(1)-N(2)-C(11)	113.89(16)
O(1)-K(1)-S(1)#1	115.31(5)	N(1)-N(2)-C(21)	114.67(17)
O(31)#2-K(1)-S(1)#1	63.0(6)	C(11)-N(2)-C(21)	120.94(16)

O(5)-N(3)-O(4)	122.73(18)	C(14)-C(13)-C(12)	120.5(2)
O(5)-N(3)-C(4)	118.81(18)	C(14)-C(13)-H(13)	119.7
O(4)-N(3)-C(4)	118.45(19)	C(12)-C(13)-H(13)	119.7
O(5)-N(3)-K(1)#5	59.60(11)	C(15)-C(14)-C(13)	119.1(2)
O(4)-N(3)-K(1)#5	69.62(11)	C(15)-C(14)-H(14)	120.4
C(4)-N(3)-K(1)#5	151.98(14)	C(13)-C(14)-H(14)	120.4
O(6)-N(4)-O(7)	124.4(2)	C(14)-C(15)-C(16)	121.5(2)
O(6)-N(4)-C(6)	117.66(17)	C(14)-C(15)-H(15)	119.3
O(7)-N(4)-C(6)	117.76(19)	C(16)-C(15)-H(15)	119.3
N(1)-C(1)-C(6)	123.37(19)	C(15)-C(16)-C(11)	119.5(2)
N(1)-C(1)-C(2)	120.7(2)	C(15)-C(16)-H(16)	120.3
C(6)-C(1)-C(2)	115.94(18)	C(11)-C(16)-H(16)	120.3
C(3)-C(2)-C(1)	121.1(2)	C(22)-C(21)-C(26)	120.0(2)
C(3)-C(2)-S(1)	118.13(16)	C(22)-C(21)-N(2)	122.07(19)
C(1)-C(2)-S(1)	120.67(15)	C(26)-C(21)-N(2)	117.9(2)
C(2)-C(3)-C(4)	119.89(19)	C(21)-C(22)-C(23)	119.4(2)
C(2)-C(3)-H(3)	120.1	C(21)-C(22)-H(22)	120.3
C(4)-C(3)-H(3)	120.1	C(23)-C(22)-H(22)	120.3
C(3)-C(4)-C(5)	121.67(19)	C(24)-C(23)-C(22)	120.8(2)
C(3)-C(4)-N(3)	119.25(18)	C(24)-C(23)-H(23)	119.6
C(5)-C(4)-N(3)	118.9(2)	C(22)-C(23)-H(23)	119.6
C(6)-C(5)-C(4)	117.4(2)	C(23)-C(24)-C(25)	119.7(2)
C(6)-C(5)-H(5)	121.3	C(23)-C(24)-H(24)	120.1
C(4)-C(5)-H(5)	121.3	C(25)-C(24)-H(24)	120.1
C(5)-C(6)-C(1)	123.74(19)	C(24)-C(25)-C(26)	119.9(2)
C(5)-C(6)-N(4)	114.00(19)	C(24)-C(25)-H(25)	120.1
C(1)-C(6)-N(4)	121.89(18)	C(26)-C(25)-H(25)	120.1
C(12)-C(11)-C(16)	118.9(2)	C(25)-C(26)-C(21)	120.2(2)
C(12)-C(11)-N(2)	120.46(18)	C(25)-C(26)-H(26)	119.9
C(16)-C(11)-N(2)	120.6(2)	C(21)-C(26)-H(26)	119.9
C(13)-C(12)-C(11)	120.5(2)	K(1)#2-O(30)-H(30A)	129.2(19)
C(13)-C(12)-H(12)	119.7	K(1)#2-O(30)-H(30B)	121(2)
C(11)-C(12)-H(12)	119.7	H(30A)-O(30)-H(30B)	105(2)

Symmetry transformations used to generate equivalent atoms:

#1 -x+1, -y+2, -z+1 #2 -x+1, -y+1, -z+1 #3 -x+1, y+1/2, -z+1/2

#4 x, -y+3/2, z+1/2 #5 -x+1, y-1/2, -z+1/2 #6 x, -y+3/2, z-1/2

Table A20: Anisotropic displacement parameters ($Å^2 \times 10^3$)for K-DP6SH. The anisotropic displacement factor exponent takes the form:

$$-2\pi^2[\, h^2 a^{*2} U^{11} + \ldots + 2\, h\, k\, a^*\, b^*\, U^{12} \,]$$

	U^{11}	U^{22}	U^{33}	U^{23}	U^{13}	U^{12}
K(1)	41(1)	31(1)	22(1)	1(1)	-7(1)	-7(1)
S(1)	21(1)	31(1)	19(1)	-3(1)	1(1)	-9(1)
O(1)	39(1)	42(1)	43(1)	4(1)	-22(1)	-12(1)
O(2)	39(1)	39(1)	50(1)	-17(1)	-2(1)	-6(1)
O(3)	51(1)	73(2)	31(1)	-9(1)	14(1)	-44(1)
O(4)	46(1)	44(1)	20(1)	-2(1)	9(1)	-6(1)
O(5)	36(1)	56(1)	29(1)	-18(1)	-3(1)	-14(1)
O(6)	35(1)	35(1)	32(1)	9(1)	-1(1)	-2(1)
O(7)	19(1)	50(1)	49(1)	6(1)	-1(1)	-13(1)
N(1)	14(1)	34(1)	18(1)	-4(1)	4(1)	-7(1)
N(2)	14(1)	36(1)	19(1)	2(1)	6(1)	0(1)
N(3)	26(1)	35(1)	19(1)	-6(1)	-4(1)	3(1)
N(4)	20(1)	27(1)	28(1)	0(1)	2(1)	-3(1)
C(1)	12(1)	28(1)	16(1)	2(1)	-2(1)	2(1)
C(2)	15(1)	25(1)	19(1)	0(1)	-2(1)	-1(1)
C(3)	18(1)	27(1)	16(1)	1(1)	0(1)	0(1)
C(4)	20(1)	29(1)	15(1)	-2(1)	-1(1)	2(1)
C(5)	17(1)	26(1)	26(1)	-2(1)	-7(1)	-1(1)
C(6)	13(1)	27(1)	21(1)	2(1)	0(1)	-1(1)
C(11)	19(1)	27(1)	19(1)	-1(1)	1(1)	-6(1)
C(12)	20(1)	39(1)	22(1)	-1(1)	1(1)	-2(1)
C(13)	27(1)	41(2)	28(1)	3(1)	-8(1)	-3(1)
C(14)	33(1)	49(2)	21(1)	6(1)	-3(1)	-12(1)
C(15)	31(1)	51(2)	23(1)	0(1)	8(1)	-7(1)
C(16)	22(1)	39(1)	24(1)	0(1)	4(1)	-1(1)
C(21)	19(1)	30(1)	15(1)	-1(1)	2(1)	0(1)
C(22)	22(1)	34(1)	29(1)	0(1)	2(1)	-5(1)
C(23)	37(1)	28(1)	34(1)	4(1)	2(1)	1(1)
C(24)	30(1)	40(2)	32(1)	-3(1)	-7(1)	10(1)
C(25)	21(1)	38(2)	48(2)	-5(1)	-6(1)	0(1)
C(26)	22(1)	31(1)	38(1)	1(1)	0(1)	-3(1)
O(30)	36(1)	43(1)	44(1)	13(1)	8(1)	6(1)

Table A21: Hydrogen coordinates (x 10^4) and isotropic displacement parameters ($Å^2$ x 10^3) for K-DP6SH

	x	y	z	U(eq)
H(1)	3148(18)	7630(30)	4475(15)	26(7)
H(3)	4084	7250	1877	24
H(5)	2087	3962	2156	27
H(12)	3317	5052	5398	32
H(13)	3402	4132	6714	39
H(14)	2172	4599	7611	41
H(15)	870	6017	7186	42
H(16)	762	6957	5873	34
H(22)	1989	9515	4303	34
H(23)	742	11062	3859	40
H(24)	-781	10075	3734	41
H(25)	-1059	7492	4015	43
H(26)	188	5925	4440	36
H(30A)	4820(20)	5340(20)	4068(16)	49
H(30B)	4810(20)	4420(30)	3429(10)	49

Table A22: Torsion angles [°] for K-DP6SH

O(3)-S(1)-O(1)-K(1)	80.4(2)	O(3)-S(1)-C(2)-C(1)	176.19(19)
O(2)-S(1)-O(1)-K(1)	-50.3(2)	O(2)-S(1)-C(2)-C(1)	-62.4(2)
C(2)-S(1)-O(1)-K(1)	-164.1(2)	O(1)-S(1)-C(2)-C(1)	55.9(2)
K(1)#1-S(1)-O(1)-K(1)	-28.8(2)	K(1)#1-S(1)-C(2)-C(1)	-52.1(2)
O(2)#1-K(1)-O(1)-S(1)	22.8(3)	C(1)-C(2)-C(3)-C(4)	-0.8(3)
O(30)#2-K(1)-O(1)-S(1)	145.6(2)	S(1)-C(2)-C(3)-C(4)	176.16(17)
O(31)#2-K(1)-O(1)-S(1)	111.5(12)	C(2)-C(3)-C(4)-C(5)	-2.5(3)
O(5)#3-K(1)-O(1)-S(1)	-65.1(2)	C(2)-C(3)-C(4)-N(3)	-177.3(2)
O(6)#2-K(1)-O(1)-S(1)	-126.2(2)	O(5)-N(3)-C(4)-C(3)	176.4(2)
O(4)#3-K(1)-O(1)-S(1)	-22.3(2)	O(4)-N(3)-C(4)-C(3)	-2.4(3)
N(3)#3-K(1)-O(1)-S(1)	-45.7(2)	K(1)#5-N(3)-C(4)-C(3)	97.7(3)
O(4)#4-K(1)-O(1)-S(1)	71.4(2)	O(5)-N(3)-C(4)-C(5)	1.3(3)
S(1)#1-K(1)-O(1)-S(1)	32.2(2)	O(4)-N(3)-C(4)-C(5)	-177.5(2)
K(1)#1-K(1)-O(1)-S(1)	26.3(2)	K(1)#5-N(3)-C(4)-C(5)	-77.4(3)
O(3)-S(1)-O(2)-K(1)#1	-79.77(19)	C(3)-C(4)-C(5)-C(6)	2.0(3)
O(1)-S(1)-O(2)-K(1)#1	50.8(2)	N(3)-C(4)-C(5)-C(6)	176.9(2)
C(2)-S(1)-O(2)-K(1)#1	163.71(15)	C(4)-C(5)-C(6)-C(1)	1.7(3)
C(1)-N(1)-N(2)-C(11)	140.7(2)	C(4)-C(5)-C(6)-N(4)	-171.42(19)
C(1)-N(1)-N(2)-C(21)	-74.0(3)	N(1)-C(1)-C(6)-C(5)	175.8(2)
K(1)#5-O(5)-N(3)-O(4)	31.0(2)	C(2)-C(1)-C(6)-C(5)	-4.7(3)
K(1)#5-O(5)-N(3)-C(4)	-147.72(16)	N(1)-C(1)-C(6)-N(4)	-11.6(3)
K(1)#5-O(4)-N(3)-O(5)	-28.3(2)	C(2)-C(1)-C(6)-N(4)	167.94(18)
K(1)#6-O(4)-N(3)-O(5)	-122.2(3)	O(6)-N(4)-C(6)-C(5)	117.0(2)
K(1)#5-O(4)-N(3)-C(4)	150.44(17)	O(7)-N(4)-C(6)-C(5)	-58.6(3)
K(1)#6-O(4)-N(3)-C(4)	56.5(4)	O(6)-N(4)-C(6)-C(1)	-56.3(3)
K(1)#6-O(4)-N(3)-K(1)#5	-93.9(3)	O(7)-N(4)-C(6)-C(1)	128.2(2)
K(1)#2-O(6)-N(4)-O(7)	142.2(2)	N(1)-N(2)-C(11)-C(12)	-29.1(3)
K(1)#2-O(6)-N(4)-C(6)	-33.0(3)	C(21)-N(2)-C(11)-C(12)	-172.0(2)
N(2)-N(1)-C(1)-C(6)	-27.6(3)	N(1)-N(2)-C(11)-C(16)	153.0(2)
N(2)-N(1)-C(1)-C(2)	152.90(19)	C(21)-N(2)-C(11)-C(16)	10.1(3)
N(1)-C(1)-C(2)-C(3)	-176.3(2)	C(16)-C(11)-C(12)-C(13)	1.5(4)
C(6)-C(1)-C(2)-C(3)	4.1(3)	N(2)-C(11)-C(12)-C(13)	-176.5(2)
N(1)-C(1)-C(2)-S(1)	6.8(3)	C(11)-C(12)-C(13)-C(14)	-0.5(4)
C(6)-C(1)-C(2)-S(1)	-172.71(16)	C(12)-C(13)-C(14)-C(15)	-0.5(4)
O(3)-S(1)-C(2)-C(3)	-0.8(2)	C(13)-C(14)-C(15)-C(16)	0.5(4)
O(2)-S(1)-C(2)-C(3)	120.66(19)	C(14)-C(15)-C(16)-C(11)	0.5(4)
O(1)-S(1)-C(2)-C(3)	-121.09(19)	C(12)-C(11)-C(16)-C(15)	-1.5(4)
K(1)#1-S(1)-C(2)-C(3)	130.98(15)	N(2)-C(11)-C(16)-C(15)	176.5(2)

N(1)-N(2)-C(21)-C(22)	-36.5(3)
C(11)-N(2)-C(21)-C(22)	106.1(2)
N(1)-N(2)-C(21)-C(26)	141.7(2)
C(11)-N(2)-C(21)-C(26)	-75.6(3)
C(26)-C(21)-C(22)-C(23)	0.5(3)
N(2)-C(21)-C(22)-C(23)	178.73(19)
C(21)-C(22)-C(23)-C(24)	0.6(3)
C(22)-C(23)-C(24)-C(25)	-1.1(4)
C(23)-C(24)-C(25)-C(26)	0.5(4)
C(24)-C(25)-C(26)-C(21)	0.5(4)
C(22)-C(21)-C(26)-C(25)	-1.0(3)
N(2)-C(21)-C(26)-C(25)	-179.3(2)

Symmetry transformations used to generate equivalent atoms:

#1 -x+1, -y+2, -z+1

#2 -x+1, -y+1, -z+1

#3 -x+1, y+1/2, -z+1/2

#4 x, -y+3/2, z+1/2

#5 -x+1, y-1/2, -z+1/2

#6 x, -y+3/2, z-1/2

Table A23: Hydrogen bonds for K-DP6SH [Å and °]

D-H...A	d(D-H)	d(H...A)	d(D...A)	<(DHA)
N(1)-H(1)...O(1)	0.89(3)	2.57(2)	3.044(3)	114.5(19)
N(1)-H(1)...O(4)#4	0.89(3)	2.50(3)	3.285(3)	147(2)
N(1)-H(1)...N(3)#4	0.89(3)	3.27(3)	3.970(3)	137.4(19)
O(30)-H(30A)...O(1)	0.860(17)	2.09(2)	2.915(3)	162(3)
O(30)-H(30A)...N(1)	0.860(17)	3.12(3)	3.535(3)	113(2)
O(30)-H(30A)...O(30)#2	0.860(17)	3.39(3)	3.786(4)	111(2)
O(30)-H(30B)...O(3)#5	0.816(17)	2.026(17)	2.823(3)	165(3)

Symmetry transformations used to generate equivalent atoms:

#1 -x+1, -y+2, -z+1 #2 -x+1, -y+1, -z+1 #3 -x+1, y+1/2, -z+1/2

#4 x, -y+3/2, z+1/2 #5 -x+1, y-1/2, -z+1/2 #6 x, -y+3/2, z-1/2